Study of Dynamics and Magnetic Field Structure of the Solar Convective Envelope using Sunspot Activity

A Thesis

submitted for the degree of

Doctor of Philosophy

In

The Faculty of Science

University of Calicut, Calicut

by

Lovely M. R.

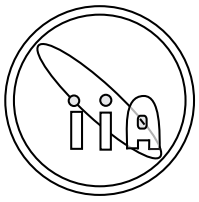

Indian Institute of Astrophysics

Bangalore 560 034, INDIA

December 2009

To my father, Late. Sri. Radhakrishnan,
for his inspiration and encouragement

DECLARATION

I hereby declare that the matter contained in this thesis is the result of the investigations carried out by me at the Indian Institute of Astrophysics, Bangalore, under the supervision of Dr. Hiremath K. M. This thesis has not been submitted for the award of any degree, diploma, associateship, fellowship etc. of any university or institute.

Dr. Hiremath K. M.	Dr. K. Neelakandan	Lovely M. R.
(Thesis Supervisor)	(Thesis Supervisor)	(Ph.D. Candidate)

Indian Institute of Astrophysics
Bangalore 560 034, INDIA
December, 2009

CERTIFICATE

This is to certify that the thesis entitled **"Study of Dynamics and Magnetic Field Structure of the Solar Convective Envelope using Sunspot Activity"** submitted to the University of Calicut by Ms. Lovely M. R for the award of the degree of Doctor of Philosophy in the faculty of Science, is based on the results of the investigations carried out by her under my supervision and guidance, at the Indian Institute of Astrophysics, Bangalore. This thesis has not been submitted for the award of any degree, diploma, associateship, fellowship etc. of any university or institute.

Dr. Hiremath, K. M.
(Thesis Supervisor)

Indian Institute of Astrophysics
II Block, Koramangala
Karnataka
December, 2009

ACKNOWLEDGMENTS

I am deeply indebted to my guide Dr. K. M. Hiremath from Indian Institute of Astrophysics (IIA) whose unconditional help, direction, suggestions and encouragement helped me throughout the duration of the research and during writing this thesis.

I owe my gratitude to my co-guide Dr. K. Neelakandan of University of Cailcut for his valuable advices and suggestions. I would like to thank Dr. B. R. S Babu, Dr. Warrier and Dr. Ramesh for all their help.

I am grateful to the Director and Dean (Academic) of IIA for giving me permission to commence this research and allowing me to use all the facilities.

I also thank Dr. Rangarajan, the then Secretary of Board of Graduate Studies for all his help and support.

This thesis utilizes the data from Kodaikanal Observatory and SOHO/MDI. SOHO is a project of international cooperation between ESA and NASA. Observers of the Kodaikanal Observatory who obtained the white light and $H\alpha$ pictures from 1969-1974 are greatfully acknowledged.

I take this opportunity to thank Prof. Raveendran, Principal, Sree Krishna College, Guruvayur, who encouraged me to take up this research.

I would like to show my gratitude to Dr. Baba Varghese and Mr. Nathan of Computer Center, all staff at Library and Administration, and support provided by Mr. Murali and Mr. Mohan Kumar.

I am thankful to research students Mr. Vigeesh, Mr. Blesson and Ms. Sreeja for supporting me with thesis style and formatting. I am also thankful to Dr. Reji Thomas, Mr. Nagaraju and Dr. Maheshwar.

Finally, I would like to express my heartfelt gratitude to my parents, especially my father, Late. Sri. Radhakrishnan for motivating and supporting me in my studies. I am grateful to my husband Sree Kumar and daughter Athira for their unconditional support all the times without which it would have been impossible for me to complete this thesis. I thank all my family members for their sincere prayers.

Table of Contents

List of Tables **viii**

List of Figures **xvii**

Abstract **xviii**

1 Introduction **2**

1.1 Historical Introduction 2

1.2 Sunspot 5

1.3 Flares 8

1.4 Sun's magnetic field 9

1.4.1 Surface magnetic field 10

1.4.1.1 Small scale magnetic fields 11

1.4.1.2 Large scale magnetic fields 13

1.4.1.3 Solar magnetic activity 13

1.4.2 Internal magnetic field 15

1.4.3 Solar MHD 17

1.5 Sun's Rotation 20

1.5.1 Surface Rotation 21

1.5.2 Internal Rotation 22

2 Flares associated with abnormal rotation rates of the sunspots **23**

2.1 Introduction 23

2.2 Data and analysis 25

2.3 Results 26

2.4 Discussion and conclusions 30

3 Growth and decay of sunspots 36

3.1 Introduction 36

3.2 Formulation of the equations 42

3.3 Solution for growth of the sunspot 43

3.4 Solution for decay of the sunspot 46

3.5 Results and conclusion 48

4 Rotation rates of the sunspots during their initial appearance 68

4.1 Introduction 68

4.2 Data and analysis 72

4.3 Results and conclusion 73

5 Inference of longitudinal magnetic flux in the convective envelope 80

5.1 Introduction 80

5.2 Data and analysis 82

5.3 Results 101

5.4 Discussion and conclusions 104

6 Inference of toroidal magnetic field structure in the convective envelope 111

6.1 Introduction 111

6.2 Data and analysis 114

6.3 Results 125

6.4 Discussion and conclusions 130

6.5 Appendix 131

7 Conclusions and future prospects 137

7.1 Conclusions 137

7.2 Future prospects 140

Bibliography 143

LIST OF PUBLICATIONS

Papers published / accepted in refereed journals:

1. Flares associated with abnormal rotation rates: Longitudinal minimum separation of leading and following sunspots, Hiremath, K. M., Suryanarayana, G. S., Lovely, M. R., 2005, A&A, 437, 297.
2. The Extreme Solar Activity during October-November 2003, Hiremath, K. M., Lovely, M. R., Kariyappa, R., 2006, ApA, 27, 333.
3. Magnetic Flux in the Solar Convective Envelope Inferred from Initial Observations of Sunspots, Hiremath, K. M., Lovely, M. R., 2007, ApJ, 667, 585.
4. Toroidal magnetic field structure in the solar convective envelope inferred from the initial observations of the sunspots.(In Preparation)
5. Initial rotation rates of leader and follower of the bipolar spots during their initial appearance. (In Preparation)
6. Growth and decay of sunspots. (In Preparation)

Papers presented in meetings

1. Lovely, M. R., Hiremath, K. M., *Magnetic Flux in the Solar Convective Envelope Inferred From the Sunspots' Initial Appearances*, 2nd UN/NASA Workshop on International Heliophysical Year and Basic Space Science. 2006.
2. Hiremath, K. M., Lovely, M. R., Kariyappa, R., *Solar Abnormal Activity During Oct-Nov. 2003*, Bulletin of the Astronomical society of India. 2005.
3. Hiremath, K. M., Lovely, M. R., *Solar internal rotation and toroidal magnetic flux inferred from sunspots*, International Solar Workshop on Transient Phenomena on the Sun and Interplanetary Medium, Nainital, India, 05 - 07, April, 2005.

List of Tables

2.1 Kodaikanal observations related to the Greenwich Group numbers . . 27

2.2 Kodaikanal observations related to the Greenwich Group numbers . . 28

2.3 Kodaikanal observations related to the Greenwich Group numbers . . 35

3.1 χ^2 fit for the laws of linear, quadratic and exponential growth of the sunspot. 49

3.2 Values of constants obtained from growth and decay of the exponential fits. 50

3.3 χ^2 fit for the laws of linear, quadratic, log-normal and exponential decay of the sunspot. 51

5.1 Measurements of line of sight component of magnetic field of the bipolar spots from SOHO/MDI magnetograms. 86

5.2 Parameters of the linear least square fit 110

6.1 Improved measurements of line of sight component of magnetic field of the bipolar spots from SOHO/MDI magnetograms 116

6.2 Strength of inferred magnetic field at different anchoring depths in the convective envelope 136

List of Figures

1.1 Sunspot picture taken by SOT on board Hinode space satellite. . . . 6

1.2 A Butterfly diagram showing the latitudinal distribution of area of sunspots from 1870 to 2000 (cf., http://wwwssl.msfc.nasa.gov /ssl /pad /solar /images /bfly.gif). 14

1.3 A typical magnetogram taken by SOHO/MDI on Feb 9^{th}, 2000. . . . 15

2.1 The evolution of a typical sunspot group that contains leader and follower spots observed from the Kodaikanal Observatory. On the images of the 22 and 25, the horizontal line represents the solar equator. For all the observations, the spot group is south of the equator. The corresponding Greenwich group number for this sunspot group is 22251. 32

2.2 (a) Left : Rotation rates and change of longitudinal separation of the leader and the follower during their evolutionary phases. The blue and green dotted lines represent the rotation rates (deg/day) of the leading and the following spots. The red dashed line represents the change of longitudinal separation (in degrees) of the spots. The red vertical continuous lines are the occurrence dates of the flares. The red numbers near the vertical lines are repetition of the scale values presented on the y axis (rotation and longitudinal separation). (b) Right: The typical rate of change of the longitudinal separation (deg/day) of the leader and the follower spots during their evolutionary phases. For both the figures the corresponding Greenwich number of the group is 22251. 33

2.3 The normalized rotation rates and rate of change of longitudinal separation of the leader and the follower during their evolutionary phases. The blue and green dotted lines represent the normalized rotation rates of the leading and the following spots. The red dashed line represents the normalized rate of change of longitudinal separation of the leader and the follower spots. The red vertical continuous lines are the occurrence dates of the flares. The corresponding Greenwich number for this sunspot group is 22251. 33

2.4 (a) The left figure represents the scatter diagram that illustrates the association between the occurrence days of the minimum separation and the flare during the evolution of the spots. The red continuous line is obtained from the linear least square fit. Here S and F represent occurrence days of minimum separation and the flares respectively. (b) The right figure represents the occurrence days of minimum separation and the flares during the evolution of spots. The symbols $\diamond$ and the square both in blue color represent occurrence day of the minimum separation and the flares respectively. 34

2.5 (a) The left figure represents minimum separation for the different classes of the flares : the square in blue color represents n (normal), the $\triangle$ with red color represents b (bright). Here 0 along the x axis represents the S subclass flare. The numbers 1, 2, 3 are higher subclass flares. (b) The right figure represents the rate of change of longitudinal minimum separation for different classes of the flares : the square in blue color represents f (faint), the $\diamond$ with green color is n (normal) and the $\triangle$ with red color represents b (bright). Here 0 along the x axis represents the S subclass flare. The numbers 1, 2, 3 are higher subclass flares. 34

3.1 The dashed and the dotted curves are the variation of the initial rotation rates of the sunspot groups with respect to their life spans. The continuous curve is the radial variation of the internal rotation as inferred from the helioseismology. 37
3.2 Evolution of growth of area A of non-recurrent sunspot group at a latitude region of 0 -10° that has lifespan of 8 days. Red line is theoretical area growth curve over plotted on the observed area growth curve (blue cross points). 52
3.3 Evolution of growth of area A of non-recurrent sunspot group at a latitude region of 0 -10° that has lifespan of 8 days. Red line is theoretical area growth curve over plotted on the observed area growth curve (blue cross points). 53
3.4 Evolution of growth of area A of non-recurrent sunspot group at a latitude region of 10 -20° that has lifespan of 8 days. Red line is theoretical area growth curve over plotted on the observed area growth curve (blue cross point). 54
3.5 Evolution of growth of area A of non-recurrent sunspot group at a latitude region of 10 -20° that has lifespan of 10 days. Red line is theoretical area growth curve over plotted on the observed area growth curve (blue cross points). 55
3.6 Evolution of growth of area A of non-recurrent sunspot group at a latitude region of 20 -30° that has lifespan of 10 days. Red line is theoretical area growth curve over plotted on the observed area growth curve (blue cross points). 56
3.7 Evolution of growth of area A of non-recurrent sunspot group at a latitude region of 20 -30° that has lifespan of 10 days. Red line is theoretical area growth curve over plotted on the observed area growth curve (blue cross points). 57

3.8 Evolution of growth of area A of non-recurrent sunspot group at a latitude region of 30 -40° that has lifespan of 8 days. Red line is theoretical area growth curve over plotted on the observed area growth curve (blue cross points). 58
3.9 Evolution of growth of area A of non-recurrent sunspot group at a latitude region of 30 -40° that has lifespan of 9 days. Red line is theoretical area growth curve over plotted on the observed area growth curve (blue cross point). 59
3.10 Evolution of decay of area A of non-recurrent sunspot group at a latitude region of 0 -10° that has lifespan of 9 days. In Fig (c), X=ln(Time) and Y=-ln(A). Red line is theoretical area decay curve over plotted on the observed area decay curve (blue cross points). . . 60
3.11 Evolution of decay of area A of non-recurrent sunspot group at a latitude region of 0 -10° that has lifespan of 9 days. In Fig (c), X=ln(Time) and Y=-ln(A). Red line is theoretical area decay curve over plotted on the observed area decay curve (blue cross points). . . 61
3.12 Evolution of decay of area A of non-recurrent sunspot group at a latitude region of 10 -20° that has lifespan of 10 days. In Fig (c), X=ln(Time) and Y=-ln(A). Red line is theoretical area decay curve over plotted on the observed area decay curve (blue cross points). . . 62
3.13 Evolution of decay of area A of non-recurrent sunspot group at a latitude region of 10 -20° that has lifespan of 9 days. In Fig (c), X=ln(Time) and Y=-ln(A). Red line is theoretical area decay curve over plotted on the observed area decay curve (blue cross points). . . 63
3.14 Evolution of decay of area A of non-recurrent sunspot group at a latitude region of 20 -30° that has lifespan of 10 days. In Fig (c), X=ln(Time) and Y=-ln(A). Red line is theoretical area decay curve over plotted on the observed area decay curve (blue cross points). . . 64

3.15 Evolution of decay of area A of non-recurrent sunspot group at a latitude region of 20 -30° that has lifespan of 10 days. In Fig (c), X=ln(Time) and Y=-ln(A). Red line is theoretical area decay curve over plotted on the observed area decay curve (blue cross points). . . 65
3.16 Evolution of decay of area A of non-recurrent sunspot group at a latitude region of 30 -40° that has lifespan of 8 days. In Fig (c), X=ln(Time) and Y=-ln(A). Red line is theoretical area decay curve over plotted on the observed area decay curve (blue cross points). . . 66
3.17 Evolution of decay of area A of non-recurrent sunspot group at a latitude region of 30 -40° that has lifespan of 8 days. In Fig (c), X=ln(Time) and Y=-ln(A). Red line is theoretical area decay curve over plotted on the observed area decay curve (blue cross points). . . 67

4.1 Left figure represents rotational isocontours inferred from the helioseismology (Antia & Chitre 1997) and right figure represents rotational isocontours obtained by the solution of MHD equations (Hiremath & Gokhale 1996). Isocontours of both the figures are in nHz. . 70
4.2 The selected number N of sunspots for different life spans are considered for the analysis. 73
4.3 Irrespective of their sizes and for different life spans, variation of rotation rates of bipolar spots during their initial appearance on the surface are compared with radial variation of rotation profile, at heliographic latitude of 5 degree, inferred from the helioseismology (continuous light green curve) from (Antia & Chitre 1997). 74
4.4 Irrespective of their sizes and for different life spans, variation of rotation rates of bipolar spots during their initial appearance on the surface are compared with radial variation of rotation profile,at heliographic latitude of 10 degree, inferred from the helioseismology (continuous light green curve) from (Antia & Chitre 1997). 75

4.5 Irrespective of their sizes and for different life spans, variation of rotation rates of bipolar spots during their initial appearance on the surface are compared with radial variation of average rotation profile (for the heliographic latitudes of 5, 10 and 15 degrees) inferred from the helioseismology (continuous light yellow curve) from (Antia & Chitre 1997). 76

4.6 For different life spans, in the left illustration blue continuous line represents difference in rotation rates of leader and the follower of the bipolar spots and a over plotted red crossed curve represents radial variation of difference of the angular velocity between two latitudes 5 and 15 deg inferred from the helioseismology. Where as right figure illustrates the variation of latitudinal rotational rates gradient for different life spans from the sunspots (blue continuous curve) and radial variation of latitudinal angular velocity gradient $\frac{d\Omega}{d\theta}$ inferred from helioseismology (red continuous curve). 77

4.7 In the left figure red crossed curve represents angular velocity for latitude 15 deg over plotted blue curve represents the angular velocity for latitudes 5 deg inferred from the helioseismology. Where as right figure illustrates the difference in latitude between leader and follower (red crossed curve). 78

5.1 A typical bipolar spot taken from SOHO/MDI observations. 84

5.2 A typical magnetogram taken by SOHO/MDI on Feb 9^{th}, 2000. . . . 85

5.3 The selected number N of sunspots for different life spans are considered for the analysis i.e., represented on the left side figure(Fig 5.3(a)) and right side figure (Fig 5.3(b)) represents the average time difference dt between the initial two observations, for different life spans. 107

5.4 For different life spans, measured initial magnetic field strength of the bipolar spots. **(a)** The left figure represents variation of the magnetic field strength of the bipolar spots during their first observation on the solar disk. **(b)** The right figure represents variation of the magnetic field strength of the bipolar spots during their second observation on the solar disk. In both the illustrations, the red continuous line represents the linear least-square fit with a law $B_i = C_1 + C_2\tau$ (where $B_i, i = 1, 2$, are the measured initial magnetic field strengths,τ is life span in days and, C_1 and C_2 are the coefficients determined from the fit) is fitted to both the data set. 107

5.5 For different life spans, measured initial magnetic flux of the bipolar spots. **(a)**The left figure represents variation of the magnetic flux of the bipolar spots during their first observation on the solar disk. **(b)** The right figure represents variation of the magnetic flux of the bipolar spots during their second observation on the solar disk. In both the left and right illustrations, the normalized (with their maximum values Flux1_Max and Flux2_Max) flux values during their first and second observations respectively are presented. The red continuous line represents the linear least-square fit to the normalized flux values with a law $F_i = C_1 + C_2\tau$ (where $F_i, i = 1, 2$, are the measured initial magnetic fluxes, τ is life span in days and, C_1 and C_2 are the coefficients determined from the fit) is fitted to both the data set. . . 108

5.6 Irrespective of their life spans, measured initial area versus initial magnetic flux of the bipolar spots. Both the left **(a)** and right **(b)** illustrations represent the normalized (with their maximum area values Area1_Max and Area2_Max and, the flux values Flux1_Max and Flux2_Max) area and flux values during their first and second observations respectively. The red continuous line represents the linear least-square fit with a law $F_i = C_1 + C_2A$ (where $F_i, i = 1, 2$, and A are the normalized flux and area and, C_1 and C_2 are the coefficients determined from the fit). 109

5.7 For different life spans, the normalized (with the maximum value of dF_Max) rate of emergence of magnetic flux of the bipolar spots respectively. The red continuous line represents the linear least-square fit with a law $dF = C_1 + C_2\tau$ (where dF (in the units of Mx/day) is the rate of emergence of initial flux, τ (in days) is the life span and, C_1 and C_2 are the coefficients determined from the fit) is fitted to both the data set. 109

6.1 Irrespective of their sizes and for different life spans of the bipolar spots with their initial appearance on the surface, figure on the left side (Fig 6.1(a)) represents variation of number of spots and figure on the right side (Fig 6.1(b)) represents central meridian distances (in degrees) of the bipolar spots considered for the analysis. In the right figure, blue continuous line represents a linear least-square fit with a law $CMD = C_1 + C_2\tau$ (where CMD is central meridian distance, τ is life span in days and, C_1 and C_2 are the coefficients determined from the least-square fit). 133

6.2 Irrespective of their sizes and for different life spans of the bipolar spots with their initial appearance on the surface, figure on the left side (Fig 6.2(a)) represents variation of measured average strength of line of sight component *Bs1* of the magnetic field structure and figure on the right side (Fig 6.2(b)) illustrates the estimated toroidal *Bts1* (blue triangles with blue continuous line) and poloidal *Bms1* (red diamonds with blue dashed line) components of the magnetic field structure. In both the figures, the blue continuous and dashed line represent the linear least-square fit with a law $B = C_1 + C_2\tau$ (where B is longitudinal or toroidal or poloidal field structures, τ is life span in days and, C_1 and C_2 are the coefficients determined from the least-square fit). 134

6.3 Irrespective of their sizes and for different life spans, inferred strengths of line of sight ($Ba1$, left figure -Fig 6.3(a)) and toroidal ($Bta1$, right figure - Fig 6.3(b)) components of magnetic field structure at different anchoring depths in the convective envelope. The blue continuous line in both the figures represents the polynomial fit with the laws indicated on the figures. The dashed red line over plotted on the Fig 6.3(b) is the radial variation of steady part of toroidal component of the magnetic field structure computed from the equation (21) of Hiremath (2001). 134

6.4 Irrespective of their sizes and for different life spans, rate of emergence of toroidal magnetic field structure $\frac{dB_\phi}{dt}$ at different anchoring depths in the convective envelope. Blue continuous line represents the exponential fit with a law indicated on the figure. 135

ABSTRACT

The sun which is an important part of solar system plays a significant role in influencing the life on Earth, disrupting electrical power grids, satellite and telecommunication facilities, air-traffic etc. This is due to various solar cycle and activity phenomena like sunspots, flares and CMEs taking place in the sun that also have effect on the earth's environment and climate. So it is important to study sunspots and associated phenomena. Before the advent of space era, from surface observations, it was difficult to infer the solar internal structure and dynamics. With the help of SOHO/MDI (Michelson Doppler Imager), it is now possible to infer internal structure by computing the velocity of sound waves passing through the sun, that provide clues to unravel the secrets of sun's eleven year cycle and associated phenomena. On the other hand MDI instruments aboard SOHO measure the line of sight component of magnetic field structure of the sun. SOT instrument on Hinode yields very high resolution longitudinal and vector magnetic field components at the photospheric levels. With the valuable data from ground based observatories and from the space observatories, from dynamics and magnetic field structure of the sunspot on the surface, now we are at a better position to understand internal structure of the convective envelope where sunspots are supposed to be originated. Hence, it is important to study sunspots' dynamics and magnetic field structure on the surface as they are supposed to be tracers of internal dynamics and magnetic field structure of solar convective envelope. This research study consists of studying of dynamics and magnetic field structure of the solar convective envelope by using dynamics and magnetic field structure on the solar surface. The thesis has been organized as follows.

The first chapter consists of introduction to solar activities like sunspot, flares and magnetic field structures associated with the sunspots.

The second chapter deals with abnormal rotation rates associated with bipolar sunspots that have leader and follower. Using six years (1969-1974) of data of sunspot groups from the white light pictures of the Kodaikanal Observatory, rotation

rates of the leading and the following sunspots and the rate of change of longitudinal separation during their life times are computed. It is found that (i) the spots that are associated with abnormal rotation rates (i.e, rotation rates that are greater than 1σ from the mean rotation) and that approach at a separation rate of $1-2\,deg/day$ also experience minimum longitudinal separation ($\sim 6^o - 10^o$) of their foot points during the course of their evolution, (ii) spots that have a minimum separation eventually trigger flares and (iii) events with abnormal rotation rates and minimum approaching distances of the foot points occur on average during between $50-80\%$ of the life spans, indicating the annihilation of magnetic energy, probably below the surface around the region of $0.935R_{\odot}$. These results support the conventional physical scenario of magnetic reconnection that may be responsible for triggering of flares. It is a first evidence of magnetic reconnection below the surface from the analysis of Kodaikanal Observatory data.

The third chapter deals with the growth and decay of sunspots. Firstly, ideas on genesis of sunspots in the convective envelope are presented. It is proposed that growth and decay of the sunspot on the surface is a net effect due to fluctuations in poloidal and toroidal magnetic and velocity (especially rotational gradient) perturbations (in the solar convective envelope) to the flux tube while it is raising along isorotational contours towards the surface. With reasonable assumptions and approximations, from MHD equations, separate analytical solutions for growth and decay parts of area curve of the sunspot are obtained. Solutions suggest that sunspots grow exponentially and rate of growth of the sunspots depends upon heliographic latitude, that is spots that are formed at high latitudes grow faster (with exponential growth) compared to the spots that are formed at low latitudes. As for another solution, spots decay at the exponential rate and depend upon the latitudes. That means spots that are formed at the high latitudes decay slowly compared to the spots that are formed near the low latitudes. In order to compare theoretical growth and decay of area curve with the observed curve of growth and decay of the sunspots, data of time evolution of corrected areas of non-recurrent sunspots from Greenwich Photoheliographic Results (GPR) are considered. For the four latitude

zones of $0-10$, $10-20$, $20-30$ and $30-40$ degrees and the spot groups that lie between $\pm$ 70 degree from the central meridian with life spans in the range of 8-10 days are considered. It is found that solution of growth and decay of area curve reasonably reproduce well the observed evolution of sunspots' growth and decay area curves.

The fourth chapter deals with the rotation rates of the leader and follower of bipolar spots during their initial appearance on the surface. For different life spans, rotation rates of the leader and the follower spots during their initial appearance on the surface are computed. Data of bipolar spots from SOHO/MDI magnetograms are considered and rotation rates of leader and follower are computed. Important conclusions drawn from this study are: (i) irrespective of their sizes and for different life spans, leaders of the bipolar spots during their initial appearance on the surface rotate faster by $\sim 5\ nHz$ than the followers, (ii) irrespective of their sizes, variation of rotation rates of the leader and follower of bipolar spots with respect to their different life spans have almost similar radial variation of the rotation profile in the convective envelope as inferred from the helioseismology, (iii) for different life spans, latitudinal difference of rotational gradient of the leader and follower is almost similar to radial variation of latitudinal rotational gradient inferred from the helioseismology and, (iv) this study suggests an independent method for inference of internal rotational profile of the sun and the stars without any information regarding internal structure that is needed in case of helioseismic inversions.

The fifth chapter deals with measurement of strength of line of sight component of magnetic field structure of the sunspots by SOHO/MDI magnetograms and inference of strength of line of sight component of magnetic field structure in the convective envelope. From the SOHO/MDI magnetograms, the strength of magnetic flux and rate of emergence of magnetic flux at different anchoring depths in the solar convective envelope by measuring *initial* magnetic fluxes of the well developed sunspots on the surface are inferred. Important findings of the study are : (i) majority of the spot groups that have *first* appearance on the surface are bipolar, (ii)

irrespective of their sizes, bipolar spots with different life spans have average magnetic field strengths of $\sim$ 500 G during their first appearance on the surface, (iii) average field strength at the site of anchoring depths of the sunspots is estimated to be $\sim 10^6$ G near base of the convective envelope and $\sim 10^4$ G near the surface, (iv) the dynamo-a source of sunspot activity- is distributed through out the convective envelope and, (v) rate of emergence of *initial* magnetic flux of such a distributed dynamo near base of the convection zone estimated to be $\sim$ 6 X 10^{19} Mx/day and is 40% higher than the the rate of emergence of *initial* magnetic flux near the surface.

The sixth chapter consists of inferring toroidal component of magnetic field structure in the convective envelope from line of sight component of magnetic field structure of the sunspots during their initial appearance on the surface. In the previous chapter, line of sight component of magnetic field structure of bipolar spots is measured that has a noise of $\sim$ 20 G. In order to estimate magnetic field structure in the convective envelope with better accuracy, measured strength of magnetic field structure of bipolar spots on the surface should have less noise in the measured parameters. Keeping in mind this objective, we used 5 minute averaged SOHO/MDI magnetogram that has noise of $\sim$ 8 G. Another important aspect of this study is that, in the previous chapter, from Parker's flux tube model, line of sight component of the magnetic field structure is only estimated in the convective envelope. As the sunspots are supposed to be toroidal magnetic field structures, it is better to modify Parker's flux tube model. Hence, Parker's equations (relevant to flux tube structure) that are in cartesian coordinates are rederived in spherical coordinates for the estimation of toroidal, poloidal and radial components. For different life spans, first we measure line of sight component of the magnetic field structure of the bipolar sunspots from the SOHO/MDI magnetograms during their initial appearance on the surface and then toroidal component of the magnetic field structure is separated. Irrespective of their sizes, strength of the measured line of sight component of the magnetic field structure varies from $\sim$ 450 G for the life span of two days to $\sim$ 300 G for the life span of twelve days. Where as strength of the estimated surface toroidal component of the bipolar spots varies from $\sim$ 10 G for the life span of two

days to $\sim$ 700 G for the life span of twelve days. Using rederived Parker's (1955b) flux tube model in spherical coordinates and Hiremath's (2002) life span anchoring depth information to infer the strength of line of sight and toroidal components of the magnetic field structures at different anchoring depths of the bipolar spots in the convective envelope and, the important findings are: (i) both the line of sight and toroidal components of the magnetic field structures at the sites of sunspots' different anchoring depths in the convective envelope have a similar radial variation and the strength ($\sim 10^4$ G near base of the convective envelope to $\sim$ 100 G near the surface) and, (ii) rate of emergence of toroidal magnetic field structure near base of the convective envelope is estimated to be $\sim 10^3$ times the rate of emergence of toroidal magnetic field structure near the surface.

The last chapter deals with conclusions and future prospects of this study.

Chapter 1

Introduction

1.1 Historical Introduction

The sun is closest star to earth that can be studied in detail with high spatial and temporal resolutions. It is a typical G2 type main sequence star which falls in the temperature range $5800°K$ and generates energy from the nuclear fusion mainly of hydrogen atoms. The sun influences life on Earth, disrupts electrical power grids, satellite and telecommunication facilities, air-traffic, etc., due to solar cycle and activity phenomena like sunspots, flares and coronal mass ejections that consist of charged particles and magnetized plasma. However, solar cycle and activity phenomena were known long ago, even prehistoric people were familiar with them. Therefore by observing and studying these solar phenomena with modern technologies it is possible to understand the solar terrestrial relationship.

Sunspots are one of the interesting aspects of solar cycle and activity phenomena. Sunspots were observed during the initial period of 17th century, particularly in China by Chinese astronomers. However early observations were misinterpreted until Galileo gave a correct explanation. He also estimated the rotation period of sun to be nearly equal to a lunar month. Sunspots were also observed telescopically in 1610 by Thomas Harriot, Johannes Fabricus, and Christoph Scheiner. The early observers like S.A.Wilson, Willian Herschel, etc., in the late 18th and 19th centuries believed that spots are 'holes' through which the 'cooler' interior of the sun could be seen. Although sunspots were discovered in the sixteenth century, they were systematically studied only after the establishment of observatories all over the world.

A German amateur astronomer, Heinrich Schwabe, from his long years of investigation from 1851, concluded that the number of visible spots on the sun's disk varied with time. Schwabe discovered the solar cycle period to be $\sim$ 11 years. Later observations however established that the period is in fact 11.2 years. The cycle of activity of Sun is repeated nearly over this period, which is known as solar cycle. Within a solar cycle, the number of sunspots and the intensity of other transient phenomena change appreciably. This lead Rodolf Wolf to make systematic observations starting in 1848. He studied historical records from 1700 AD onwards and established the cyclic behavior of sunspot activity.

Solar activity is best measured by a quantitative index, the sunspot number, related to number of sunspot groups and individual sunspots present on the sun on a given day. Rudolf Wolf introduced in 1848, a simple and globally used Wolf number of sunspots or Relative sunspot number defined as R = k(10g + f), where 'g' is the number of spot groups, 'f' the number of all individual spots in these groups and 'k' is the reduction factor.

Solar rotation is variable with latitude, time and depth. The sun which is in the fourth state of matter i.e., plasma and behaves differently from normal gas. Sun rotates differentially, i.e., different latitude zones rotate at different rates. Each rotation of the sun is given a unique number called Carrington Rotation number starting from Nov 9, 1853. Richard Carrington's observations of sunspots indicated that in the beginning of the solar cycle, sunspots appear around 40 degree north and south of heliographic latitude and drift towards the equator as the cycle progresses.

At the beginning of a solar cycle, sunspots tend to form at high latitudes, but as the cycle reaches a maximum the spots form at lower latitude. At the minimum of cycle, sunspots appear closer to the equator and as the new cycle starts sunspots again appear at high latitudes. This recurrent behavior of sunspots give rise to a butterfly diagram and was first discovered by English astronomer, Edward Walter Maunder in 1904. The period from 1645-1715 of greatly reduced level of solar activity is known as Maunder Minimum. This period of very low solar activity is closely associated with one of the coldest periods known as 'Little Ice Age' (1350-1850 AD) on the Earth. In this period most of the European countries experienced unusually

long and harsh cold winter leading to shortened growing seasons, failed crops and widespread famine. Eddy (1976) succeeded in convincing many researchers that there a was real evidence for the absence of sunspot during the Maunder Minimum period. This has led scientists to study the possible influences of solar activity on terrestrial climate. In fact recent studies (Hiremath & Mandi 2004; Hiremath 2009b) confirm Eddy's findings and one cannot neglect the solar influence on the Earth's climate and environment.

Motion of material within a sunspot can be derived from analysis of spectroscopy of spot. Within a spot group, velocity of the flow appears to be very complex. From an analysis of H-alpha spectroheliograms of spot, Hale observed the inflow of gas into the spot. The most correct picture of gas flow in the spot was proposed soon after by J. Evershed, who found that at the photospheric level, the gas flows outward from umbra into penumbra. Measurements of intensity and Doppler shifts in the spot spectra reveal that Evershed motion vary with distance from the center of the spot. At the upper levels of solar atmosphere a reverse flow is observed. This is known as Evershed effect.

Using Zeeman splitting of spectral lines, Hale measured magnetic field structure of sunspots and showed that it is in the range of 100 G for small spots to about 3000 G or more for larger ones. Remnant magnetic field persisted in the spot region even when the spot disappeared. The sunspot groups are classified into three classes according to the nature of magnetic polarity in the following way.

1. The unipolar groups consist of individual spots or groups of spots with similar magnetic polarity.

2. The bipolar groups that have two main spots with opposite polarity. One of these is called a leader spot while the other is called a follower spot.

3. The complex groups of spots contain spots with opposite polarity mixed together. Statistics shows that about 90% spot groups are bipolar, about 10% are unipolar, while complex spot groups are rare.

The unipolar spots are generally identified as the last visible preceding spots in

bipolar groups when the following spots have already completely decayed on the photosphere.

The most remarkable feature observed in a bipolar spot group is the reversal of magnetic polarities in either hemisphere with the beginning of a new cycle. Thus when magnetic polarities are taken into account, a complete cycle has a period of about 22 years. This is known as 22 year magnetic cycle.

1.2 Sunspot

Magnetic flux emerges as bipolar regions with a wide range of sizes through the sun's photosphere. Sunspots are identified as active regions, a localized region on solar surface, which develops from larger magnetic dipoles. Sunspots are sites of intense magnetic field structures which are visible on solar surface but appear dark because they are cooler than the photosphere owing to the partial suppression of convective energy transport by magnetic field. A typical sunspot picture taken by solar optical telescope (SOT) on board Hinode, a Japanese space satellite is shown in Fig 1.1.

The Sun is typically very active when sunspot counts are high. Sunspots can generate solar events like solar flares and coronal mass ejections. Well developed sunspots consist of two distinct regions, viz., umbra and penumbra. Outer section of the sunspot is called the penumbra, and a darker central region is named the umbra. Some sunspots contain light bridges which are bright bands crossing the umbra. The umbra contains small bright structures called umbral dots. On the closer look, penumbra is found to be containing several filaments. The fibrils of the filament extend up to the umbra. Matter flows outwards along these filaments. This outflow is known as Evershed effect. Near the solar limb the penumbral distribution is asymmetric and this effect is known as Wilson effect. Sunspots exhibit considerable range of sizes, and the size is well approximated by a log-normal size distribution (Bogdan et al. 1988; Baumann & Solanki 2005). Large sunspots can reach diameters of 60,000 km, but are relatively rare. Sunspots smaller than 3000 km in diameter are also rare. Small sunspots live for hours, the largest ones for months.

Sunspots' lifetime τ, increases linearly with their maximum area, then decay

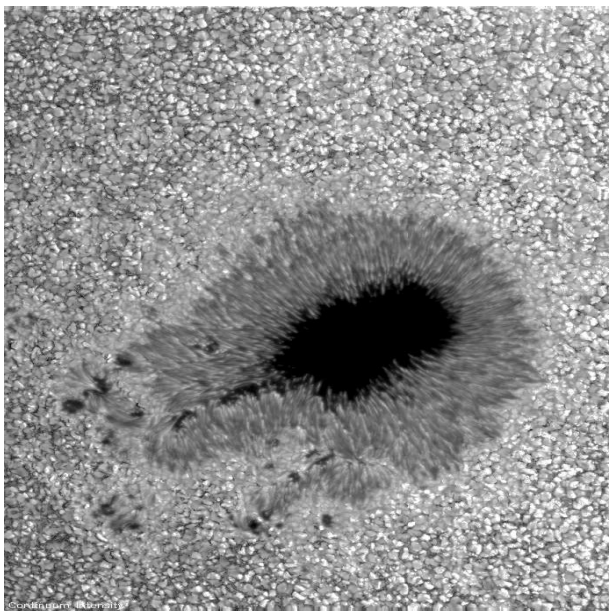

Figure 1.1: Sunspot picture taken by SOT on board Hinode space satellite.

slowly until they vanish from the surface. The decay is thought to be driven by turbulent diffusion of the magnetic field (Meyer et al. 1974; Petrovay & van Driel-Gesztelyi 1997) structure.

Sunspots usually show up as small forms that are irregularly shaped, and grow within days or weeks to their full size. While they can last weeks or months, they do eventually disappear, often by breaking into smaller and smaller sunspots. The number of sunspots observed on the surface of the sun varies from year to year.

The sunspot cycle maximum is the term for the maximum solar activity and solar minimum is the lowest point of solar activity that takes place approximately every eleven years. Along with the number of sunspots, the location of sunspots varies throughout the sunspot cycle. At solar minimum, sunspots tend to form around latitudes of 30 degree to 45 degree north and south of the sun's equator. As the solar cycle progresses from solar maximum to minimum, sunspots tend to appear closer to the equator, around a latitude region of 15 degree. Towards the end of a cycle, with solar minimum once again approaching, sunspots form quite close to solar equator, around 7 degree north and south latitude zones. There is often an overlap in this latitudinal migration trend around solar minimum, when sunspots

of the outgoing cycle are forming at low latitudes and sunspots of the upcoming cycle begin to form at high latitudes once again. This gradual equatorward drift of sunspots throughout the sunspot cycle, which was first noticed in the early 1860's by the German astronomer Gustav Sporer and the Englishman Richard Christopher Carrington, is often called Sporer's Law.

Using Zeeman effect Hale discovered sunspots' magnetic field structure and Zeeman effect is the amount of splitting of spectral lines in the presence of strong a magnetic field structure that depends upon strength of magnetic field and Lande g factor. Observations show that magnetic field structure is strongest at the center of the sunspot, i.e. at the umbra and decreases gradually outwards. Magnetogram is a pictorial representation of the variation in strength of magnetic field. It shows mainly "line-of-sight" component of magnetic field structure. MDI is an instrument that is used to take magnetograms of the sun in order to measure velocity and magnetic field structure in sun's photosphere, to learn about the convection zone and about the magnetic field structure that controls the structure of solar corona. Typical SOHO/MDI magnetograms (Fig 1.3) show that the darkest areas in a magnetogram are regions of south magnetic polarity and white areas are regions of north polarity. Grey areas indicate that there is no magnetic polarity. From the magnetograms it is observed that sunspots usually occur in bipolar pairs, with negative and positive polarities. In case of bipolar spots, the magnetic field lines emerge from one polarity towards the outer solar atmosphere and enter into other opposite polarity.

Sunspots can be used for determination of sun's rotation as tracers. Hence, from the movement of sunspots on the surface, it was discovered that the sun rotates on its axis and differentially. That is sun rotates differently at various latitude zones. The speed being greatest in the equatorial region where the period is almost 25 days and least at poles where the period of rotation is almost 35 days. Rotation for all latitudes can be expressed as

$$\omega = A + Bsin^2\theta + Csin^4\theta, \tag{1.1}$$

where ω is the rotation, A, B, C are coefficients and θ is the latitude.

Present consensus is that the sunspots originate below the solar surface. In the convective envelope, owing to differential rotation and cyclonic turbulence, so called "dynamo mechanism" is supposed to wind the poloidal magnetic field structure into toroidal magnetic field structure leading to formation of the sunspots. It is believed that solar cycle and activity phenomena are produced and maintained by such a dynamo mechanism although such mechanisms have fundamental difficulties and inconsistent with physics of convective envelope (Hiremath 2009a). Once sunspots are formed, they have lower density structure and due to buoyancy raise towards the surface. Yet there are no satisfactory theories for explanation of the formation and evolution of the sunspots and, the solar cycle and activity phenomena.

1.3 Flares

One of the most frequently observed events are solar flares which are sudden, localized transient events with increase in brightness that occur in active regions near sunspot. Solar flares are the most energetic explosions in the solar system that have a direct effect on the earth's atmosphere. Energetic particles that escape into interplanetary space are dangerous to astronauts and cause damage to electronic components of satellites. The intense radiations from a solar flare travels to earth in eight minutes which directly affect the ionosphere and radio communications at the Earth.

Typical energy probably due to annihilation of oppositely directed magnetic field structures, released in a large flare is of the order of 10^{27}-10^{32} erg/second. When magnetic energy is released energetic particles including electrons, protons and heavy nuclei, are heated and accelerated in the solar atmosphere. Here flares can be defined as powerful, sudden, rapid eruptions that have intense variations in the brightness of solar radiations and occur in the atmosphere of sun in magnetically active regions.

Two scientists R. C. Carrington and R. Hodgson independently observed a large flare in white light picture of the sun. The first solar flare was recorded in an astronomical literature was on September 1, 1859. During the occurrence of flares, the sun emits radiations across the entire electromagnetic spectrum. Typically there

are three stages of solar flare occurrence. They are precursor stage, impulsive stage and decay stage. In precursor stage, the release of magnetic energy is triggered. Emission of soft x-ray is detected in this stage. In the second or impulsive stage, protons and electrons are accelerated to energies exceeding 1 MeV and radiations such as radio waves, hard x-rays, and gamma rays are emitted. In the last stage, i.e., decay stage, a gradual build up and decay of soft x-rays can be detected. Solar flares extend to the outermost atmosphere of the sun called "corona". The corona is visible during solar total eclipses and in soft x-rays. Corona is concentrated around solar equator in loop-shaped structures and these connect areas of strong magnetic fields called active regions. Sunspots are located within these active regions.

Flare classes are classified based on their output of x-ray brightness in the wavelength range of 1 to 8 $\mathring{A}$. There are four categories of solar flares that in turn are classified into 9 subclasses. X-class flares are the largest energetic transient having intensity greater than $10^{-4}\ W/m^2$. M-class flares are medium sized energetic events with intensity lying between 10^{-5} and $10^{-4}\ W/m^2$. C-class flares are small sized with intensity lying between 10^{-6} and $10^{-5}\ W/m^2$. Finally, B-class flares have intensity less than $10^{-6}\ W/m^2$. The structure of magnetic field around sunspot gives an idea of understanding and predicting flares. If this structure becomes twisted and sheared then magnetic field lines can cross and reconnect with the explosive release of energy.

We study flares because these high energetic phenomena provide an opportunity to study physical processes in nature that are similar to those that occur in laboratory devices designed for the purpose of achieving controlled thermonuclear fusion.

1.4 Sun's magnetic field

During the solar total eclipse, one can notice from the white light picture that sun is pervaded by a large scale dipole like magnetic field structure. Strength of large scale magnetic field structure is ~ 1 G, whereas sun also consists of localized strong ($\sim 10^3$ G) magnetic field structure such as sunspots.

The sun with a strong and complex magnetic field structure which may impact (Hiremath & Mandi 2004; Hiremath 2009b) weather and climate on Earth. The sun's magnetic field give rise to many effects such as sunspot, flares which are collectively called solar activity. Much of solar activity seems to be directly connected with the properties of magnetic field. In a precise and direct manner the magnetic field of sun can be probed, because in the presence of magnetic field the energy levels of atoms, ions and molecules are split into more than one level. This causes the spectral lines to split into more than one line and amount of splitting is proportional to the strength of ambient magnetic field. This physical process is called Zeeman effect.

One can measure the strength of magnetic field structure by measuring the amount of Zeeman splitting. The number of sunspots and levels of solar activity vary with an 11 year period known as solar cycle.

The magnetic field of sun extends far out of space and it is called "interplanetary magnetic Field" (IMF). The solar wind, the stream of charged particles that flows outward from sun, carries the IMF to planets and interact with planetary magnetic fields in complex ways and thus generating phenomena such as aurora. Active regions are places on solar surface where the magnetic field is strong and these regions produce sunspots. Plasma interacts strongly with sun's magnetic field. Due to this gaseous nature and convection in the outer part of 30% of radius, sun does not rotate uniformly but rotates differentially such that different latitude of sun rotates at different rates. At its equator, sun's period of rotation is 25 days whereas at poles it is 36 days.

1.4.1 Surface magnetic field

Solar magnetism is mainly observed via the Zeeman splitting of the photospheric Fraunhofer lines. The source of surface magnetism in sun probably lies in the convection zone, the layer of solar interior just below the photosphere. Sunspots which are the regions of intense magnetic field structures on the solar surface are visible component of magnetic flux tubes that are formed in the sun's convective zone. Due to differential rotation and cyclonic turbulence, the dynamo mechanism is supposed

to wind the poloidal magnetic field structure into toroidal magnetic field structure leading to the formation of sunspot structures.

It is believed that the solar cycle and activity phenomena are produced and maintained by such dynamo mechanism, although recently many doubts (Hiremath 2009a) are raised regarding such a process. Coronal loops formed from magnetic field lines from the sunspot stretch out into corona. The toroidal magnetic fields linked to sunspots and coronal loops are linked to flare activity and are also associated with CMEs. Surface magnetic activity appears to be related to age and rotation rate of sunspot.

Features occurring above the solar surface i.e., photosphere, is divided into chromospheric features and coronal features. Chromospheric features include chromospheric network, plage, prominences or filaments and spicules. While coronal features consist of coronal holes, coronal loops, coronal mass ejections, helmet structures, polar plumes and solar flare. Granulation and super granulation patterns observed on the surface of the sun are the result of underlying convective processes.

1.4.1.1 Small scale magnetic fields

Howard (1967) classified the surface magnetic fields into small scale and large scale magnetic field structure. The small scale magnetic field structures are associated with small-scale structures of solar atmosphere, the development of active regions and the decay of active regions. The large scale field consists of background-field, large scale distribution of solar activity and polar fields.

Hale (1922a,b) discovered small regions on the sun where the magnetic field measured was several hundred guass. He named these "Invisible Sunspots". Many of these features later developed into sunspots, or the remains of sunspots and some were not connected with sunspots even though they were within active regions.

Solar magnetic field structures are not smoothly distributed over the surface, but appear as small scale and concentrated in bundle. Most of these clumps are bipolar and typical sizes of these clumps are $\sim$ 100 Kms, with field strengths $\sim 1-2$ KG. Stenflo (1989) has observed that, nearly 90% of the total magnetic flux penetrating the photosphere outside the sunspots occurs in such clumps. Since,

the sizes of these clumps are near the angular resolution limit, the mechanism of formation and evolution is poorly understood. It is believed that magnetic flux which appears to emerge from the solar interior as large coherent structures (example sunspots) decay by fragmentation at a rate of 10^{15} $Mxsec^{-1}$ (Gokhale & Zwaan 1972). The fragmentation implies transferring of flux from smaller to larger spatial wave numbers (Harvey & Harvey 1973; Stenflo 1976) leading to sizes of $\sim$ 100 Km flux tubes.

The magnetic field structure in the photospheric layers is concentrated in active regions and in a network distributed over the whole sun (Solanki et al. 2006). In active regions (outside sunspots) the magnetic field is concentrated in faculae or plage areas. In the quiet sun (i.e., outside active regions) the magnetic flux elements form a network along the borders of super granular cells with a length scale of $\sim 20-40$ Mm. Another type of magnetic feature in the quiet sun located in the interiors of super granular cells are the internetwork elements that have horizontal magnetic field structures. Recent spectropolarimetric observations (Lites et al. 1996; Harvey et al. 2007; Lites et al. 2009) from Hinode show that: (i) horizontal fields are ubiquitous on the surface of the sun; (ii) they have structural dimension that are smaller than granules and larger than vertical fields; (iii) horizontal fields are spatially separated from the vertical fields; (iv) these horizontal magnetic field structures have strengths ($\sim$ 55 G) five times larger than vertical fields and (v) strong horizontal fields in plages appear as small islands with strength $\sim$ 600 G.

Another magnetic feature present on the solar surface is sunspot. Sunspot covers only a fraction of a percent of solar surface even at the times of greatest solar activity. Other magnetic activities are pores that have diameters a couple of thousand of kilometers and are dark. Smaller and more common structures that appear on the solar surface are magnetic elements and bright structures that have diameters smaller than a few kilometers. High resolution observation shows magnetic features having spatial resolution of $\sim$ 150 km (Keller 1992). Indirect observations suggest the existence of internetwork field structure of diameter 50 km (Lin 1995). Observations also indicate the presence of omnipresent turbulent field structure in photospheric layers (Solanki et al. 2003). Magnetic elements have many features in common with

sunspots. These two structures together with pores are thought to be manifestations of intense magnetic flux and are described by the theory of magnetic flux tube. The magnetic structure both in active and quiet sun are similar and magnetic field is concentrated in less discrete elements of magnetic flux separated by regions with comparatively little magnetic flux.

1.4.1.2 Large scale magnetic fields

Howard (1967) showed that there exists large-scale monopolar and bipolar magnetic field structure in the of photosphere with sizes $\sim 10^3$ times larger, field strengths $\sim 10^3$ times weaker (~ 5 G) and fluxes of the same order as those of active regions. The unipolar regions seem to be created by breaking up the 'following' polarity parts of the active regions. These unipolar regions seem to migrate pole ward and to build up a general polar magnetic field.

These photospheric large-scale fields lead to the large-scale structures in the corona which are seen in the white light photographs and in the x-ray pictures. The examples of these are : (i) prominences, (ii) coronal loops, extending up to one solar radius, (iii) coronal streamers, extending often beyond $\sim 10R_\odot$ and (iv) coronal holes extending up to $0.1R_\odot$.

1.4.1.3 Solar magnetic activity

Interaction of sun's convection, differential rotation and magnetic field plays an important role in the generation of solar activity and solar cycle. But the exact mechanism of solar activity is not understood. Sunspots act as tracers of solar magnetic activity cycle. Active region of the sun consists mainly of the sunspots and the magnetic loops connecting them. The magnetic field in the sun is continuously altered and the active region is always varying which means that number of sunspots observed on the sun is not a constant but vary with time. Time variation is predominantly cyclic, i.e., mean period is 11 years. However, there are large amplitude fluctuations. This cyclic phenomenon is termed as sunspot cycle.

Early in solar cycle, sunspots appear at higher latitudes and at the end of the cycle appear closer to the equator.When a new cycle starts again sunspots appear at

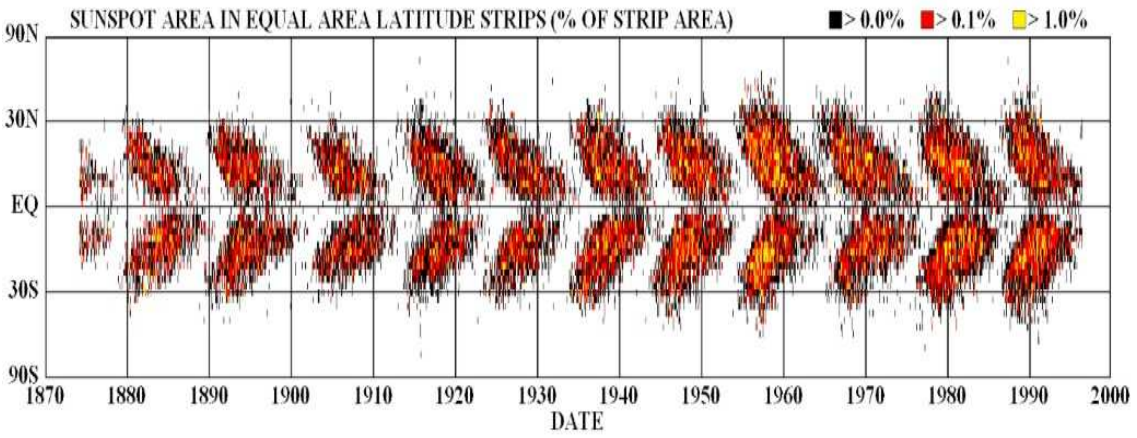

Figure 1.2: A Butterfly diagram showing the latitudinal distribution of area of sunspots from 1870 to 2000 (cf., http://wwwssl.msfc.nasa.gov /ssl /pad /solar /images /bfly.gif).

high altitudes. The latitude distribution of sunspot is a good method to determine the time of sunspot minimum for a given cycle. This recurrent behavior of sunspots give rise to the butterfly pattern and was discovered by Edward Maunder in 1904 and it is shown in Fig 1.2. Butterfly diagram shows equatorward migration of sunspots, poleward migration of weak surface radial field, pole reversal at the time of sunspot maximum and both have an average periodicity of 11 years. The reason for this sunspot migration pattern is unknown. Understanding this pattern could tell us something about generation of sun's internal magnetic field structure.

Most of the sunspot groups are bipolar which contain two principal members, the one which leads the group in the direction of sun's rotation is called leader and the other is called the follower. In general, leader spot is found to be larger than the follower. The leading and following parts in a spot group have opposite polarities. The most remarkable feature observed in a bipolar spot group is the reversal of magnetic polarities in either hemisphere with the beginning of the new cycle. Thus, when magnetic polarities are taken into account, a complete sunspot cycle has a period of about 22 years. This is known as 22 year magnetic cycle. Magnetic interaction can sometime trigger sudden explosions called solar flares and coronal mass ejections (CMEs) which are the biggest explosions in the solar system

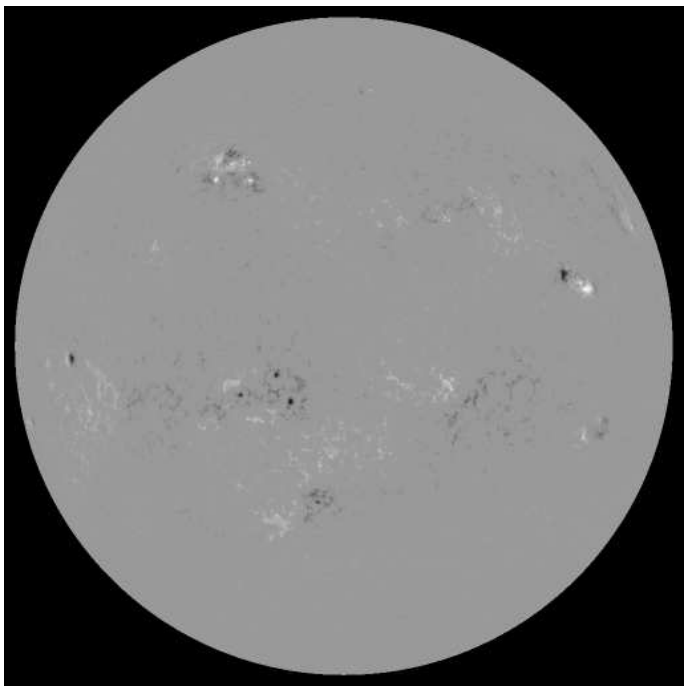

Figure 1.3: A typical magnetogram taken by SOHO/MDI on Feb 9^{th}, 2000.

and these eject magnetized plasma and charged particles into the space. These disrupt satellite operations and telecommunications facilities, electrical power grids, air-traffic on polar routes etc.

1.4.2 Internal magnetic field

Direct measurement of strength of internal magnetic field is impossible. Hence internal magnetic field structure can be studied only by theoretical modelling and comparing the consequences at the solar surface with the observed photospheric field (Hiremath 1994).

Many theoretical models have been developed for explaining the surface field structure that has near 22 periodicity. According to turbulent dynamo theory, the surface time varying field structure is maintained and periodically reversed by cyclonic turbulence and rotation inside the sun (Parker 1955a; Krause 1976; Raedler 1974; Yoshimura 1972; Gilman 1974). In order to produce a dynamo field structure a weak seed field is required. High conductivity of solar plasma suggests that the sun

might have retained some of the fossil field structure from the collapse in its proto-star phase (Cowling 1953; Hiremath 1994; Hiremath & Gokhale 1995). In fact, only on theoretical grounds such a field of primordial origin is possible (Cowling 1953; Bahcall & Ulrich 1971). Chitre et al. (1973) and Dicke (1977, 1979) had postulated the existence of fields of $\sim 10^8$ G in the central regions of the sun to explain the dearth of solar neutrinos. The meridional circulation can be induced by large scale internal magnetic field resulting in mixing of material in the solar interior. This could possibly explain the deficit of observed solar neutrinos and splitting of acoustic modes of oscillations, although recent observational evidences suggest a solution in neutrino physics.

The presence of a 'steady' quadrupole toroidal field structure of $\sim 2 \pm 1$ MG at the bottom of convection zone was derived by Dziembowski & Goode (1991) by analyzing the Libbrecht's (1989) data on rotational splittings of acoustic frequencies. Mestel (1968) suggested that a field of ~ 1 G is required for uniform rotation. The deficit of lithium with a normal beryllium abundance in the solar atmosphere was explained by Parker (1984) and Moss (1987) by proposing that a strong magnetic field $\sim 10^6$ G may be existing below base of the convection zone. Dudorov et al. (1989) concluded that the presence of a weak large-scale magnetic field in the radiative zone could lead to the establishment of rigid-body rotation in a short time scale compared with the age of the sun. The oscillatory theories of solar magnetic cycle also require large-scale weak magnetic fields ~ 100 G in the radiative interior of the sun.

A large-scale weak field in the radiative core was proposed by Stenflo & Vogel (1986) and Gough (1986) based on the analysis of global magnetic resonances. A large-scale poloidal field ($\sim 10^{-5}$ - 1G) was suggested by Rosner & Weiss (1985) from the analysis of rotational frequency splittings. Spruit (1990) suggested the existence of a large-sale field of ~ 1 G, with poloidal and toroidal components of similar strengths on the grounds of evolution of sun's angular momentum.

With reasonable assumptions and approximations, recently steady part of poloidal magnetic field structure in the solar interior is modelled (Hiremath 1994; Hiremath & Gokhale 1995) as an analytical solution of the equation for magnetic

diffusion in an incompressible medium of constant diffusivity such that field lines must isorotate with solar plasma. Characteristic diffusion time scales are estimated to be $\sim$ 10.6 and 2.7 billion year respectively.

1.4.3 Solar MHD

Sun is in the fourth state of matter i.e., plasma. Specifically, plasma is ionized gas i.e., gas that has been given an electrical charge by stripping of electrons. The theory of plasma involves the study of interaction between magnetic field and plasma, treated as a continuous medium. Large scale plasma structure like sun can be defined by magnetohydrodynamics (MHD) equations. MHD describes the dynamics of macroscopic plasma where magnetic field $\mathbf{B}$ and velocity field $\mathbf{V}$ are coupled using a simplified set of Maxwell's equations along with Ohm's law, the ideal gas law, equations of continuity, equations of motion and equations of energy. Any movement of conducting material in a magnetic field generates an electric current $\mathbf{j}$, which in turn induces a magnetic field, $\mathbf{B}$. Each unit volume of liquid having $\mathbf{j}$ and $\mathbf{B}$ experiences MHD forces approximately equal to

$$\mathbf{j} \times \mathbf{B}, \tag{1.2}$$

known as Lorentz force.

Alfven was the first to introduce the term MHD. MHD applies quite well to astrophysical objects since 99% of baryonic matter of the universe is made up of plasma, including stars, the interplanetary medium, the interstellar medium and nebulae. Solar atmosphere is dominated by magnetic fields. Sunspots are the source of intense magnetic field. To understand the surface activity of sun and solar cycle it is necessary to outline the principles of MHD. The basic building blocks of MHD are Maxwell's equations, fluid dynamic equations and Ohm's law. The properties of electromagnetic field is described by the following Maxwell's equations:
Ampere's Law

$$\nabla \times \mathbf{B} = \mu \mathbf{j} + \frac{1}{c^2} \frac{\partial \mathbf{E}}{\partial t}, \tag{1.3}$$

Faraday's Law

$$\nabla \times \mathbf{E} = \frac{\partial \mathbf{B}}{\partial t}, \tag{1.4}$$

Coulomb's Law

$$\nabla.\mathbf{E} = \frac{q}{\epsilon}, \tag{1.5}$$

and divergence of magnetic field

$$\nabla.\mathbf{B} = 0, \tag{1.6}$$

where $\mathbf{B}$ is the magnetic field, $\mathbf{E}$ is the electric field, $\mathbf{D}$ is the electric displacement, $\mathbf{j}$ is the current density and c is the velocity of light. If μ_0, ϵ_0 are permeability and permittivity of free space respectively, then for most gaseous media in the universe,

$$\mathbf{B} = \mu_0 \mathbf{H}, \tag{1.7}$$

and

$$\mathbf{D} = \epsilon_0 \mathbf{E}. \tag{1.8}$$

Generalized Ohm's law is

$$\mathbf{j} = \sigma[\mathbf{E} + \mathbf{v} \times \mathbf{B}], \tag{1.9}$$

where σ is the electrical conductivity and $\mathbf{v}$ is the velocity of the plasma and it relates the electric current density to the fields producing it. In fluid mechanics, equation of motion is

$$\rho \frac{d\mathbf{v}}{dt} = -\nabla p + \rho \mathbf{g}, \tag{1.10}$$

equation of continuity is

$$\frac{d\rho}{dt} + \rho \nabla.\mathbf{v} = 0, \tag{1.11}$$

perfect gas equation is

$$p = \frac{R}{\mu} \rho T, \tag{1.12}$$

where p is the pressure, $\mathbf{g}$ is accelaration due to gravity, R is the universal gas constant, μ is the permeability, ρ is the density and T is the temperature. The equation of motion is given by Navier-Stokes equation extended by including Lorentz force which is

$$\rho \frac{d\mathbf{v}}{dt} = -\nabla p + \mathbf{j} \times \mathbf{B} + \rho \mathbf{g}. \tag{1.13}$$

Lorentzian force ($\mathbf{j}\times\mathbf{B}$) can be decomposed into two terms. The first term represents the change of $\mathbf{B}$ along a particular field line and is therefore a magnetic tension force whose strength is proportional to B^2. The second term is the magnetic pressure force. The last term $\rho\mathbf{g}$ in equation(1.13) is a force due to gravity.

Magnetic induction equation follows from the Maxwell's equations and the generalized Ohm's law under the non-relativistic approximation as follows

$$\frac{\partial \mathbf{B}}{\partial t} = \nabla \times (\mathbf{v} \times \mathbf{B}) - \nabla \times (\eta \nabla \times \mathbf{B}) \tag{1.14}$$

with

$$\nabla.\mathbf{B} = 0, \tag{1.15}$$

and the magnetic diffusivity η is defined as

$$\eta = \frac{1}{\mu\,\sigma}, \tag{1.16}$$

or

$$\frac{\partial \mathbf{B}}{\partial t} = \nabla \times (\mathbf{v} \times \mathbf{B}) + \eta \nabla^2 \mathbf{B} \tag{1.17}$$

if η is uniform. The first term on the right hand side of magnetic induction equation is due to convection, i.e., due to fluid motion and second term represents field diffusion. The ratio of convection term to diffusion term gives magnetic Reynold's number, i.e., $\frac{\nabla\times(\mathbf{v}\times\mathbf{B})}{\eta\nabla^2\mathbf{B}} \sim \frac{\frac{\mathbf{VB}}{L}}{\frac{\eta\mathbf{B}}{L^2}} = \frac{VL}{\eta} \equiv R_m$. where V is the velocity, L is the length scale.

When $R_m \ll 1$, then induction reaction reduces to $\frac{\partial \mathbf{B}}{\partial t} \simeq \eta\nabla^2\mathbf{B}$, i.e. induction equation reduces to a pure diffusion equation and therefore typical diffusive time scale is $\tau = \frac{L^2}{\eta}$.

When $R_m \gg 1$, then induction reaction reduces to $\frac{\partial \mathbf{B}}{\partial t} \simeq \nabla \times (\mathbf{v} \times \mathbf{B})$, such that the frozen flux theorem of Alfven applies (Priest 1981) which states that in a perfectly conducting fluid, i.e., in ideal MHD, the magnetic lines move with the fluid or the field lines are frozen into plasma. Some basic assumptions of MHD are

1. The plasma is treated as a continuum.

2. The coefficients η (the magnetic diffusivity) and μ (the magnetic permeability) are assumed to be uniform. Also most of the plasma properties are assumed to be 'isotropic'. The exception is the coefficient of thermal conductivity, whose value along and normal to the magnetic field may differ greatly.

3. The plasma is assumed to be in thermodynamic equilibrium with velocity distribution function close to a Maxwellian. This holds for time-scales much larger than the collision time scales and length-scales much longer than the mean free paths.

4. The equations are written for inertial frame. The extra terms that arise for a frame rotating with the sun may be important for large-scale processes.

5. 'Relativistic' effects are neglected, since the flow speed, sound speed and Alfven speed are all assumed to be much smaller than the speed of light.

6. The simple form of 'Ohm's Law' is adopted for most applications, rather than more general version.

7. The plasma is treated as a 'single fluid' although two or three fluid models may be more relevant for the coolest or rarest parts of the solar atmosphere.

1.5 Sun's Rotation

Nearly 400 years ago (soon after the discovery of the sunspots), sun's rotation was discovered from the movements of the sunspots over the sun's disk, since sunspots serve as tracers that help us to compute the rotation of sun. Pioneers of this discovery were Galileo Galilee (1564-1621), Goldschmidt (1587-1615), Thomas Harriet (1560-1621) and Schiener (1575-1650).

Study of sun's rotation started systematically from 1850 AD onwards. It was Richard Carrington and Gustav Sporer who carried out observations of the apparent motion of sunspots. From the study of sunspots, it is seen that sun rotates differentially at its surface and extends throughout the convective zone. Below the base of convection zone, i.e., in the radiative zone and core, there is an abrupt change in

rotation, with rotation like a solid body. On the surface sun's rotation is observed to be fastest at the equator and tend to decrease as latitude increases, i.e., equatorial region rotates faster than polar region. At the equator, the solar rotation period is about 25 days and at the poles it is about 36 days. The sun's rotational axis is tilted by about 7.25 degrees from the axis of the earth's orbit. Since sun is in plasma state and due to convection, it exhibits differential rotation. The 11-year sunspot cycle and associated 22 year magnetic solar cycle phenomena are believed to be due to this differential rotation and convective motion of sun.

1.5.1 Surface Rotation

By observing the positions of stable and long-lived structures, tracers such as sunspots, faculae and filaments, super granules and coronal features etc., solar rotation can be determined. Doppler velocity measurements are also used to measure sun's surface rotation which reveal narrow bands of weakly slower and faster rotation rate as a function of latitude that migrate towards the equator (Howard & Labonte 1980). These variations are known as *torsional oscillations*. Measurements from Doppler velocity also reveal nonrotational flows on the surface. These include flows from the equator towards the pole which may represent *meridional flow* in the convection zone (Hathaway 1996; Hathaway et al. 2003). Sun's rotational profile on the surface can be derived by measuring the apparent motions of sunspots over the sun's disk (Newton & Nunn 1951; Ward 1966; Balthasar & Woehl 1980; Godoli & Mazzucconi 1979). For example, a typical rotational profile of the Sun on the surface using sunspot as tracers is given by Gilman & Howard (1984) as follows:

$$\Omega(R_\odot, \phi) = 467.0(\pm 0.2) - 91.4(\pm 1.4) sin^2\phi \ \ nHz, \tag{1.18}$$

where $R_\odot$ is the observed radius of the sun and ϕ is the heliographic latitude. Sun's rotational profile can also be derived by measuring the Doppler shift in the spectral lines east and west limbs (Snodgrass 1991) and is given as follows:

$$\Omega(R_\odot, \phi) = 453.8(\pm 1.0) - 54.6(\pm 0.8) sin^2\phi - 75.5(\pm 1.1) sin^4\phi \ \ nHz. \tag{1.19}$$

This is $\approx$ 4% slower than the rotation rate of sunspot groups. This significant difference, amounts to $\approx 80\ msec^{-1}$ in relative velocity at the equator. Later measurements (Livingston & Duvall 1979; Duvall 1982) also confirm this result. The rotation of photospheric magnetic fields outside sunspots was first examined by Wilcox & Howard (1970). This rotation is similar to the rotation of sunspots. Later studies (Stenflo 1974, 1977) confirmed this result. Snodgrass (1983) also determined surface rotation from the Mount Wilson magnetograph data as follows.

$$\Omega(R_\odot, \phi) = 461.9(\pm 0.3) - 73.8(\pm 2.9)sin^{\phi} - 52(\pm 5)sin^4\phi\ \ nHz. \tag{1.20}$$

1.5.2 Internal Rotation

Sun's interior is not accessible to direct observation. But the advent of helioseismology helped us to understand the sun's interior and solar activities. Helioseismic investigations of internal rotation rate of the sun reveal that latitudinal differential rotation seen at the surface extends up to the base of the convection zone. From base of convection zone to the center, sun rotates rigidly. Sun's internal rotation can also be inferred from the rotation rates of the sunspots during their initial appearance on the surface (Hiremath 2002). Due to very high conductivity of solar plasma, sunspots isorotate with internal plasma, and due to buoyancy rise toward the surface along the path of rotational isocontours. This implies that sunspots are very good tracers of internal dynamics and magnetic field structure of solar convective envelope. Recent studies (Javaraiah & Gokhale 1997; Sivaraman et al. 2003; Hiremath 2002) have shown that variation of initial rotation rates of the sunspot groups with different lifespans is almost similar to the radial variation of internal rotation as inferred from helioseismology.

Chapter 2

Flares associated with abnormal rotation rates of the sunspots

2.1 Introduction

The sunspots are supposed to be associated with many solar activity phenomena like flares, prominences, coronal mass ejections, etc. It is believed (Priest 1981; Parker 1994) that the magnetic reconnection is one of the physical phenomenon in releasing the required amount of flare energy. However, it is not known at what level of the solar region reconnection events take place. Moreover, it is not known why some set of sunspots trigger flares and others do not. Though following studies indicate the relevance of sunspot motions for triggering the flares, much quantitative and statistical evidences are lacking. In this study, using daily motions of the bipolar spot groups observed from the Kodaikanal observatory same is presented.

The previous studies (Tanaka & Nakagawa 1973; Ambastha & Bhatnagar 1988; Sundara Raman et al. 1998) have shown that the proper motions of sunspot pairs can cause the energy build up and provide the required amount of energy involved in flaring. Sivaraman (1969) has demonstrated that the flares coincide with the period of maximum area in the evolutionary phase. Zirin & Liggett (1987) have studied the case of δ spots and showed that such spot groups are the potential candidates for the great flares. They further conclude that the driving force for one of the flare precursor such as magnetic shear may be due to spot motion, either flux emergence or the forward motion of p spots in an inverted magnetic configurations. Many studies (Hagyard et al. 1982; Hagyard 1984; Venkatakrishnan et al. 1989; Ambastha

et al. 1993), from the vector magnetograms, show the relevance of magnetic shear with the eventual triggering of the solar flares.

By considering the H-α filament as a proxy for the magnetic neutral line, Sivaraman et al. (1992) quantitatively estimated change in the shear that corresponds with the occurrence of the flare. Schmieder et al. (1994) showed that in order to have the flare occurrences, the following two conditions are necessary : (i) the break up motions of different polarity regions maintained a high shear level for the continuous build up of the magnetic flux and, (ii) the rapid motions and the changes in the magnetic sources.

Most of the aforementioned studies clearly indicate that the occurrence of the flares is associated with the complex movement and magnetic topology of the sunspots. That means flares may be attributed not only to magnetic flux build up and reconnection but also to dynamics of the active regions that acquire during the course of their raising from the convection zone towards the surface.

The conventional picture of the formation of sunspots is that they originate below the solar surface due to an unknown dynamo mechanism. Due to the very high conductivity of the solar plasma, sunspots are glued to the internal plasma and due to buoyancy raise towards the surface. This implies that sunspots are very good tracers of the internal dynamics and structure of the solar interior. Previous studies (Gokhale & Hiremath 1984; Javaraiah & Gokhale 1997; Hiremath 2002; Sivaraman et al. 2003; Zuccarello & Zappalá 2003) show that variation of the initial rotation rates obtained from the daily motion of sunspot groups with respect to their life spans is similar to the radial variation of the internal rotation profile of the solar plasma.

In order to know whether dynamics of the sunspots-especially the dynamics due to rotational rates-give clues about the triggering of flares, (Hiremath & Suryanarayana 2003) computed the daily rotation rates of sunspots (that have leaders and followers) during their life time and have shown that the abnormal rotation rates of either leading or following spots or both eventually trigger the flares. In that study, because of the strong association between abnormal rotation rates of sunspots and the occurrence of flares, it is possible to estimate the probable region

of the depth of magnetic reconnection below the surface. For such reconnection events to occur, a close approach of their foot points and contact of the flux tubes below the surface may be necessary. In the present study, it is searched for such events and showed that triggering of a flare occurs at the time of minimum distance between the leading and the following spots. In section 2.2, data used and the method of analysis is described. Results are presented in section 2.3. The physical phenomenon of magnetic reconnection that may be responsible for triggering the flare is discussed in section 2.4 and overall conclusions are presented.

2.2 Data and analysis

For the years 1969-74, both the data set of positional measurements (heliographic latitude and longitude from the central meridian) of the sunspot groups (that have leading and following sunspots) taken from daily white light images and the flare events in the $H\alpha$ images from the Kodaikanal Observatory are used. The details of the telescope and observations of daily white light images are given by Sivaraman, Rausaria and Aleem (1992). Using similar criteria (Hiremath 2002) in selecting the sunspot groups, rotation rate ω_i of the leading and following sunspots are computed as follows:

$$\omega_i = \frac{(l_{i+1} - l_i)}{(t_{i+1} - t_i)}, \tag{2.1}$$

where l is the heliographic longitude from the central meridian, t is the time of observation, i= 1,2,3,..n, and n is the age of the spot group. The term *rotation rate* of the sunspots means the *(synodic) angular rotation velocity*. Daily *longitudinal separations* $d_i = l_L - l_F$ (l_L and l_F are the longitudes of the *leader* and the *follower*) of the foot points of the spots are computed. Following equation (2.1), the *rate of change of longitudinal separation* S_i is computed as follows.

$$S_i = \frac{(d_{i+1} - d_i)}{(t_{i+1} - t_i)}\,. \tag{2.2}$$

In the following analysis combined data (1969-74) set for the whole region of heliographic latitudes of 0^o to 40^o in both the solar hemispheres is used. The combined data set is presented in Tables 2-1-2.3. The columns are : (i) Kodaikanal

spot group number, (ii) Greenwich spot group number, (iii) the year of observation, (iv) the month of observation, (v) the date of flare occurrence and (vi) the flare type. From the Kodaikanal data archive, it is not possible to obtain the flare types for the following Kodaikanal sunspot group numbers : 13621, 13784, 13859, 13875, 14652-14784. The stars (attached to the Greenwich group numbers) in the second column of Tables 2.1-2.3 indicate the ambiguity in identifying the Kodaikanal group numbers with the Greenwich group numbers.

2.3 Results

For the period of observations, 57 well-developed spot groups that have leader and follower spots are selected. Using equation (2.1) and (2.2), daily rotation rates ω_i and rate of change of longitudinal separation S_i are computed.

Typical white light images of the evolutionary phase of a spot group that has leading and following sunspots are illustrated in Fig 2.1. The spot group grows and decays in the southern hemisphere of the solar disk. Although from the 25th onwards new complex sunspots emerge near the equator, the identity of the leading and the following spots can still be traced unambiguously. In Fig 2.2(a), the rotation rates (in units of *deg/day*) and the daily longitudinal separation (in units of *deg*) of the leader and the follower of such a spot group are presented. In Fig 2.2(a), the numbers near the vertical lines are the scale values presented along the y axis (rotation and longitudinal separation). In Fig 2.2(b), the rate (in units of *degrees/day*) of change of longitudinal separation are presented. In Fig 2.3, the normalized values of daily rotation rates and the rate of change of longitudinal separation are presented. The normalized values are defined as follows. If x_i are the data points for different i days, $\overline{x}$ is the average of all data points and σ is the standard deviation of rotation rates of the leading and the following spots and the rate of change of separation of their foot points, then the normalized value is $y_i = (x_i - \overline{x})/\sigma$. Since all three parameters (rotation rates of the leader and the follower and the rate of change of longitudinal separation) that have different ranges of magnitudes are to be presented, the normalization allows presentation of the three variables in a single plot.

Table 2.1: Kodaikanal observations related to the Greenwich Group numbers

$Kodai\ No$	$Green\ No$	$Year$	Mon	$Date\ of\ flare$	$Flare\ Type$
13105	21482	1968	1	29	$1-n$
”	”	”	2	2	$s-b$
13483	21894	1969	2	20	$1-n$
”	”	”	2	25	$2-b$
”	”	”	2	26	$2-b$
13510	21936	1969	3	21	$2-n$
13621	22064	1969	8	2	
”	”	”	8	3	
13625	22068	1969	8	2	$s-n$
13640	22086	1969	9	26	$1-b$
13683	22138	1969	10	8	$1-n$
”	”	”	10	10	$1-f$
13696	22152	1969	11	2	$1-f$
13713	22176	1969	11	24	$2-b$
13743	22210	1969	12	26	$s-n$
13776	22247*	1970	1	17	$1-n$
13778	22251	1970	1	25	$1-n$
”	”	”	1	28	$2-b$
”	”	”	1	30	$1-n$
13783	22255	1970	1	26	$1-n$
13784	22261	1970	1	29	
13791	22272	1970	2	9	$2-b$
”	”	”	1	10	$1-n$
”	”	”	1	11	$2-b$
”	”	”	1	12	$s-b$
13792	22274	”	2	7	$1-b$
13811	22291	1970	2	21	$s-n$
”	”	”	2	25	$s-n$
13859	22351	1970	4	9	
13860	22349*	1970	4	9	$s-n$
”	”	”	4	11	$s-n$
”	”	”	4	13	$s-b$

* Ambiguity in identifying these spot group numbers with Greenwich group numbers

In Figure 2.3, whenever there are minimum approaching distances (represented by the negative values of the variation of separation) between the foot points of the leading and the following spots, on the same day or later the spots experience abnormal rotation rates leading to triggering of flares. From the same figure, one can also notice that in order to trigger flares, foot points of the leading and the following sunspots should move towards each other at a rate of $1-2\,deg/day$. For the 57 spot groups, occurrence of longitudinal minimum separation and the corresponding occurrence of the flare are noted. The resulting correlative analysis is presented in the scatter diagram of Fig 2.4 (a) (left). In 6 years many flares do not satisfy

Table 2.2: Kodaikanal observations related to the Greenwich Group numbers

$Kodai\ No$	$Green\ No$	$Year$	Mon	$Date\ of\ flare$	$Flare\ Type$
13870	22362	1970	4	24	$1-b$
”	”	”	4	25	$s-n$
13875	22370*	1970	4	25	
13881	22379	1970	5	7	$s-n$
”	”	”	5	8	$1-n$
13891	22392	1970	5	15	$s-n$
”	”	”	5	16	$1-b$
13901	22411	1970	5	30	$1-b$
13916	22433	1970	6	13	$1-n$
”	”	”	6	14	$s-n$
”	”	”	6	16	$1-n$
13932	22448	1970	6	27	$s-n$
”	”	”	6	30	$1-n$
13937	22454	1970	6	30	$s-n$
”	”	”	7	1	$s-n$
13973	22495*	1970	8	6	$s-n$
13980	22508	1970	8	24	$2-n$
14021	22556	1970	9	27	$1-n$
”	”	”	9	28	$s-n$
”	”	”	9	29	$s-n$
14064	22608*	1970	11	13	$1-n$
”	”	”	11	14	$1-n$
14108	22664	1970	12	1	$s-n$
14120	22679	1971	1	21	$1-n$
”	”	”	1	25	$1-n$
14128	22686	1971	1	31	$1-b$
”	”	”	2	3	$1-n$
14144	22710	1971	2	16	$1-b$
14175	22738	1971	3	21	$s-b$
14184	22755	1971	4	11	$1-n$

* Ambiguity in identifying these spot group numbers with Greenwich group numbers

the criterion of a strong association between the minimum longitudinal separation and triggering of the flare. However, only those H-α flares that correspond to the sunspot groups' heliographic coordinates and time on that day are selected.

Moreover, the correlation coefficient is found to be 94% with a very high significance ($\sim 100\%$). One has to be cautious in interpreting the magnitudes of very high correlation coefficients (~ 1). In the present analysis the Spearman Rank-Order correlation coefficient and its significance (Press et al. 1992) are computed. This method of finding the correlation between two variabilities is more robust than the usual method (*i.e.,* by linear correlation). From this method, one can not only find a very high correlation but also with very high significance can be confirmed.

In order to know at what stage of a sunspot's life span the events of minimum separation and flares occur, spot groups of different life spans are separated. In Fig 2.4(b) (right), the results with life span along the x axis and the corresponding occurrence of the minimum separation and the flares along the y axis are presented. The errors are determined using the formula $\sigma/(N)^{1/2}$, where N is the total number of events of minimum separation and flares and σ is the standard deviation. Abnormal rotation rate is defined as follows. Fist the daily rotation rates ω_i for each pair of the bipolar spots is computed and then the mean $\bar{\omega}$ with their standard deviation σ is computed. If the absolute value of the difference $(\bar{\omega} - \omega_i) > 1\sigma$, then the corresponding rotation rate at that date is considered as abnormal rotation rate of the spot. As in the previous study (Hiremath & Suryanarayana 2003) , for the events with abnormal rotation rates, a spot with a 4 day life span experiences on average a minimum separation and correspondingly the occurrence of a flare on the second day. A spot with a life span of six days experiences the same events on the third day and so on. In other words, abnormal rotation rates of the spots and the minimum distances of the foot points on average occur at between $50 - 80\%$ of the life span during the course of their evolution, probably indicating annihilation of magnetic energy below the surface (Hiremath & Suryanarayana 2003). If we assume that the flares occur due to magnetic reconnection, then it is interesting to know the magnitude of minimum separation during the occurrence of the flare. In Fig 2.5(a), minimum separation (in degrees) of the leading and the following foot points during the occurrence of the flare are presented. In order that reconnection events occur below the surface, the approaching spots that experience abnormal rotation rates should have a minimum longitudinal separation, on average $6^o - 10^o$ in the photosphere. It is also interesting to know the speed at which foot points of the spots approach each other during the occurrence of the flare. In Fig 2.5(b), rate of change of minimum separation for different classes of flares are presented. The foot points of the spots that eventually trigger the flares approach each other on average at a rate of $\sim 1^o - 2^o$/day.

2.4 Discussion and conclusions

Since the majority of spots that have leading and following parts are bipolar (Zirin 1988), it is assumed that all the spot groups that are considered in the present study from white light images are *bipolar*. Thus we can invoke the theory of *magnetic reconnection* for the interpretation of the results.

Presently it is believed (Priest 1981; Parker 1994) that the source of energy produced in solar flares is due to *magnetic reconnection* in a very compact region wherein oppositely directed magnetic fluxes, in the limit of finite electric conductivity, annihilate each other and release the required amount of flare energy. Oppositely directed magnetic flux of large length scale L merges with inflow velocity v_{in}. This merging of flux will form a current sheath. The law of magnetic induction dictates the course of evolution of the plasma. The condition of infinite electric conductivity fails in the region of magnetic field reconnection by producing very high gradients of current and electric fields. Dissipation of these strong currents leads to annihilation of the magnetic field in the region of magnetic reconnection where a steady state exists so that convective and resistive terms in the induction equation are equal. There are two crucial requirements for the reconnecting region that eventually produce the flares. The first requirement is the amount of energy released by the annihilation of the magnetic field B and a cube of length L, estimated to be $\sim L^3B^2$. That means that in order to produce the observed typical flare energy of $\sim 10^{27} - 10^{30}$ ergs, the length (L) of the reconnecting region below the surface must be $\sim 10^5 - 10^8$ cms and the strength of the magnetic field should be $10^5 - 10^3$ G. The second requirement, from the standard flare mechanism (Petschek 1964), yields the relation $v_{in} = 0.1v_a$, where v_{in} is the inflow velocity with which magnetic lines merge and v_a is the Alfven velocity in the vicinity of the magnetic reconnection. From the present study, we satisfy the two requirements as follows.

Based on the size and visual appearance of the intensity, traditionally, the flares are classified as follows : (i) sf, 1f, 2f, 3f, 4f; (ii) sn, 1n, 2n, 3n, 4n; and (iii)sb, 1b, 2b, 3b, 4b. Since we considered the dynamic events, it is interesting to know whether occurrence of different class and subclass of flares depends upon the magnitudes

of the abnormal rotation rates of the spots. To satisfy the first requirement, the present analysis (see the Fig 2.5(a)) shows that on the surface the average minimum separation between bipolar spots is $\sim 6^o - 10^o$ in longitude ($\sim 10^9$ cms) during the occurrence of flare events. By taking a clue from the previous study (Hiremath & Suryanarayana 2003) that the reconnection may be occurring below the surface at a depth of $0.935R_\odot$, from simple plane trigonometry, one can estimate the thickness (length) of the reconnecting region to be $\sim 10^5$ cms which is in the required range of $10^5 - 10^8$ cms.

For the second requirement, the strength of the background magnetic field in the vicinity of the reconnecting region is required. The region outside the sunspot has a background magnetic field strength of ~ 1 G (Stenflo 1994). This is not the same as the strength of the magnetic field (~ 40 G) of the localized small scale magnetic structures as determined by the Hanle method. On the other hand, I want to determine the strength of the large-scale global magnetic field in the sunspot-free region. Observational (Duvall et al. 1979; Stenflo 1994) and theoretical (Hiremath & Gokhale 1995) estimates of the magnetic field strength of such a region shows that it is ~ 1 Guass.

Thus, at the surface of the photosphere, in the region outside the sunspot, the Alfven velocity $v_a (= B/(4\pi\rho)^{1/2}$, where B is the strength of the magnetic field and ρ is the density) is found to be $\sim 10^5$ cms/sec. The results from Fig 2.3 show that the leading and the following spots that approach each other during the occurrence of the flare have a separation velocity of $\sim 1^o/day$ (10^4 cms/sec). This result satisfies the requirement that $v_{in} = 0.1 v_a$. *Thus, this study strengthens the conventional view that flares may be occurring due to magnetic reconnection.*

The overall conclusion of the present study is that during the course of the evolution of leading and following sunspots and in order to trigger flares, the foot points associated with the abnormal rotation rates of the leading and following spots should have an approaching velocity of $1 - 2\, deg/day$ and ultimately reach a minimum separation of $\sim 6^o - 10^o$ for probable magnetic reconnection below the surface around $0.935R_\odot$.

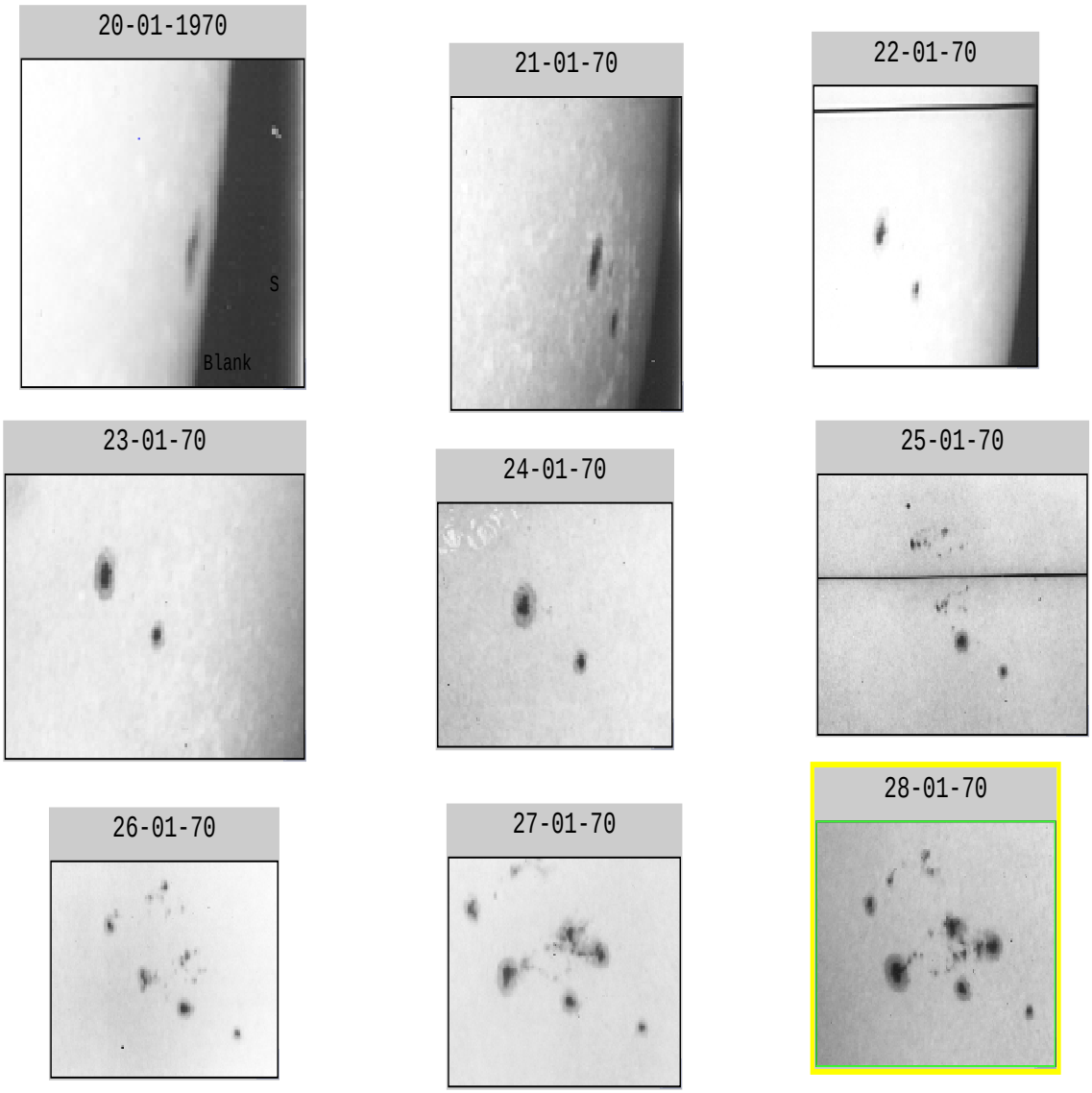

Figure 2.1: The evolution of a typical sunspot group that contains leader and follower spots observed from the Kodaikanal Observatory. On the images of the 22 and 25, the horizontal line represents the solar equator. For all the observations, the spot group is south of the equator. The corresponding Greenwich group number for this sunspot group is 22251.

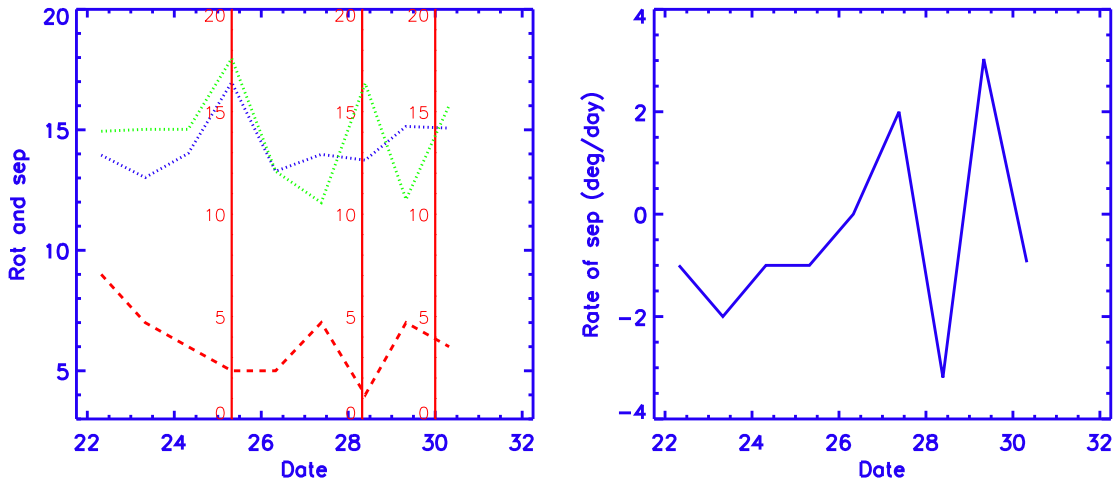

Figure 2.2: (a) Left : Rotation rates and change of longitudinal separation of the leader and the follower during their evolutionary phases. The blue and green dotted lines represent the rotation rates (deg/day) of the leading and the following spots. The red dashed line represents the change of longitudinal separation (in degrees) of the spots. The red vertical continuous lines are the occurrence dates of the flares. The red numbers near the vertical lines are repetition of the scale values presented on the y axis (rotation and longitudinal separation). (b) Right: The typical rate of change of the longitudinal separation (deg/day) of the leader and the follower spots during their evolutionary phases. For both the figures the corresponding Greenwich number of the group is 22251.

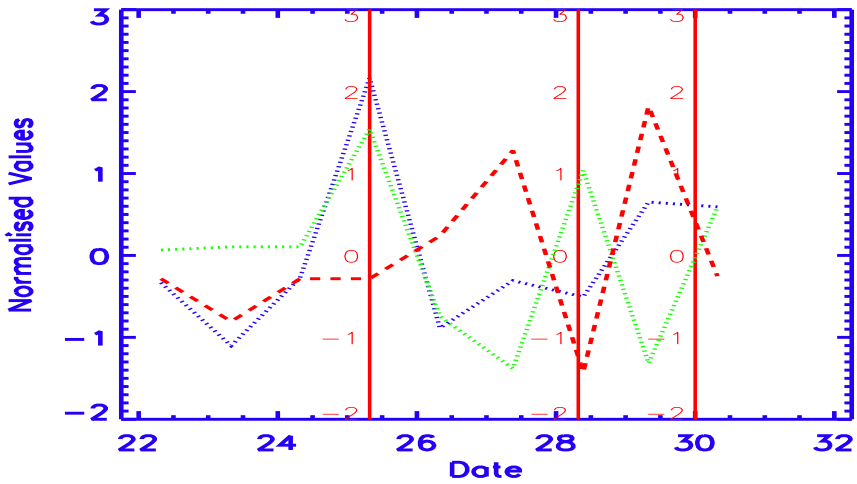

Figure 2.3: The normalized rotation rates and rate of change of longitudinal separation of the leader and the follower during their evolutionary phases. The blue and green dotted lines represent the normalized rotation rates of the leading and the following spots. The red dashed line represents the normalized rate of change of longitudinal separation of the leader and the follower spots. The red vertical continuous lines are the occurrence dates of the flares. The corresponding Greenwich number for this sunspot group is 22251.

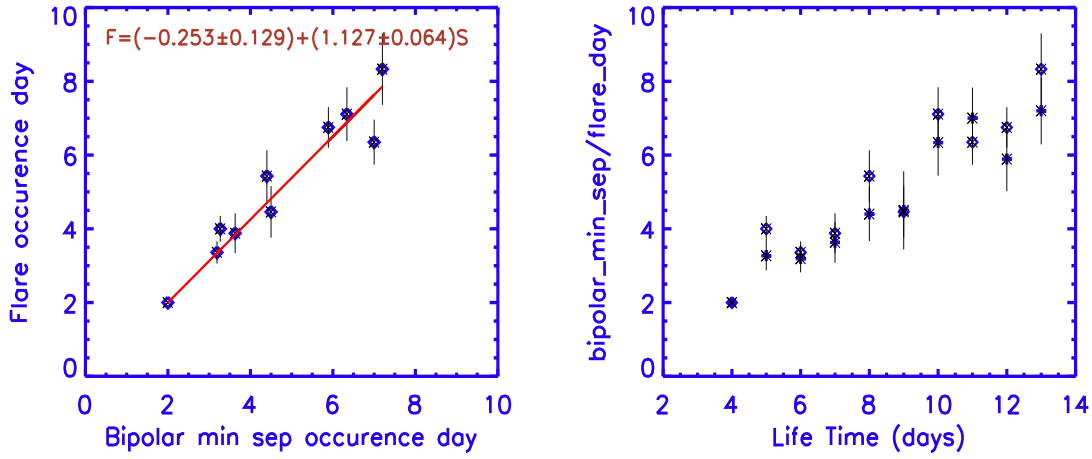

Figure 2.4: (a) The left figure represents the scatter diagram that illustrates the association between the occurrence days of the minimum separation and the flare during the evolution of the spots. The red continuous line is obtained from the linear least square fit. Here S and F represent occurrence days of minimum separation and the flares respectively. (b) The right figure represents the occurrence days of minimum separation and the flares during the evolution of spots. The symbols $\diamond$ and the square both in blue color represent occurrence day of the minimum separation and the flares respectively.

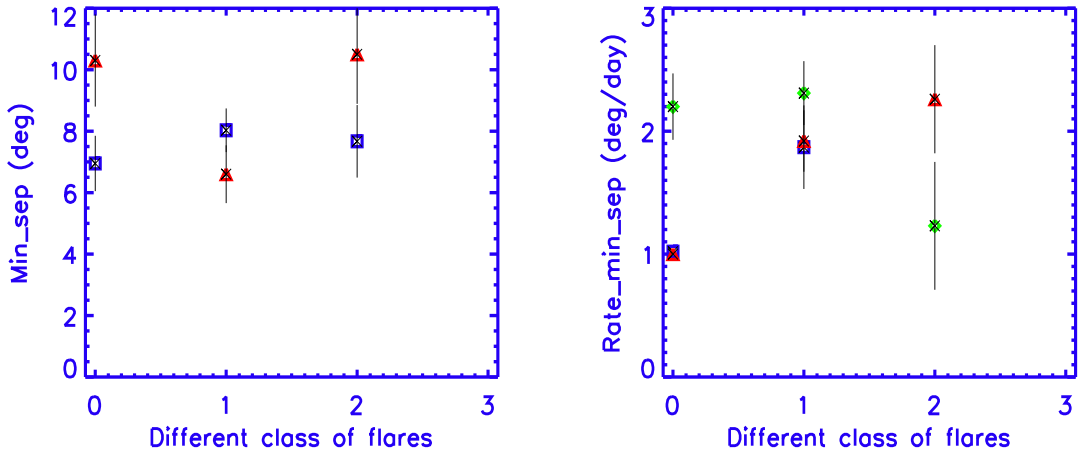

Figure 2.5: (a) The left figure represents minimum separation for the different classes of the flares : the square in blue color represents n (normal), the $\triangle$ with red color represents b (bright). Here 0 along the x axis represents the S subclass flare. The numbers 1, 2, 3 are higher subclass flares. (b) The right figure represents the rate of change of longitudinal minimum separation for different classes of the flares : the square in blue color represents f (faint), the $\diamond$ with green color is n (normal) and the $\triangle$ with red color represents b (bright). Here 0 along the x axis represents the S subclass flare. The numbers 1, 2, 3 are higher subclass flares.

Table 2.3: Kodaikanal observations related to the Greenwich Group numbers

Kodai No	*Green No*	*Year*	*Mon*	*Date of flare*	*Flare Type*
14191	22764	1971	4	16	$2-n$
”	”	”	4	20	$2-b$
14277	22877	1971	8	19	$1-n$
”	”	”	8	27	$s-n$
14290	22894*	1971	9	15	$1-n$
”	”	”	9	17	$s-n$
14322	22931	1971	11	16	$s-n$
”	”	”	11	17	$s-n$
14325	22940	1971	12	2	$1-b$
14381	23013	1972	2	15	$1-b$
”	”	”	2	18	$s-b$
”	”	”	2	21	$1-n$
14384	23020	1972	2	18	$1-n$
”	”	”	2	19	$s-n$
”	”	”	2	21	$s-b$
”	”	”	2	24	$s-n$
”	”	”	2	25	$s-n$
14458	23110	1972	5	27	$2-n$
”	”	”	5	28	$1-n$
”	”	”	5	30	$1-b$
”	”	”	6	5	$s-b$
14462	23113	1972	6	5	$s-n$
14517	23179	1972	7	7	$2-b$
14593	23272	1972	11	24	$s-n$
”	”	”	11	25	$s-n$
14635	23312	1973	2	5	$1-n$
14647	23328	1973	2	25	$s-b$
14652	23332	1973	3	$6-7$	
14657	23338	1973	3	20	
”	”	”	3	24	
14681	23377	1973	6	$8-10$	
14712	23412	1973	9	$2-4$	
14743	23453	1973	12	21	
14776	23491	1974	4	13	
14784	23500	1974	4	26	

* Ambiguity in identifying these spot group numbers with Greenwich group numbers

Chapter 3

Growth and decay of sunspots

3.1 Introduction

Since discovery of the sunspots by Galileo, genesis of their 22 year cyclic activity in general and, their formation and decay during their evolutionary stages in particular still remain a mystery. The study of sunspots' origin, formation and decay is important owing to the observed fact that variation of sunspot occurrence activity is related with the solar irradiance that in turn affect the earth's environment and the climate (Prabhakaran Nayar et al. 2002; Hiremath & Mandi 2004; Badruddin et al. 2006; Pereira & Girish 2009; Hiremath 2009a).

Present general consensus is that the sunspots originate below the solar surface due to an unknown dynamo mechanism. Due to very high conductivity of the solar plasma and assuming that raising flux tube does not acquires extra flux from the ambient medium, sunspots isorotate with the internal plasma and due to buoyancy raise towards the surface along the path of rotational isocontours. This implies that sunspots are very good tracers of the internal dynamics and structure of the solar interior. Hence if the sunspots that have first and second days appearance on the surface, and if one computes their initial rotation rates, then one can infer rotation rate of the internal solar plasma where the sunspots' foot points are anchored. Recent studies (Hiremath 2002) show that variation of initial rotation rates obtained from the daily motion of sunspot groups with respect to their life spans on the surface is almost similar to the radial variation of the internal rotation profile of the solar plasma.

From Hiremath's (2002) paper, results are reproduced in Fig 3.1 that illustrates

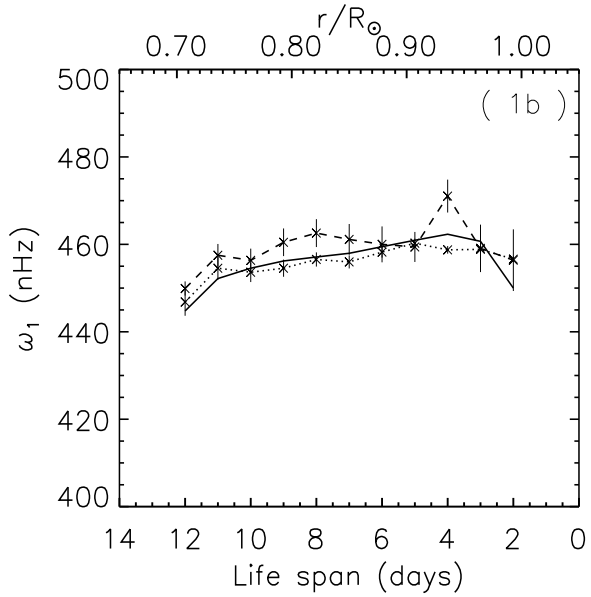

Figure 3.1: The dashed and the dotted curves are the variation of the initial rotation rates of the sunspot groups with respect to their life spans. The continuous curve is the radial variation of the internal rotation as inferred from the helioseismology.

a comparison between the variation of initial rotation rates of the sunspot groups for different life spans and radial variation of internal rotation profile as inferred (Antia et al. 1998) from the helioseismology. Note the striking similarity between these two profiles. In order to reach closer to the reality of the physics of convection zone and dynamics of the flux tubes, in the same study, the rate of change of initial rotation rates of the sunspot groups (that represent the acceleration or deceleration of the flux tubes in the ambient plasma) are compared (the Fig 5(b) of Hiremath (2002)) with the radial profile of gradient of rotation (that is computed from the radial variation of rotation of the plasma inferred from the helioseismology). Again we get a striking similarity between these profiles. To conclude from that study (Hiremath 2002), for different life spans, initial sunspot dynamics over the surface represents the internal dynamics in different layers of the convection zone. For example initial anchoring of a flux tube whose life span is 10 days is near base of the convection zone and initial anchoring of a flux tube whose life span is 5 days is in the middle of the convective envelope.

Observations show that there are three important stages in the sunspot's evolutionary history : (i) a well developed sunspot (that consists of umbra and penumbra) is formed due to coalescing of the emerging flux regions, (ii) once stabilized sunspot is formed, its area increases and reach the maximum area and, (iii) decay of the sunspot from it's maximum area to minimum area and ultimately disintegrating into smaller active regions and diffusion of the flux on the surface.

As for the first and last stages, there are many studies that explain the formation and decay parts the sunspot's evolutionary history. The first stage is supposed to be due to convective collapse, a kind of instability that has been invoked to explain the kilo gauss fields on the surface (Parker 1978; Spruit 1979; Hasan 1985). Once flux element is formed, different adjacent flux elements coalesce and sunspot is formed. Owing to their strong magnetic field structure, sunspots inhibit the ambient convection resulting in reduction of temperature and density. Ultimately lower density of the flux tube results in raising (due to buoyancy) from the convection zone to the surface. Contrary to this conventional view, Parker (1992) has proposed that sunspots are basically formed due to coalescence of magnetic elements by the vortices. According to him, flux tubes are surrounded by vortex flows that attract other vortices leading to coalescence of different flux elements. On the other hand Meyer et al. (1974), have different view on the formation of the flux tubes. According to them a strong converging flow is necessary to form the sunspots. That means sunspots might be formed at the boundary of the convective cells, with an outflow at the surface and an inflow in the deeper layers. Where as Hiremath (2009a), by updating Alfven's (1943) seminal idea of sunspot formation, came to the conclusion that sunspots are formed due to superposition of Alfven wave perturbations of the underlying steady part of large scale toroidal magnetic field structure and travel along isorotational contours in order to reach at the proper activity belt on the surface.

There are many studies on the decaying phase of the sunspot. Cowling (1946) was the first person to investigate the decay part of the sunspot area. Bumba (1963) obtained a linear decay law for the recurrent spot groups and exponential decay law for the non-recurrent spot groups. Where as some studies (Petrovay & van Driel-

Gesztelyi 1997) indicate the quadratic decay (*i.e.*, sunspot area as quadratic function of time) and other studies indicate the linear decay law. Moreno-Insertis & Vazquez (1988) and Martinez Pillet et al. (1993) conclude that the present sunspot data do not allow any distinction between either linear or quadratic decay law. To add to these decay laws, log-normal distribution (Martinez Pillet et al. 1993) also fit the decay of umbrae.

There are following theoretical studies to understand the sunspot decay. First theoretical study in supporting the results of linear decay laws is by Gokhale & Zwaan (1972). Such a linear decay law suggests that flux loss takes place everywhere within the spot irrespective of their different sizes. Gokhale & Zwaan (1972) assumed a current sheet around the sunspot and turbulent diffusion inside the tube. In this case Ohmic diffusion dictates the decay of the current sheet and hence as spot decays to smaller area, thickness of the current sheet reduces. In fact such current sheets around the sunspots have been observed (Solanki et al. 1992). In contrast, Simon & Leighton (1964) and Schmidt (1968) propose that the sunspots are decayed by the erosion of the sunspot boundary which implies that dA/dt is proportional to $A^{1/2}$, where A is area of spot. Supporting the erosion model, Petrovay & Moreno-Insertis (1997) proposed that turbulent diffusivity depends strongly on the field strength. Their model predicts the quadratic decay and spontaneous current sheet around the sunspot.

Though there are many studies on the first and last phases of the sunspot evolution, the second stage of a sunspot, viz., physics of a growth phase, during it's life time is not understood. Moreover, it is not clear whether all the three phases in a sunspot's life time remain same or different over the whole solar cycle. That means: is there any year to year variations in the area gradients (rate of change of area dA/dt with respect to time, where A(t) is time dependent area of the sunspots and t is time variable) of the sunspots during it's increasing (second phase) and decaying (last phase)? Is there any connection between the evolutionary history of the sunspots and underlying deeper dynamics or this phenomenon is simply due to surface convection. Some of these important issues are addressed in this study.

As for year to year changes in gradient of sunspots' area, for the year 1955-1965

and for different life spans, (Hiremath 2005), with summer student Mr. Subba Rao, computed both growth dA_1/dt and the decay dA_2/dt rates of the sunspots and came to the following conclusions. For the same life span, to reach their maximum areas sunspots take different times as cycle progresses. That is, in the beginning of the cycle, area-age curves are nearly gaussian and as cycle progresses area-age curve follow the simple linear decay law. Further they conclude: (i) during the beginning of the solar cycle, sunspots' *rate of growth* and *rate of decay* are larger compared at end of the solar cycle, (ii) in the beginning of the solar cycle, in order to reach their maximum areas, sunspots increase their area at a rate of $\sim$ 100 mh (millionths hemisphere)/day where as at the end of solar cycle sunspots increase their area at the rate of $\sim$ 50 mh/day and, (iii) sunspots decay faster ($\sim$ 75 mh/day) in the beginning of the solar cycle compared to the end of the solar cycle ($\sim$ 25 mh/day).

Active regions are centers of solar activity ranging from flares to CMEs. They are believed to be locations where magnetic flux bundles erupt from deep in the convection zone to emerge at solar surface in the form of sunspots due to magnetic buoyancy. Further the complexity of sunspot groups plays an important role in determining the active regions (Zirin 1988). The difference in energy between a solar minimum and a solar maximum is about 0.1% and even this small energy changes in the sun's output over 11-year solar cycle can intensify wind and rainfall pattern and therefore have a major impact on global weather pattern and this is one of the great challenges facing scientists. Therefore it will be useful to investigate how the sunspot groups themselves eventually grow and decay. The growth and decay of sunspot groups also play an important role in irradiance variations (Wilson 1981).

If decay of sunspots were purely by ohmic dissipation, sunspots would have lifetimes of about 300 years by considering their size and photospheric conductivity (Cowling 1946). However, the sunspots have shorter life span of $\sim$ weeks for non-recurrent spot groups and $\sim$ months for recurrent spot grops. How to reconcile these observed phenomena, viz., three phases of growth and decay of the sunspots. In the present study, we assume that sunspots are formed due to Alfven wave perturbations of large-scale global toroidal magnetic structure (Hiremath 2009a) that coexists with

the poloidal magnetic field structure in the solar interior and both the magnetic field structures assumed to have diffusion time scales of the $\sim$ sun's age.

In the recent study (Hiremath 2009a), it is proposed that sunspots are formed by the superposition of many Alfven wave perturbations of the embedded toroidal magnetic field structure. Once sunspots are formed, due to buoyancy, at different depths in the convective envelope raise along isorotational contours and reach the surface at different latitudes. One can notice the internal rotational profile (continuous curve) as inferred from helioseismology (Antia et al. 1998), from Fig 3.1 that there are two rotational gradients, viz., a positive rotational gradient from base of the convective envelope to $0.935R_{\odot}$ and a negative rotational gradient from $0.935R_{\odot}$ to $1.0R_{\odot}$. From the magnetic induction equation it is proposed in this study that growth and decay of either sunspots' area or magnetic flux is due to interplay of both convective source term (that in turn depends mainly upon fluctuations in the positive rotational gradient and convection) and sink term (that in turn depends upon fluctuations in negative rotational gradient, magnetic eddy diffusivity and radiation effects near the surface). That means sunspots that formed in the region of positive rotational gradient, while raising towards the surface, accumulate magnetic flux from the ambient magnetic turbulent medium and reduction of magnetic flux in the region of negative rotational gradient. The net magnetic flux of the sunspot that formed in the region of positive rotational gradient in the convective envelope while raising it's anchoring feet and reaching towards $0.935R_{\odot}$, should increase and, magnetic flux should decrease as flux tubes' anchoring feet lifts from $0.935R_{\odot}$ to $1.0R_{\odot}$. On the other hand, the sunspots that formed in the region of negative rotational gradient while raising towards the surface mainly experience decay phase only. These reasonable ideas will be clear in the following section. In order to understand and test these ideas on growth and decay phases of the sunspots, magnetic induction equation is solved by considering separately the source and the sink terms respectively. In section 3.2, formulation of the equations are presented. Solution of magnetic induction for the growth of area is presented in section 3.3 and solution for decay part is presented in section 3.4. In section 3.5, both the solutions are fitted with observed sunspots growth and decay phases of the sunspots and conclusions

are presented.

3.2 Formulation of the equations

It is assumed that, in the convective envelope, fluid is incompressible. We also assume that the magnetic eddy diffusivity η and the eddy diffusivity ν are constants with values represented by the appropriate averages. Magnetic field $\mathbf{B}$ and the velocity field $\mathbf{V}$ vectors are expressed as

$$\mathbf{B} = P\hat{\mathrm{I}}_{\vartheta} + T\hat{\mathrm{I}}_{\varphi} \ , \tag{3.1}$$

$$\mathbf{V} = U\hat{\mathrm{I}}_{\vartheta} + r\Omega sin\theta\hat{\mathrm{I}}_{\varphi} \ , \tag{3.2}$$

where $\hat{\mathrm{I}}_{\vartheta}$ and $\hat{\mathrm{I}}_{\varphi}$ are the unit vectors along heliographic latitude ϑ and longitude φ of the sun; P, T, U and Ω are scalar functions. P and T are scalar functions that represent poloidal and toroidal parts of the the magnetic field structures and U and Ω are scalar functions that represent poloidal (meridional) and toroidal (angular velocity) parts of the velocity field structures. Equation of continuity is

$$\frac{\partial \rho}{\partial t} + \rho \nabla . \mathbf{V} = 0. \tag{3.3}$$

As the life spans ($\sim$ weeks to months) of sunspots are very much larger than the time scales ($\sim$ minutes) of ambient density perturbations in the convective envelope, we have $\frac{\partial \rho}{\partial t} = 0$ and the resulting equation is

$$\rho \nabla . \mathbf{V} = \mathbf{0} \tag{3.4}$$

where ρ is the density. Similarly as magnetic diffusivity is assumed to be constant, magnetic induction equation is

$$\frac{\partial \mathbf{B}}{\partial t} = curl(\mathbf{V} \times \mathbf{B}) + \eta \nabla^2 \mathbf{B}. \tag{3.5}$$

This magnetic induction equation determines growth and decay of the sunspot. The first term on right hand side (RHS) is the source term that enhances the magnetic

flux of the sunspot and second term on RHS is the sink term that attempts to destroy the generated magnetic flux. As magnetic induction equation in turn depends upon velocity and diffusivity η, these two source and sink terms are important and dictate the growth and decay of the sunspots. We solve the induction equation by considering the source and sink terms separately for the following reasons. In case of region of positive rotational gradient from base of convective envelope to $0.935R_{\odot}$ in the convective envelope, rate of increase of magnetic flux that mainly depends upon fluctuations of increase in rotational gradient is dominant compared to magnetic diffusivity. As for region of negative rotational gradient from $0.935R_{\odot}$ to $1.0R_{\odot}$, fluctuations in decreasing rotational gradient, increasing magnetic diffusivity (as magnetic diffusivity $\eta \sim T^{-3/2}$, where T is ambient temperature) and dominant radiational effects near the surface remove and destroy the magnetic flux.

3.3 Solution for growth of the sunspot

After substituting equations (3.1) and (3.2) in equation (3.5) and also by satisfying the continuity equation (3.4), by considering a source (first) term of the toroidal component of the induction equation in spherical coordinates is

$$\frac{\partial T}{\partial t} = (\frac{UTcot\theta}{r}) + (Psin\theta\frac{\partial \Omega}{\partial \theta} - \frac{U}{r}\frac{\partial T}{\partial \theta}) + (T\frac{\partial \Omega}{\partial \phi} - \Omega\frac{\partial T}{\partial \phi}) \ , \tag{3.6}$$

where r, θ and ϕ are radial, latitudinal and longitudinal variables in spherical coordinates. The last term in RHS of the above equation can be simplified further as follows

$$\Omega = \frac{\phi_2 - \phi_1}{t_2 - t_1} = \frac{\partial \phi}{\partial t} \ , \tag{3.7}$$

where Ω is the angular velocity, ϕ_1 and ϕ_2 are changes in longitudinal displacement from time t_1 and t_2 respectively. Hence we have following equations

$$\partial \phi = \Omega \partial t \ , \tag{3.8}$$

$$T\frac{\partial \Omega}{\partial \phi} = \frac{T}{\Omega}\frac{\partial \Omega}{\partial t} \ , \tag{3.9}$$

and

$$\frac{\partial T}{\partial \phi} = \frac{\partial T}{\partial t}\frac{\partial t}{\partial \phi} = \pm\frac{\partial T}{\partial t}\frac{1}{\Omega}. \tag{3.10}$$

Hence,

$$(T\frac{\partial \Omega}{\partial \phi} - \Omega\frac{\partial T}{\partial \phi}) = (\frac{T}{\Omega}\frac{\partial \Omega}{\partial t} - \frac{\partial T}{\partial t}). \tag{3.11}$$

The reason for inclusion of $\pm$ symbol in (3.10) is that Alfven wave perturbations are along (positive sign) and opposite (negative sign) directions of the angular velocity. With these equations, equation (3.6) can be written as

$$2\frac{\partial T}{\partial t} = (\frac{UTcot\theta}{r}) + (Psin\theta\frac{\partial \Omega}{\partial \theta} - \frac{U}{r}\frac{\partial T}{\partial \theta}) + (\frac{T}{\Omega}\frac{\partial \Omega}{\partial t}). \tag{3.12}$$

Perturb this induction equation by taking the variables $\Omega = \Omega_0 + \Omega^{'}$ and $T = T_0 + T^{'}$ such that $\frac{\partial \Omega_0}{\partial t} = \frac{\partial T_0}{\partial t} = 0$ and magnitudes of fluctuating $\Omega^{'}$ and $T^{'}$ components are assumed to be very small compared to steady parts Ω_0 and T_0. This condition also implies that magnitudes of products of the fluctuating components are nearly zero. Further it is assumed that poloidal component of the magnetic field structure P is constant and it's magnitude is very small compared to magnitude of toroidal magnetic field structure. This reasonable assumption is consistent with the observed strength of solar magnetic field structure that during 11 years period strength of poloidal field structure ($\sim$ 1 G) is << strength of toroidal magnetic field structure ($\sim 10^3$ G). That means the fluctuating term ($Psin\theta\frac{\partial \Omega^{'}}{\partial \theta}$) is neglected. Hence resulting time dependent part of toroidal component of global magnetic field structure for the Alfven perturbations along the direction of rotation is given as follows

$$2\frac{\partial T^{'}}{\partial t} = (\frac{U_0T^{'} + U^{'}T_0}{r})cot\theta - (\frac{U_0}{r}\frac{\partial T^{'}}{\partial \theta} + \frac{U^{'}}{r}\frac{\partial T_0}{\partial \theta}) + (\frac{T_0}{\Omega_0}\frac{\partial \Omega^{'}}{\partial t}). \tag{3.13}$$

Derivative $\frac{\partial T^{'}}{\partial \theta}$ can be modified as follows

$$\frac{\partial T^{'}}{\partial \theta} = \frac{\partial T^{'}}{\partial t}\frac{\partial t}{\partial \theta} = \frac{\partial T^{'}}{\partial t}\frac{1}{U_0}\ , \tag{3.14}$$

where U_0 is steady part of meridional circulation.

On both sides of the equation (3.13), multiply area $A = \pi S^2$ of the flux tube (where S is radius of the tube at a particular depth) and resulting equation for rate

of change of magnetic flux or area (as area of the sunspot is directly proportional to magnetic flux) of the sunspot is given as follows

$$\frac{\partial A}{\partial t} = \frac{U_0 cot\theta A}{2r+1} + \frac{S^2 U^{'}}{2r+1}(T_0 cot\theta - \frac{\partial T_0}{\partial \theta}) + \frac{r S^2 T_0}{(2r+1)\Omega_0}\frac{\partial \Omega^{'}}{\partial t}. \tag{3.15}$$

This equation suggests that rate of change of area of the sunspot is a function of steady part of poloidal and toroidal velocity field structures, radial variations in the fluctuations in the meridional velocity and steady part of toroidal component of magnetic field structure respectively. Although momentum equation is necessary (for the hydrostatic equilibrium of internal structure of the sun, as $\frac{\partial \Omega^{'}}{\partial t}$ is proportional to fluctuating parts of advective terms, Lorentzian force and variation in the second derivative of angular velocity), as fluctuating terms assumed to be small (although in principle not to be neglected), radial variation of last two terms in RHS is neglected. Hence, with the initial conditions that at time $t = 0$, area $A = A_0$ (initial area), solution yields the following relationship between increase of flux tube area (while it raises in the positive rotational gradient) with respect to time.

$$A(t) = A_0 e^{\frac{(U_0 cot\theta)t}{2r+1}} \tag{3.16}$$

As for Alfven perturbations that are opposite to the direction of angular velocity, solution for growth of the sunspot is

$$A(t) = A_0 e^{\frac{(-U_0 cot\theta)t}{2r+1}} . \tag{3.17}$$

Hence, in the region of positive rotational gradient, simultaneous growth and decay of the Alfven wave perturbations exist yielding net exponential growth of the sunspot. Another interesting property of solution (equation 3.16) is that exponent of the growth part depends upon magnitude of meridional velocity U_0, $cot\theta$ and the depth of the foot point of the flux tube where it is anchored. It is not known how the meridional velocity varies with depth and it is assumed to be constant. Thus as time progresses, due to buoyancy, anchored feet lifts from interior in the positive rotational gradient (until it reaches maximum angular velocity at the depth $0.935 R_{\odot}$), there is an exponential growth of area of the sunspot.

If one keeps the ratio $\frac{U_0}{2r+1}$ constant at a particular depth (say near the surface), exponent of solution for growth of area is directly proportional to $cot\theta$. That means by the property of $cot\theta$ function, spots at the lower co-latitudes θ (or higher heliographic latitudes) grow very fast compared to the spots that grow at the lower co-latitudes (or lower heliographic latitudes, i,e., near the equator). This important property of sunspot's growth will be tested in the following sections.

Once sunspot's anchoring enter the negative rotational gradient, the picture will be different and it will be known from the next section that area of the sunspot decays exponentially and ultimately disappears on the surface.

3.4 Solution for decay of the sunspot

After substituting equations (3.1) and (3.2) in equation (3.5) and also by satisfying the continuity equation (3.4), resulting toroidal component of the induction equation with a sink term in spherical coordinates is

$$\frac{\partial T}{\partial t} = \eta\big[\frac{1}{r^2}\frac{\partial^2 T}{\partial \theta^2} + \frac{1}{r^2 sin^2\theta}\frac{\partial^2 T}{\partial \phi^2} + \frac{cot\theta}{r^2}\frac{\partial T}{\partial \theta} - \frac{T}{r^2 sin^2\theta}\big]. \tag{3.18}$$

Adopting a similar method in the previous section, this equation can be transformed into following equation for steady part of toroidal component of the induction equation

$$\frac{\partial^2 T}{\partial t^2} - (r^2 sin^2\theta\frac{\partial \Omega}{\partial t} + \frac{\Omega^2 r^2 sin^2\theta}{\eta})\frac{\partial T}{\partial t} + \frac{\Omega sin^2\theta}{\eta}\frac{\partial^2 T}{\partial \theta^2} + \frac{\Omega sin^2\theta cot\theta}{\eta}\frac{\partial T}{\partial \theta} - \frac{\eta T}{r^2 sin^2\theta} = 0. \tag{3.19}$$

Following similar perturbation method in the previous section, we get the following time dependent component of the toroidal component of magnetic field structure

$$A_1\frac{\partial^2 T'}{\partial t^2} + A_2\frac{\partial T'}{\partial t} + A_3 T' = 0\ , \tag{3.20}$$

where

$$A_1 = 1 + \frac{\Omega' sin^2\theta}{\eta {U_0}^2}\ , \tag{3.21}$$

$$A_2 = r^2 sin^2\theta\frac{\partial \Omega'}{\partial t} + \frac{\Omega_0^2 r^2 sin^2\theta}{\eta} + 2\frac{\Omega_0\Omega' r^2 sin^2\theta}{\eta} + \frac{\Omega' sin^2\theta}{\eta {U_0}^3}\frac{\partial U_0}{\partial t} - \frac{\Omega' sin^2\theta cot\theta}{\eta U_0}\ , \tag{3.22}$$

and

$$A_3 = -\Omega_0. \tag{3.23}$$

On both sides of the equation (3.20), multiply area $A = \pi S^2$ of the flux tube (where S is radius of the tube). As amplitude $\Omega^{'}$ of fluctuations in angular velocity assumed to be negligible compared to steady part of the angular velocity, then we have the analytical solution for variation of the sunspot area with respect to time in case of perturbations along the direction of angular velocity

$$A(t) = c_1 e^{D_1 t} + c_2 e^{-D_2 t} \ , \tag{3.24}$$

where c_1 and c_2 are integrational constants and,

$$D_1 = \frac{1}{2}[\frac{\Omega_0^2 r^2 sin^2\theta}{\eta} + \sqrt{(\frac{\Omega_0^2 r^2 sin^2\theta}{\eta})^2 + 4\Omega_0}] \ , \tag{3.25}$$

and

$$D_2 = \frac{1}{2}[\frac{\Omega_0^2 r^2 sin^2\theta}{\eta} - \sqrt{(\frac{\Omega_0^2 r^2 sin^2\theta}{\eta})^2 + 4\Omega_0}] \ , \tag{3.26}$$

As second term in the square root is negligible compared to the first term, solution for decay part of the area of the sunspot with respect to time is given as

$$A(t) = c_1 e^{(\frac{\Omega_0^2 {R_\odot}^2 x^2 sin^2\theta}{\eta})t} + c_2 \ , \tag{3.27}$$

where $x = \frac{r}{R_\odot}$ and $R_\odot$ is the radius of the sun. Although, mathematically, solution has an exponential growth, physically, in the region of negative rotational gradient as flux tube lifts its anchored feet (due to buoyancy) towards surface, the distance (difference between sunspot's anchored depth and the surface) r decreases, angular velocity Ω_0 decreases and magnetic diffusivity η ($T^{-3/2}$, where T is ambient temperature) increases and hence resulting area decreases.

If one keeps the ratio Ω_0^2/η constant at a particular depth (say near the surface), exponent of the decay is directly proportional to $sin^2\theta$. That means spots at the lower co-latitudes θ (or higher heliographic latitudes) decay very slow compared to the spots that decay at the higher co-latitudes (or lower heliographic latitudes, i,e.,

near the equator). This important decay property will be tested in the following sections.

As for the Alfven perturbations opposite to the direction of angular velocity in the solar interior, solution yields

$$A(t) = c_1 e^{(\frac{-\Omega_0^2 {R_\odot}^2 x^2 sin^2\theta}{\eta})} t + c_2 \tag{3.28}$$

Hence, in the region of negative rotational gradient, at a particular latitude and depth, summation of these two solutions effectively constitutes the decay of area of the sunspots.

3.5 Results and conclusion

In order to test results of the physical ideas on the growth and decay of the sunspots that are presented in the previous sections, data of time evolution of corrected areas of non-recurrent sunspot groups from Greenwich Photoheliographic Results (GPR) are used. For the four latitude zones of $0-10$, $10-20$, $20-30$ and $30-40$ degrees two spot groups that lie between $\pm$ 70 degree from the central meridian and life spans in the range of 8-10 days are considered.

In Figures 3.2-3.9 time evolution of growth of area of the non-recurrent sunspot groups are presented. It is assumed that sunspot area grows linearly, quadratically and exponentially and relevant laws are fitted with the observed growth of area of the sunspot groups. As measured uncertainties in the areas of sunspot groups are not available in GPR, it is assumed that growth and decay of area curves follow the Poisson distribution and hence uncertainty in each of measured area $A(t)$ (where t day of observation) is taken as $A(t)^{1/2}$. By knowing area $A(t)$ values and their uncertainties, all the three laws are fitted to the observed sunspots' area growth curves and are over plotted on top of the each plot. In all the Figures 3.2-3.9, the plots in the top are for the linear and quadratic fits and the the plot at the bottom is fit for the exponential growth law.

Similarly, in Figures 3.10-3.17, observed decay of area of the sunspot groups for all the four latitude zones are presented. In addition to three (viz., linear, quadratic,

exponential) decay laws, a law of log-normal distribution is also considered for fitting the observed decay curves. In all the Figures 3.10-3.17, first and second plots in the top row are for linear and quadratic decay fits respectively. In the second row of Figures 3.10-3.17, log-normal and exponential decay fits are presented.

As for growth of the sunspots, it is interesting to note that among all the Figures 3.2-3.9, exponential fit is best one. This is also clearly evident from the χ^2 values presented in Table 3.1. In the Table 3.1, first column represents latitude of occurrence of the sunspot, second column represents lifespan and, columns 3-5 represent χ^2 values for linear, quadratic and exponential fits. It is to be noted that low value of χ^2 means, observed and expected curves are almost similar. In Table 3.2, constants C_1 and C_2 of exponential growth and decay parts of the area curve are presented. First column represents latitude of occurrence of the spot group, second and third columns represent the constants C_1 and C_2 that are determined from the exponential growth and, fourth and fifth columns represent the constants that are determined from fits of exponential decay of the sunspot area curve respectively. Another important property, according to theoretical expectations presented in section 3.3 regarding growth of the sunspot, as is evident from Table 3.2 (see the third column) that the exponent of the exponential fit for the high heliographic latitude is high compared to the exponential fits for the low heliographic latitudes. That means the spots that formed at the high latitudes grow fast (with exponential growth) and the spots that are formed near the low heliographic latitudes grow slowly.

Table 3.1: χ^2 fit for the laws of linear, quadratic and exponential growth of the sunspot.

Latitude	Life span (Days)	Linear	Quadratic	Exponential
0 - 10°	9	6.65	4.15	0.03
0 - 10°	9	26.35	1.64	0.02
10 - 20°	9	4.39	2.54	0.29
10 - 20°	10	0.19	0.18	0.02
20 - 30°	10	257.98	69.37	0.11
20 - 30°	10	487.63	9.67	0.13
30 - 40°	8	2.60	2.60	0.02
30 - 40°	9	46.68	16.75	0.39

Table 3.2: Values of constants obtained from growth and decay of the exponential fits.

	Growth		Decay	
Latitude	C_1	C_2	C_1	C_2
0 - 10°	39.65±15.93	0.26±0.66	395.44±6.17	0.93±0.56
0 - 10°	4.57±3.22	0.59±0.41	208.51±4.71	0.98±0.28
10 - 20°	12.31±4.18	0.72±0.58	138.38±1.08	0.43±0.35
10 - 20°	60.95±7.10	0.54±0.93	403.434±6.17	0.55±0.48
20 - 30°	36.23±5.31	0.63±0.54	5.02±1.45	0.14±0.27
20 - 30°	12.18±3.86	0.65±0.34	212.73±6.23	0.27±0.53
30 - 40°	29.08±5.53	0.14±0.62	92.76±4.02	0.38±0.26
30 - 40°	30.27±5.10	0.68±0.61	391.51±6.11	0.46±0.50

As for decay of the sunspots, even though log-normal fit appears to be a very good fit among all the Figures 3.10-3.17, from criterion of goodness of fit of χ^2 value, exponential decay fit is best one. In fact this result is also clearly evident from the values of χ^2 presented in Table 3.3. Similarly we have another important property from these results. According to theoretical expectations presented in section 3.4 regarding decay of the sunspots, exponent of the exponential fit (see the 5^{th} column of Table 3.2) for the high heliographic latitude is very low compared to exponent of the exponential fits for the low heliographic latitudes. That means the spots that are formed at the high latitudes decay slowly compared to the spots that are formed near the low heliographic latitudes.

Even with approximations by neglecting fluctuations in poloidal (meridional) and toroidal (angular) components of velocity fields, theoretical solutions of growth (equation 3.16) and decay (equation 3.28) parts of sunspot's area evolutionary phases match with the observed area evolutionary phases. In order to understand a unique single solution for understanding growth and area decay curve, one should solve consistently full set of MHD equations (as the neglected fluctuations $\frac{\partial \Omega'}{\partial t}$ in turn depend upon fluctuations in the momentum equations).

From the observed characteristics of growth and decay of the sunspots and from the theoretical ideas and inferences one can safely conclude that sunspots are formed due to constructive interference of toroidal Alfven wave perturbations and, after attaining a critical strength in the convective envelope, due to buoyancy, sunspots

raise along isorotational contours and reach the respective latitudes. It is understood from this study that growth and decay phases of the sunspots do not depend upon not only on the surface physical characteristics , as this problem was treated by the earlier studies, but also evolutionary history of internal dynamics and magnetic field structure of the sunspot while it raising towards the surface. As the sunspot is a three dimensional structure whose evolutionary history not only depends upon it's internal structure but also one has to consider the ambient dynamic properties for the combined solution of growth and decay of the sunspot.

Table 3.3: χ^2 fit for the laws of linear, quadratic, log-normal and exponential decay of the sunspot.

Latitude	Life span (Days)	Linear	Quadratic	Log-normal	Exponential
0 - 10°	8	19.82	7.77	1.17	0.29
0 - 10°	9	9.12	3.29	0.05	0.03
10 - 20°	10	53.27	6.37	0.23	0.08
10 - 20°	8	101.64	62.45	0.26	0.13
20 - 30°	10	16.60	17.28	0.13	0.08
20 - 30°	10	24.56	3.29	0.08	0.05
30 - 40°	8	17.38	17.28	2.44	0.91
30 - 40°	8	36.84	31.51	0.36	0.12

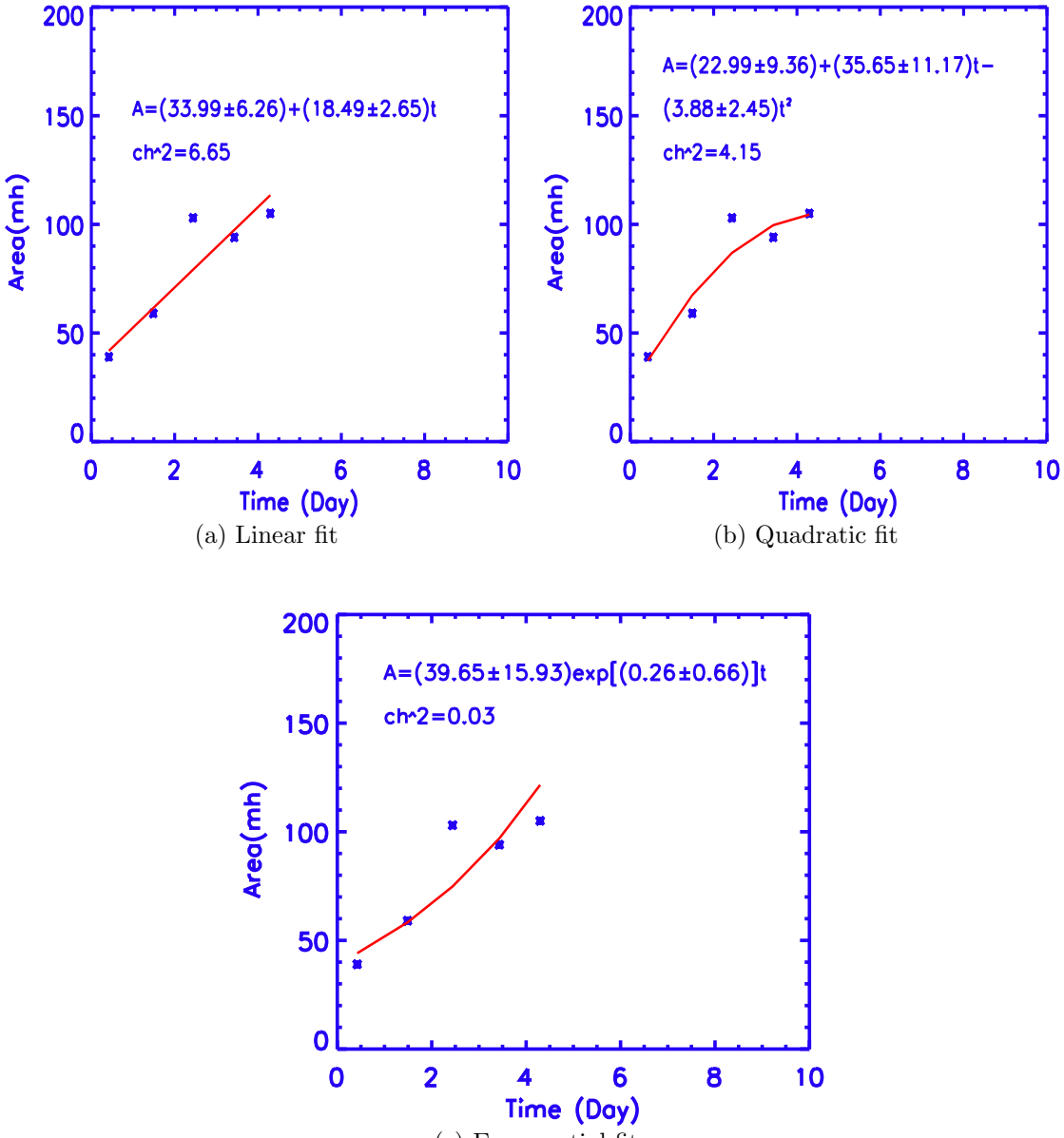

(a) Linear fit

(b) Quadratic fit

(c) Exponential fit

Figure 3.2: Evolution of growth of area A of non-recurrent sunspot group at a latitude region of 0 -10° that has lifespan of 8 days. Red line is theoretical area growth curve over plotted on the observed area growth curve (blue cross points).

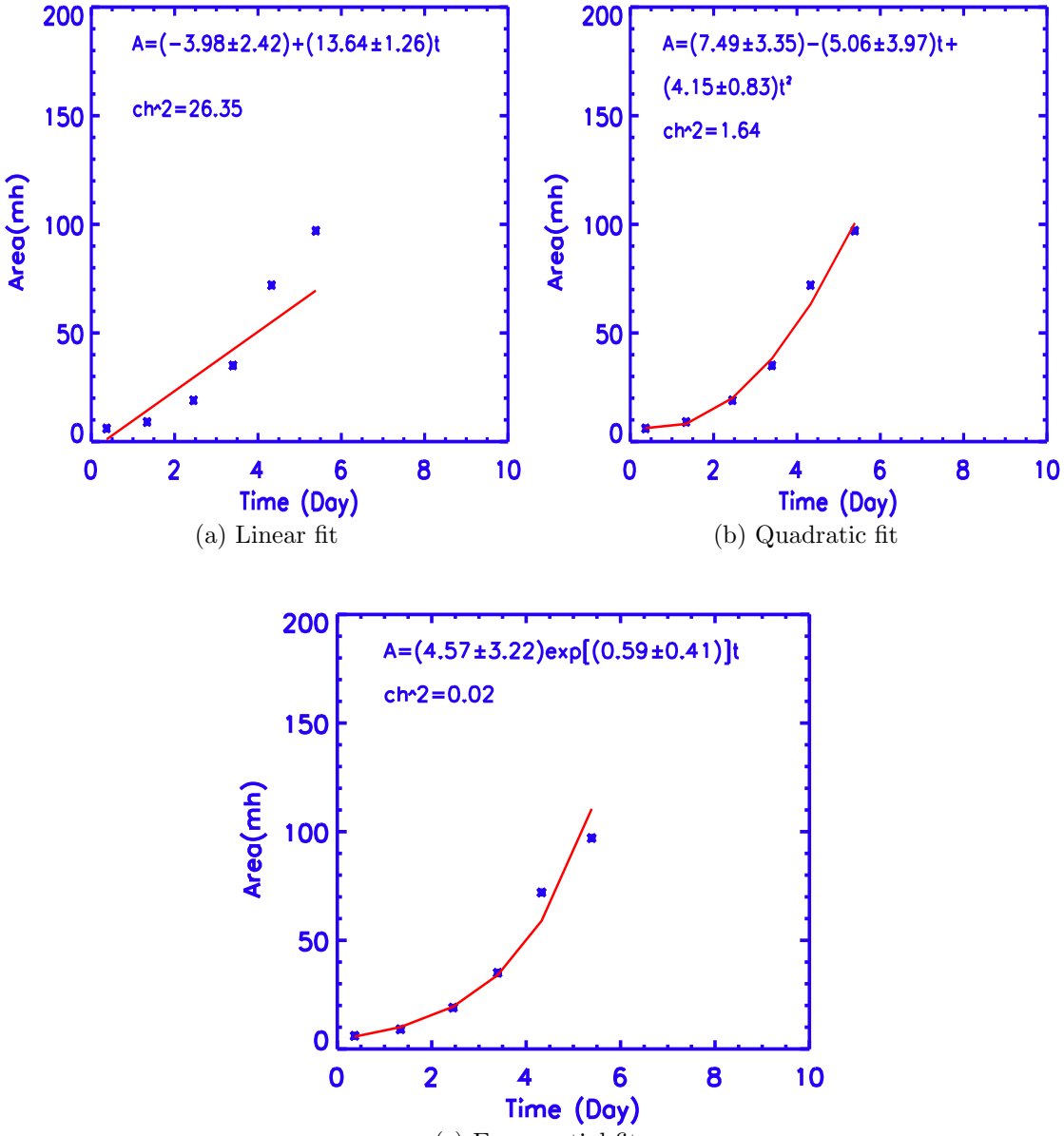

(a) Linear fit

(b) Quadratic fit

(c) Exponential fit

Figure 3.3: Evolution of growth of area A of non-recurrent sunspot group at a latitude region of 0 -10° that has lifespan of 8 days. Red line is theoretical area growth curve over plotted on the observed area growth curve (blue cross points).

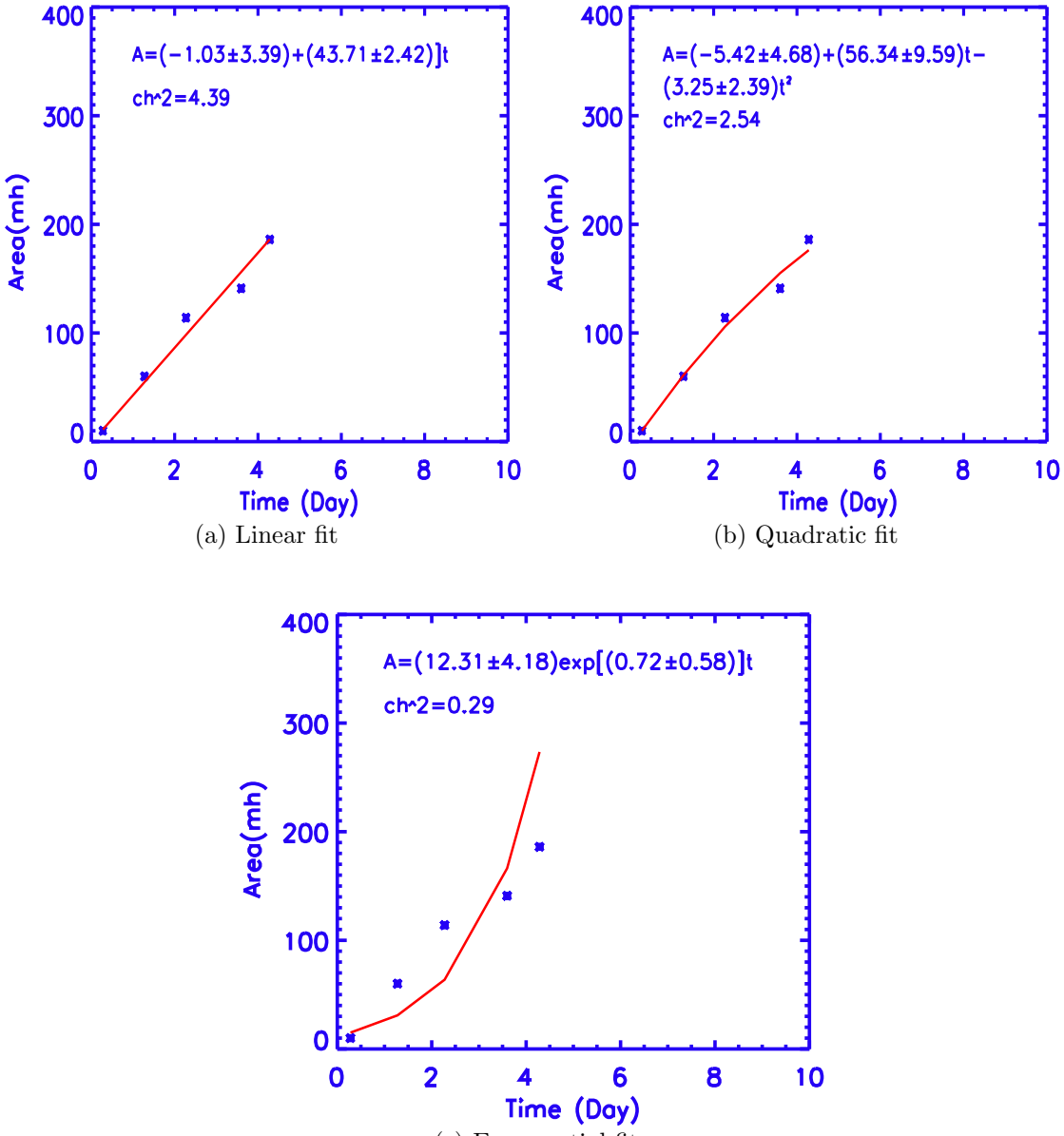

(a) Linear fit

(b) Quadratic fit

(c) Exponential fit

Figure 3.4: Evolution of growth of area A of non-recurrent sunspot group at a latitude region of 10 -20° that has lifespan of 8 days. Red line is theoretical area growth curve over plotted on the observed area growth curve (blue cross point).

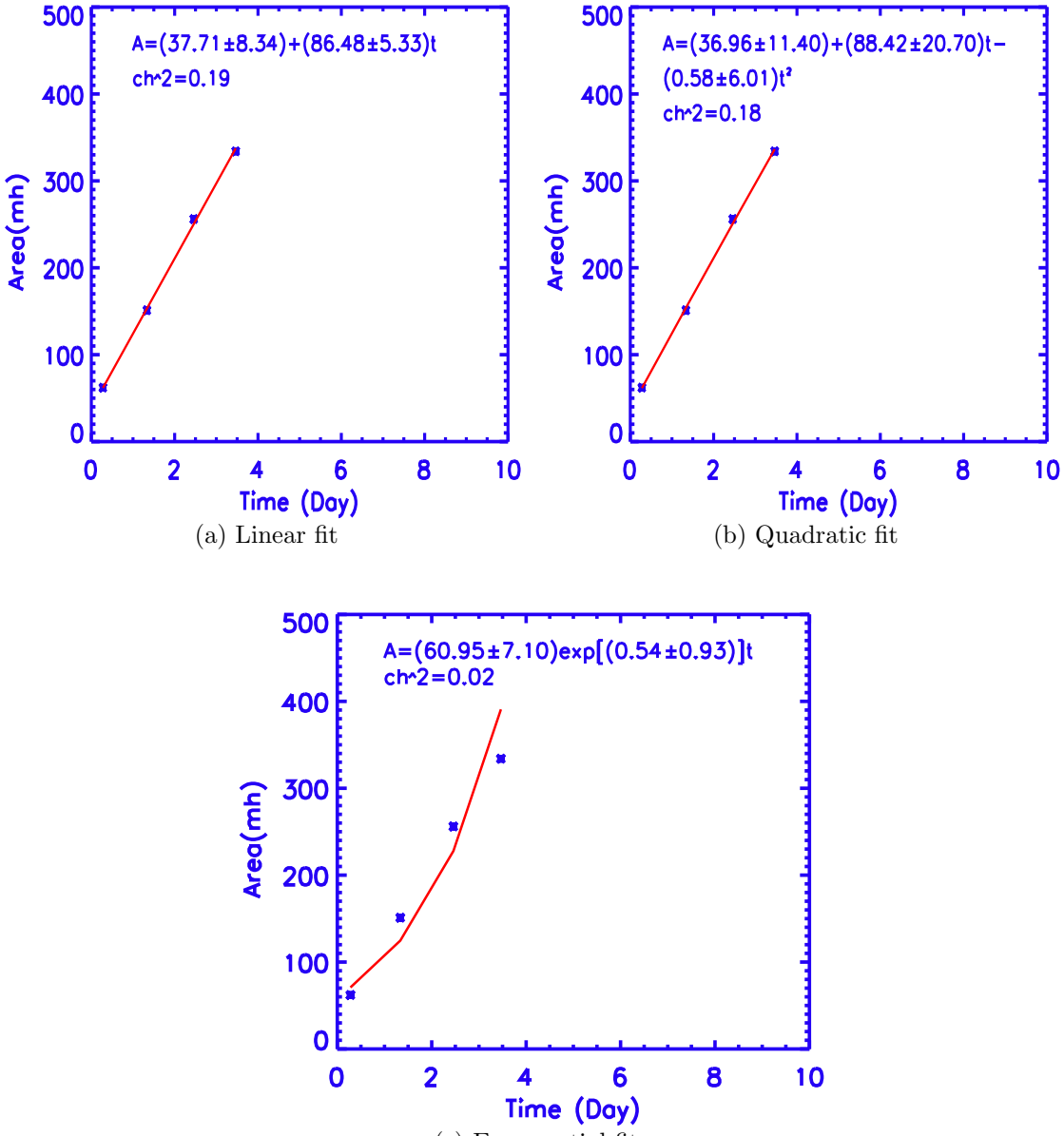

(a) Linear fit

(b) Quadratic fit

(c) Exponential fit

Figure 3.5: Evolution of growth of area A of non-recurrent sunspot group at a latitude region of 10 -20° that has lifespan of 10 days. Red line is theoretical area growth curve over plotted on the observed area growth curve (blue cross points).

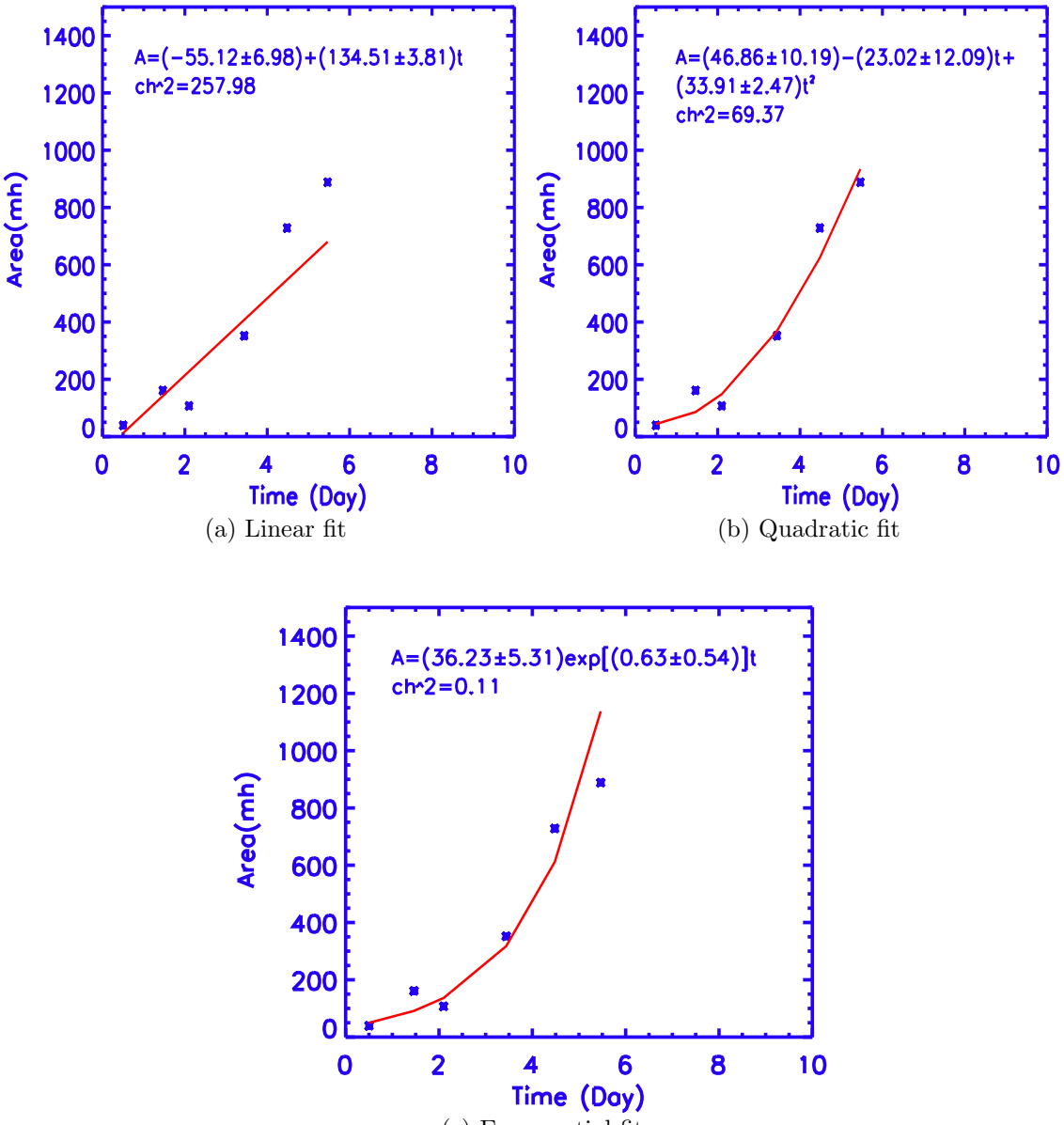

(a) Linear fit

(b) Quadratic fit

(c) Exponential fit

Figure 3.6: Evolution of growth of area A of non-recurrent sunspot group at a latitude region of 20 -30° that has lifespan of 10 days. Red line is theoretical area growth curve over plotted on the observed area growth curve (blue cross points).

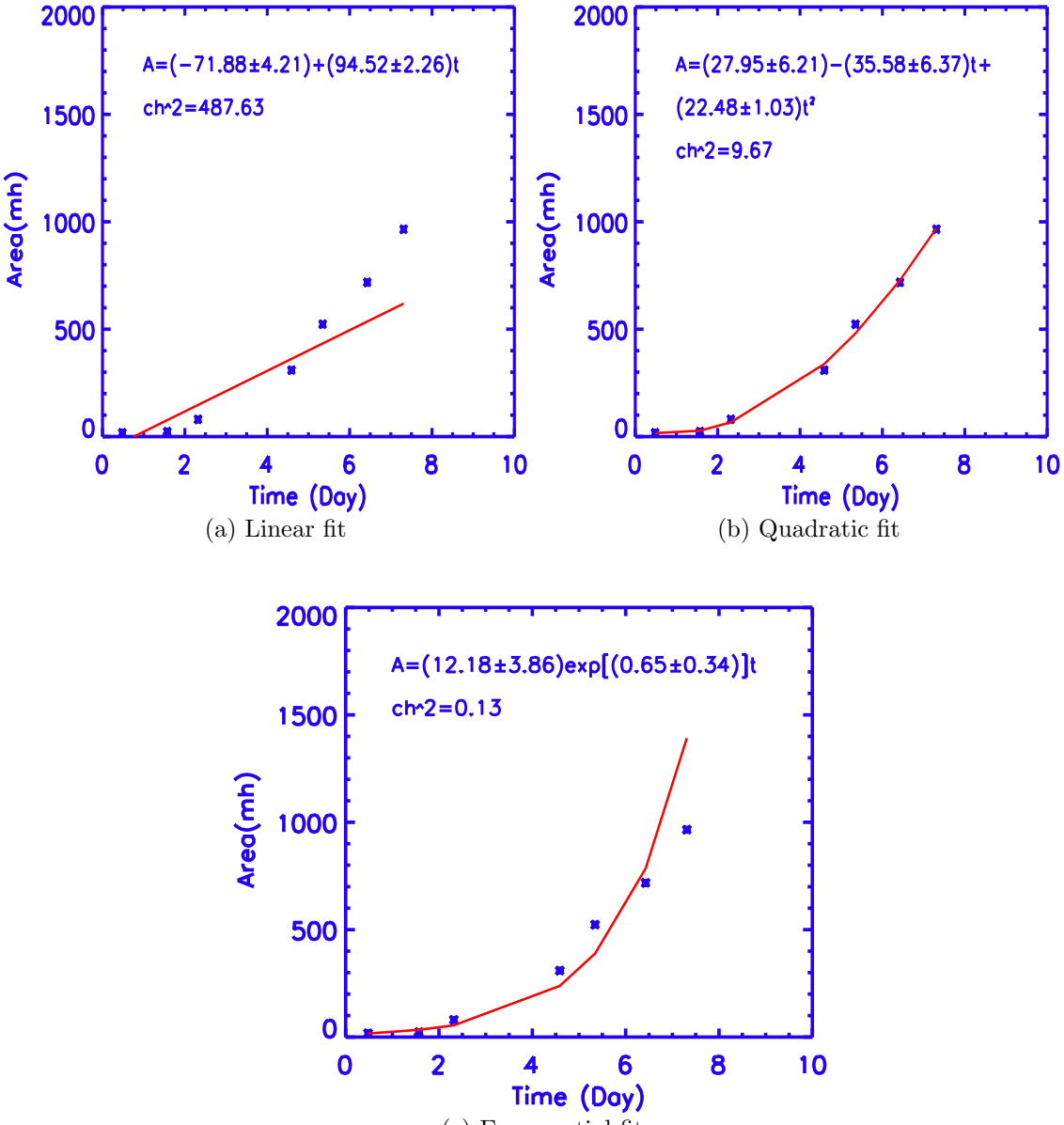

(a) Linear fit

(b) Quadratic fit

(c) Exponential fit

Figure 3.7: Evolution of growth of area A of non-recurrent sunspot group at a latitude region of 20 -30° that has lifespan of 10 days. Red line is theoretical area growth curve over plotted on the observed area growth curve (blue cross points).

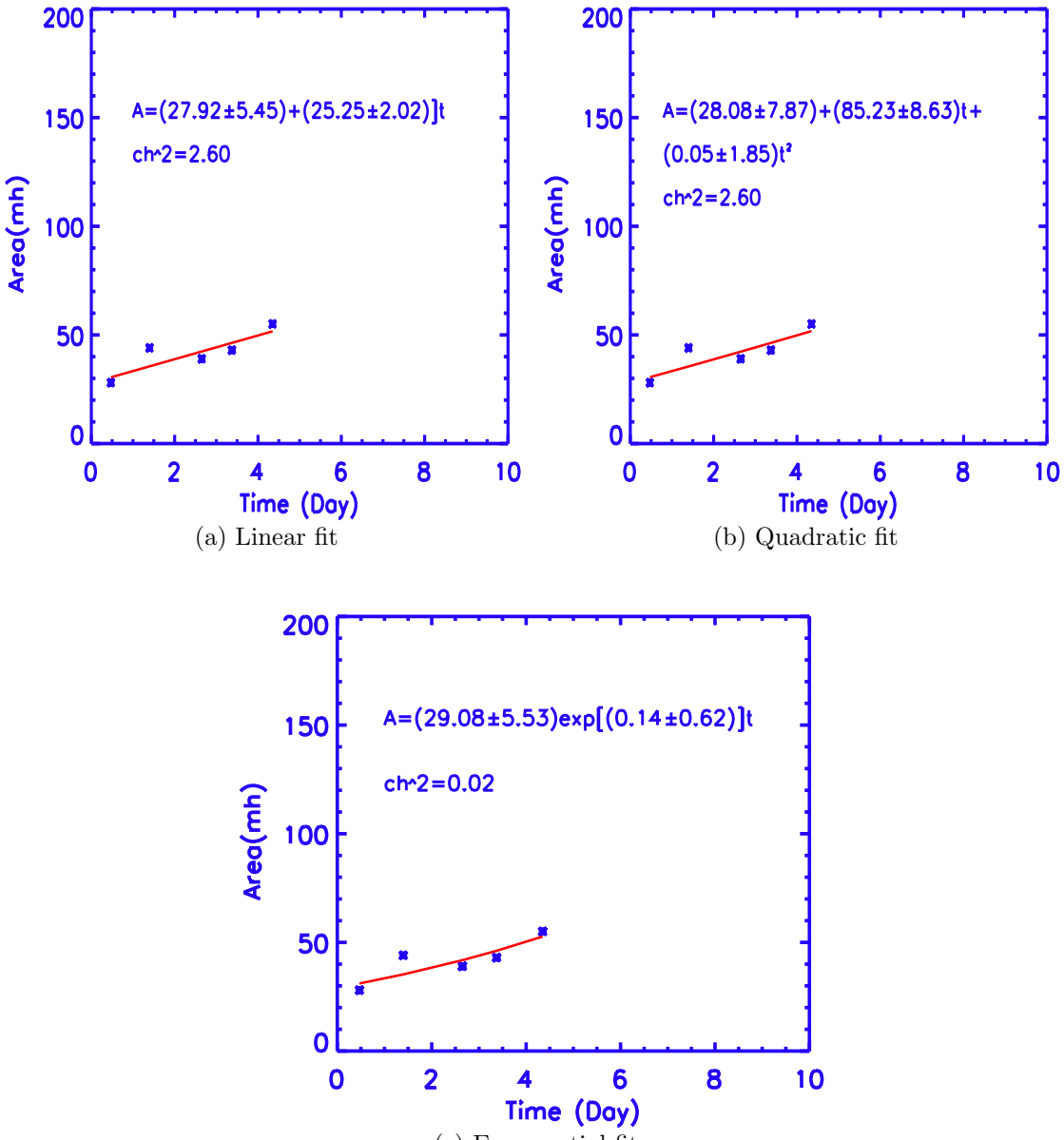

(a) Linear fit

(b) Quadratic fit

(c) Exponential fit

Figure 3.8: Evolution of growth of area A of non-recurrent sunspot group at a latitude region of 30 -40° that has lifespan of 8 days. Red line is theoretical area growth curve over plotted on the observed area growth curve (blue cross points).

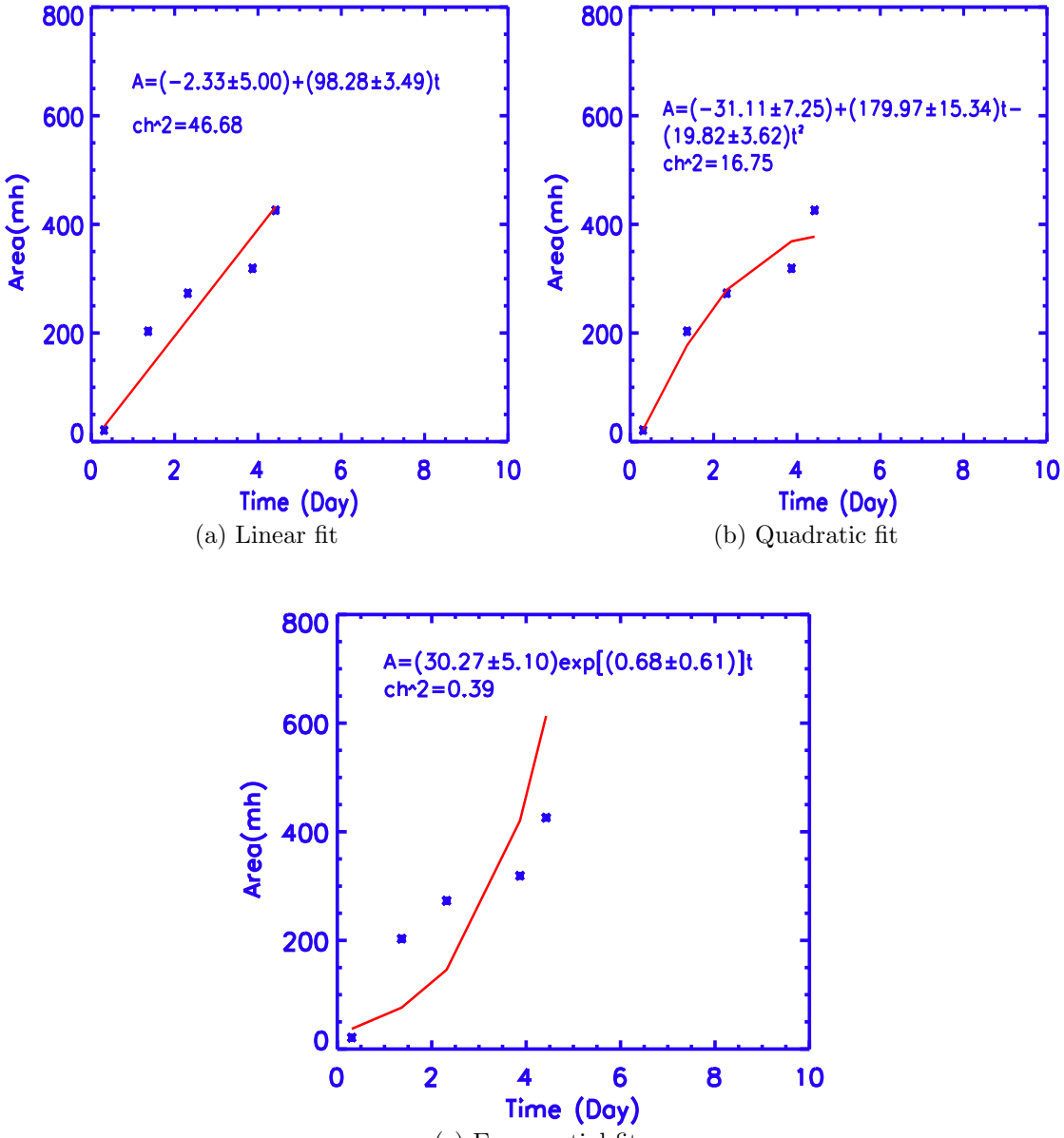

(a) Linear fit

(b) Quadratic fit

(c) Exponential fit

Figure 3.9: Evolution of growth of area A of non-recurrent sunspot group at a latitude region of 30 -40° that has lifespan of 9 days. Red line is theoretical area growth curve over plotted on the observed area growth curve (blue cross point).

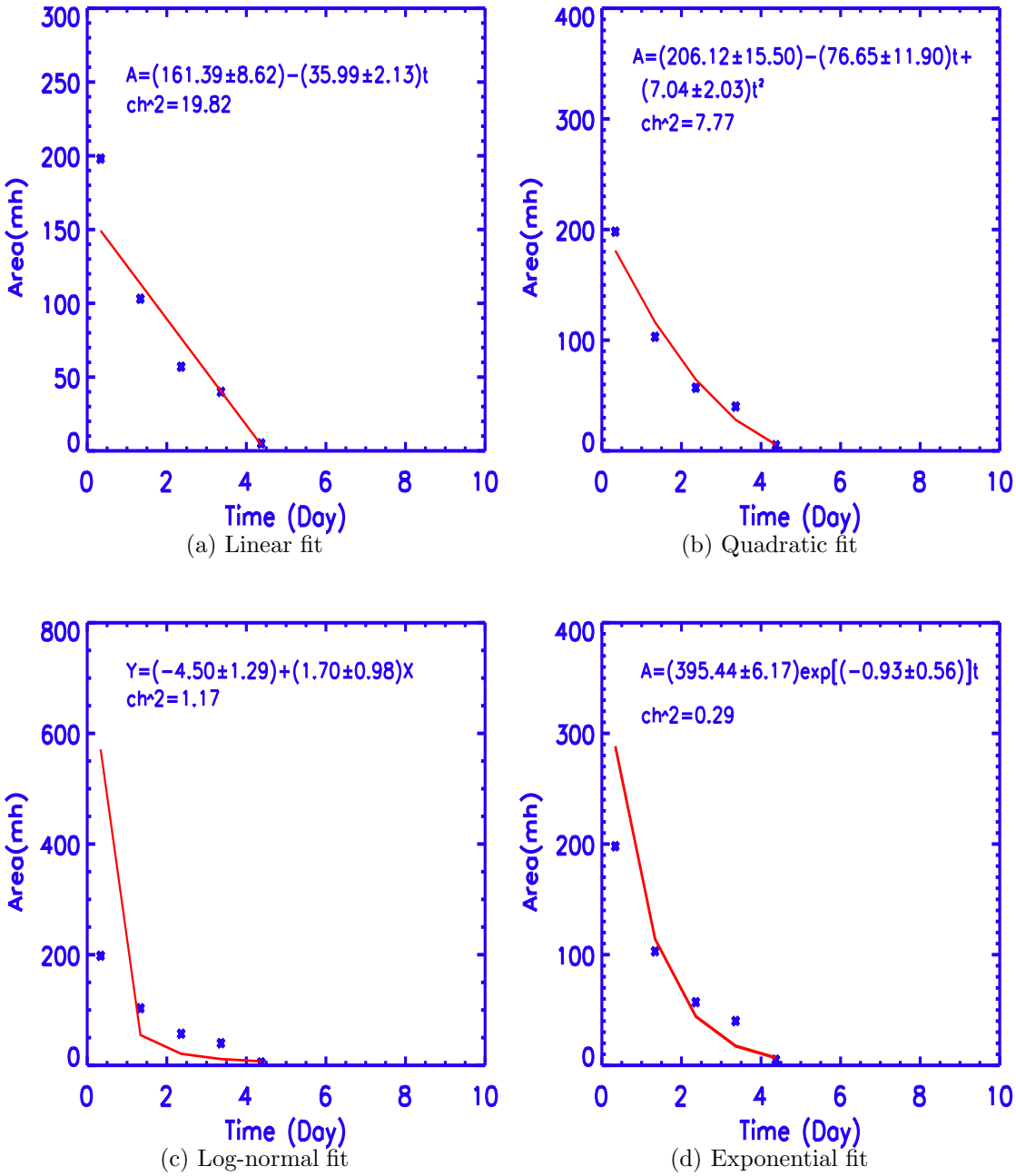

(a) Linear fit (b) Quadratic fit

(c) Log-normal fit (d) Exponential fit

Figure 3.10: Evolution of decay of area A of non-recurrent sunspot group at a latitude region of 0 -10° that has lifespan of 9 days. In Fig (c), X=ln(Time) and Y=-ln(A). Red line is theoretical area decay curve over plotted on the observed area decay curve (blue cross points).

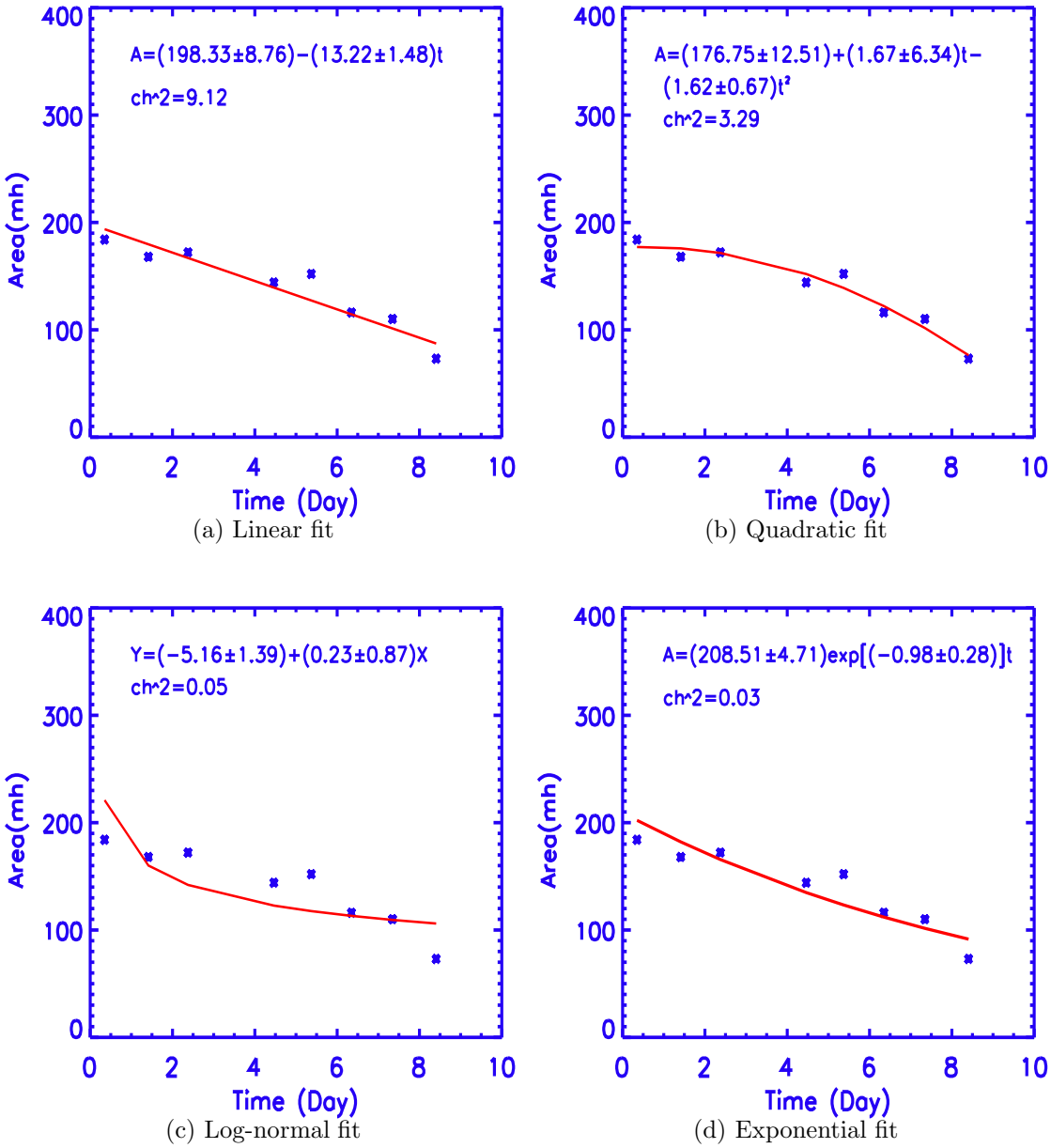

(a) Linear fit (b) Quadratic fit

(c) Log-normal fit (d) Exponential fit

Figure 3.11: Evolution of decay of area A of non-recurrent sunspot group at a latitude region of 0 -10° that has lifespan of 9 days. In Fig (c), X=ln(Time) and Y=-ln(A). Red line is theoretical area decay curve over plotted on the observed area decay curve (blue cross points).

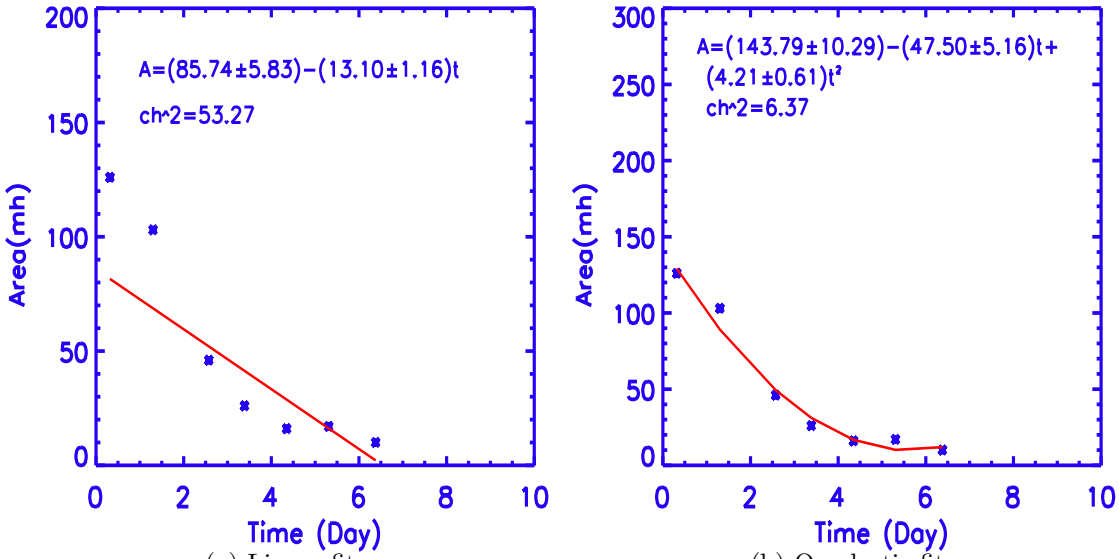

(a) Linear fit (b) Quadratic fit

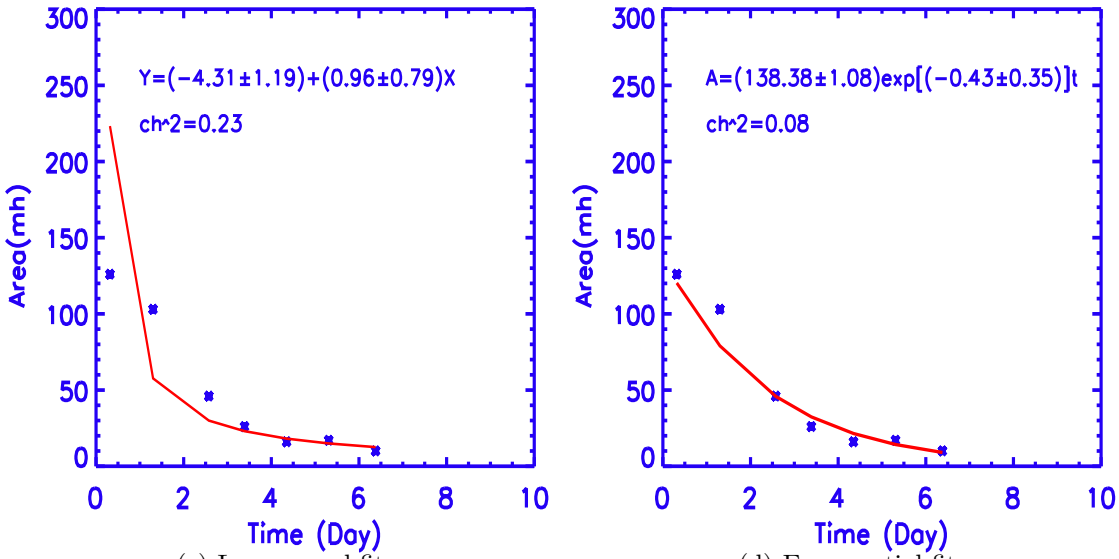

(c) Log-normal fit (d) Exponential fit

Figure 3.12: Evolution of decay of area A of non-recurrent sunspot group at a latitude region of 10 -20° that has lifespan of 10 days. In Fig (c), X=ln(Time) and Y=-ln(A). Red line is theoretical area decay curve over plotted on the observed area decay curve (blue cross points).

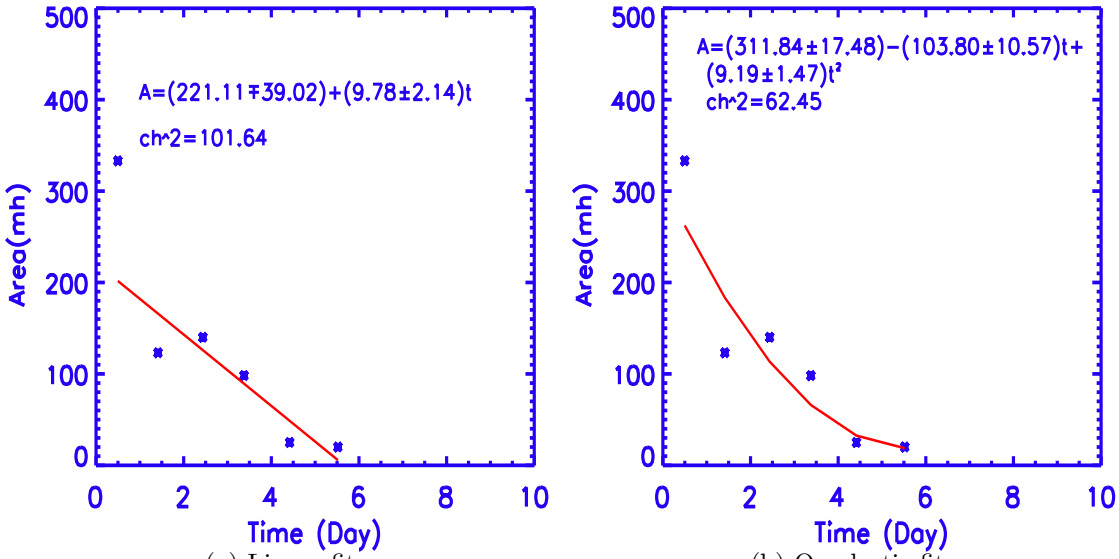

(a) Linear fit (b) Quadratic fit

(c) Log-normal fit (d) Exponential fit

Figure 3.13: Evolution of decay of area A of non-recurrent sunspot group at a latitude region of 10 -20° that has lifespan of 9 days. In Fig (c), X=ln(Time) and Y=-ln(A). Red line is theoretical area decay curve over plotted on the observed area decay curve (blue cross points).

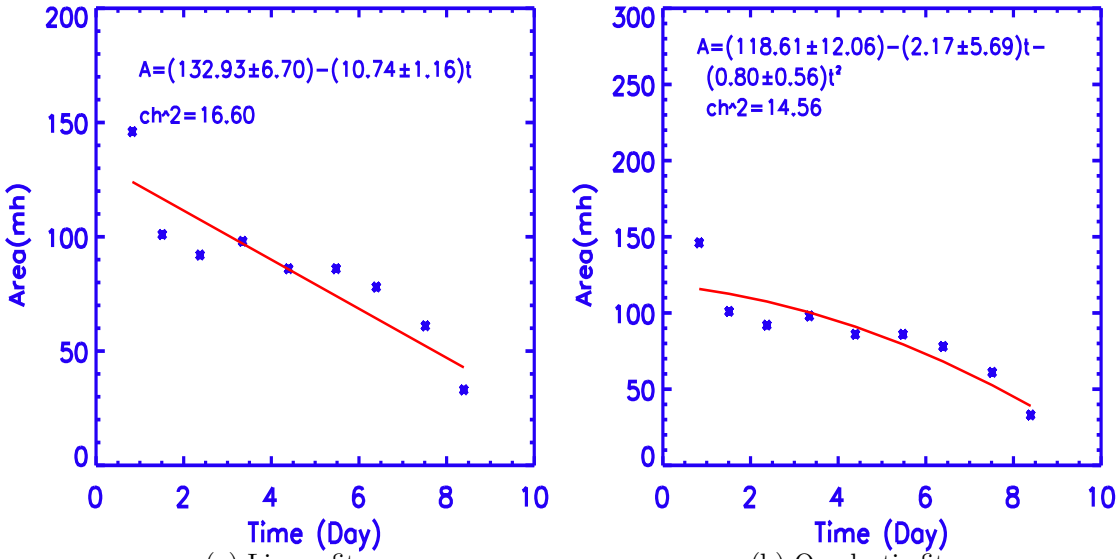

(a) Linear fit (b) Quadratic fit

(c) Log-normal fit (d) Exponential fit

Figure 3.14: Evolution of decay of area A of non-recurrent sunspot group at a latitude region of 20 -30° that has lifespan of 10 days. In Fig (c), X=ln(Time) and Y=-ln(A). Red line is theoretical area decay curve over plotted on the observed area decay curve (blue cross points).

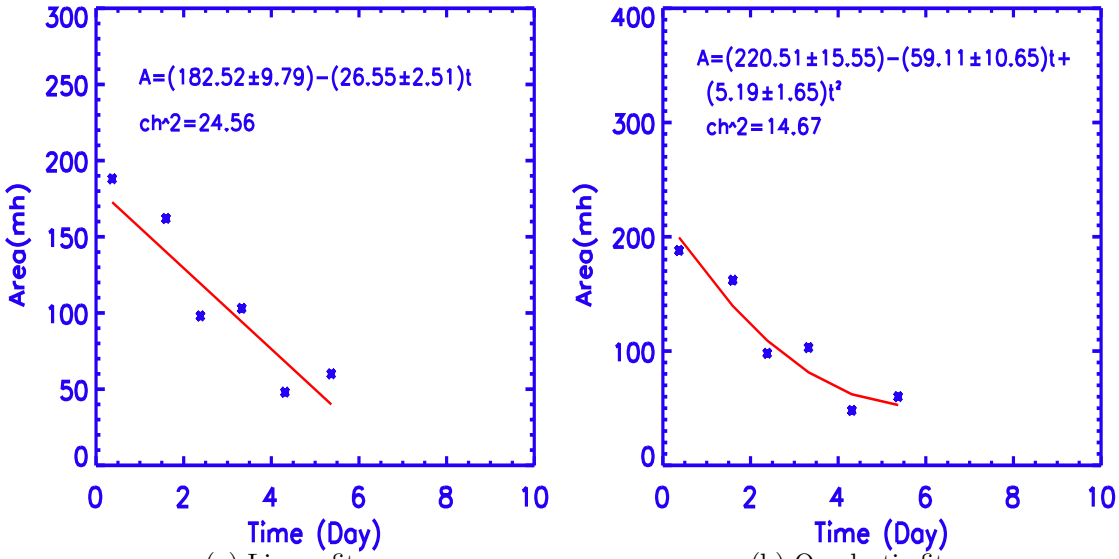

(a) Linear fit (b) Quadratic fit

(c) Log-normal fit (d) Exponential fit

Figure 3.15: Evolution of decay of area A of non-recurrent sunspot group at a latitude region of 20 -30° that has lifespan of 10 days. In Fig (c), X=ln(Time) and Y=-ln(A). Red line is theoretical area decay curve over plotted on the observed area decay curve (blue cross points).

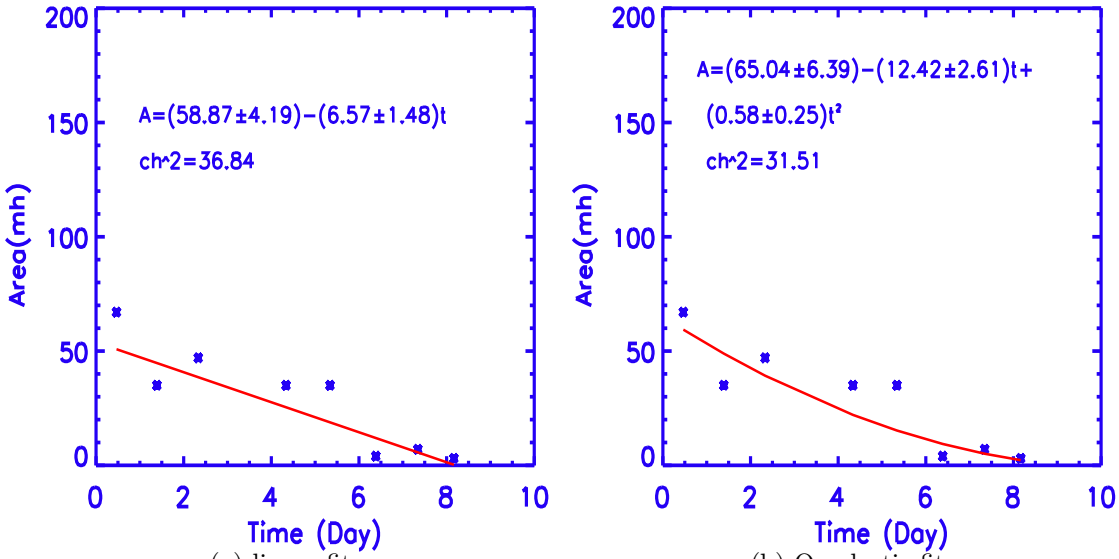

(a) linear fit (b) Quadratic fit

(c) Log-normal fit (d) Exponential fit

Figure 3.16: Evolution of decay of area A of non-recurrent sunspot group at a latitude region of 30 -40° that has lifespan of 8 days. In Fig (c), X=ln(Time) and Y=-ln(A). Red line is theoretical area decay curve over plotted on the observed area decay curve (blue cross points).

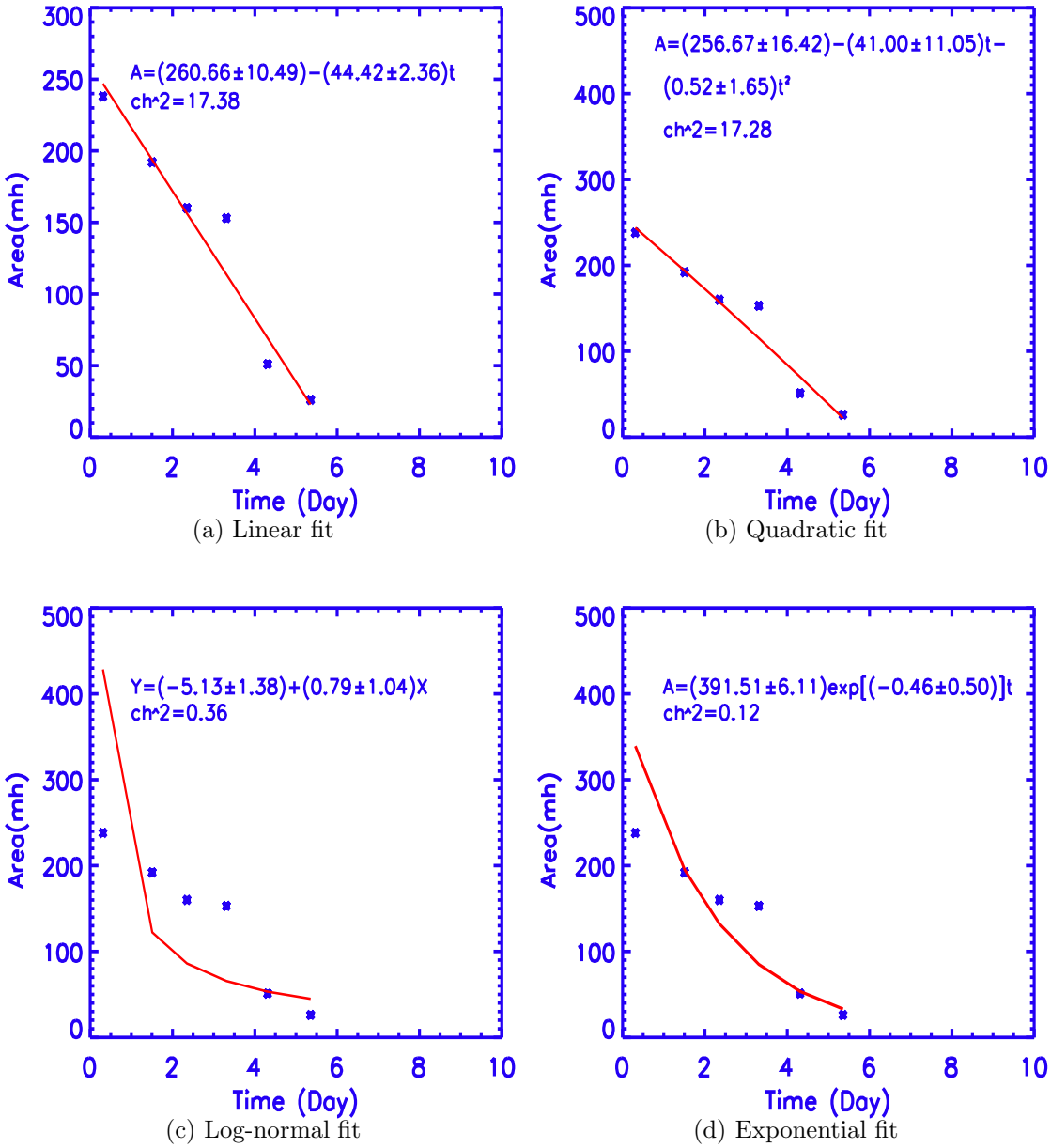

(a) Linear fit (b) Quadratic fit

(c) Log-normal fit (d) Exponential fit

Figure 3.17: Evolution of decay of area A of non-recurrent sunspot group at a latitude region of 30 -40° that has lifespan of 8 days. In Fig (c), X=ln(Time) and Y=-ln(A). Red line is theoretical area decay curve over plotted on the observed area decay curve (blue cross points).

Chapter 6

Inference of toroidal magnetic field structure in the convective envelope

6.1 Introduction

General consensus is that the observed bipolar sunspots are Ω shaped toroidal field structures that are supposed to be formed in the convective envelope and due to buoyancy rise towards the surface. Owing to sunspots' close relationship with the solar magnetic cycle and activity phenomena that are sustained by the underlying unknown dynamo mechanism, it is of considerable interest to know their magnetic field strengths at different anchoring depths in the convective envelope.

It is believed that the dynamo-the source and maintenance of the solar cycle and activity phenomena-is operating just below the base of convection zone, probably in the tachocline region (a transitional region between the differentially rotating convective envelope and rigidly rotating outer part of the radiative envelope)-wherein time dependent toroidal magnetic field structure erupts with the phase of the solar cycle. In order that erupted toroidal field structure reaches at the proper latitude, strength of the magnetic field structure at base of the convection zone is one of the crucial parameter.

For example, in order to satisfy the observed properties such as sunspots' appearances in particular latitude zones, tilts of the bipolar spots and properties of rotation rates of the bipolar spots, numerical simulations (D'Silva & Choudhuri 1993; D'Silva

& Howard 1993, 1994) of thin flux tube approximations put the limit on strength of the toroidal magnetic field structure near base of the convection zone to be in the range of 60-160 kG ruling out either equipartition field ($\sim 10^4$ G) as expected by the dynamo models (Parker 1987) or the mega Gauss field structure as inferred from the helioseismology (Dziembowski & Goode 1989). The numerical MHD simulations with realistic physics (van Ballegooijen 1983; Fan et al. 1992; Fisher et al. 2000; Wissink et al. 2000; Nordlund et al. 2000; Dorch & Nordlund 2001; Abbett et al. 2001; Fan 2004; Fan et al. 1992; Ferriz-Mas & Steiner 2007; Fan 2008; Brun & Rempel 2009) and studies on MHD instabilities (Gilman & Fox 1999; Durney 2000; Arlt et al. 2007; Dikpati et al. 2009) near tachocline region arrive at almost similar conclusion.

With reasonable assumptions and approximations relevant to the physics of the solar convective envelope, Hiremath (2001) obtained the steady part of the toroidal component of the magnetic field structure that is compatible with the strength of rotational profile as inferred by the helioseismology. The solution yields a dipole like toroidal field structure near the surface and a quadruple like toroidal field structure with a strength ~ 30 kG near base of the convection zone. If such a steady toroidal field structure exists in the convective envelope, perturbation of such a steady field structure with a similar constraint used in the solution of a thin flux tube approximation leads to standing MHD oscillations along the toroidal field ring that superpose to yield the required sunspot structure. Recently an independent study (Itoh et al. 2007) from the cross-helicity-driven dynamo magnetic field structure with the influence of rotation predicts the existence of such a toroidal field structure with a similar geometrical structure in the convective envelope. Lastly in order to explain the seasonal oscillations of the solar neutrino fluxes existence of such a toroidal magnetic field structure (Kubota et al. 1994) in the convective envelope is essential.

Aims of the present study in this chapter are three fold : during their initial appearance on the surface, (i) measure strength of line of sight component of the bipolar magnetic field structure from the SOHO/MDI magnetograms, (ii) separate and estimate the toroidal component of the magnetic field structure from the line of sight component and, (iii) following Parker's (1955b) flux tube model, derive

the same equations in the spherical coordinates and use Hiremath's(2002) life span anchoring depth information to infer the line of sight and toroidal components of the magnetic field structures at different anchoring depths of the bipolar spots in the convective envelope.

In order to estimate strength of toroidal component of the magnetic field structure of the bipolar spots at different anchoring depths, one should have an idea of strength of the toroidal component of the magnetic field structure of the sunspots when they appear initially on the surface. Although line of sight component of sunspots' magnetic field structure on the surface is measured on the surface, toroidal component can not be directly measured and one has to separate toroidal field component from the line of sight component of the magnetic field structure.

In the previous chapter using seven years of SOHO/MDI magnetograms, line of sight component of the magnetic field structure of bipolar spots that have initial appearance on the surface is measured (Hiremath & Lovely 2007). With the measured initial field strength on the surface, line of sight component of the magnetic field structure near base and near the surface of the convective envelope is estimated. However, as the aforementioned theoretical studies put severe constraints on strength of the toroidal field structure, estimated strength of line of sight component of the magnetic field structure is too high ($\sim 10^6$ G near base of the convection zone) compared with the strength of equipartition magnetic field. The main reason for the estimated high flux could be due to 96 minute SOHO/MDI magnetograms data that have 20 G noise that is larger than the 8 G noise of 5 minute averaged data used in the present study. Another problem with the previous study is that corrections for the projectional effects of the sunspots are not taken into account. Plan of this chapter is as follows : (i) in section 6.2, data used and method of analysis are presented, (ii) results are presented in section 6.3 and, (iii) discussion and conclusions that emerge from this study are presented in section 6.4.

6.2 Data and analysis

Six years (2000-2005) of primary (at 1.8 level) calibrated 5 minute averaged full disk SOHO/MDI magnetograms (Scherrer et al. 1995) are used that have 8 G of noise level for estimation of the longitudinal component of magnetic field structure of the sunspot on the surface. Detailed explanation of the data can be found from the previous studies (Scherrer et al. 1995; Meunier 2003, 2005). As in the previous chapter and published study (Hiremath & Lovely 2007), for the latitude zones of $0-15^o$ in both the hemispheres, non-recurrent sunspots for the present study are considered and, similar definition for estimating the life span of a sunspot, similar procedure and criteria in selecting and estimating strength of longitudinal part of the magnetic field structure of the sunspots are adopted. However, present analysis differs in the following aspects: (i) observed time difference of the first two initial appearances of the sunspot is $\sim$ 3 hours, whereas in the previous study it is $\sim$ 12 hours, (ii) Peter Meadows software (http://www.petermeadows.com/html/software.html) is used for measuring the positional measurements (such as heliographic latitude, longitude and hence the longitude from the central meridian) of the individual bipolar sunspots, (iii) instead of 20 G isocontours, 8 G isocontour is used for estimation of strength of magnetic field structure and, (iv) measured strengths of bipolar spots are corrected for the projectional effects (the observed fields are divided by $cos\theta$, where θ is angle from the central meridian).

Using Peter Meadows software, with their initial appearance on the surface, well developed (with umbra and penumbra) sunspots' positions on the SOHO/MDI magnetograms are located and their heliographic latitude, longitude from the central meridian are noted. As described in the previous chapter and published study (Hiremath & Lovely 2007) and by using FV interactive fits file editor[1], average magnetic field strength of line of sight component in each of the bipolar whole spots (that have well developed regions of umbra and penumbra) with in 8 iso-gauss contour is computed.

By applying the Hale's law (*i.e* in a particular solar cycle, polarities of leading

[1] (http://heasarc.gsfc.nasa.gov/docs/software/ftools/fv/)

and following sunspots in both the northern and southern hemis pheres are in opposite signs) of magnetic polarity, irrespective of their polarities in the northern and southern hemispheres, strength of magnetic field structure of the leading and the following spot in the northern and southern hemispheres respectively are collected. For the sake of statistical significance, both the leading and following spots' data set are merged.

As the SOHO/MDI magnetograms are observed in Ni I 6768 $\mathring{A}$ line (Scherrer et al. 1995) whose line formation occurs at 200 kms above the photosphere (Jones 1989; Meunier 1999), there is every possibility that the measured sunspot flux partly contains the plage flux also. Assuming that Parker's (1955b) flux tube model is valid (i.e, strength of the flux tube is directly proportional to square root of the ambient plasma pressure; as this idea is used in the discussion part of the previous chapter (Hiremath & Lovely 2007) and by knowing the observed average magnetic field strength and the pressure (Vernazza et al. 1981) at the height of the line formation ($\sim$ 200 kms above the photosphere), average magnetic field strength at the photosphere level is computed. Such an improved measured and corrected data set from the SOHO/MDI magnetograms is presented in Table 6.1. In this table, first column represents the date of observation, second to fifth columns represent measured parameters for the leader and sixth to ninth columns represent measured parameters for the follower spots. As for the measured parameters of the leader and follower, Lat and Long are the helographic latitude and longitudes respectively.

Here onwards, the computed average magnetic field strength of whole spot at the photospheric level is called as *initial* magnetic field strength of a sunspot. If Bs_1 and Bs_2 are the measured initial surface magnetic field strengths for the two consecutive times of the observations, the *rate of emergence of the magnetic activity* (REM) is computed from the following relation

$$REM = \frac{(Bs_2 - Bs_1)}{(t_2 - t_1)}\,, \tag{6.1}$$

where t_1 and t_2 are the time of observations for the first and second *initial* observations respectively.

Table 6.1: Improved measurements of line of sight component of magnetic field of the bipolar spots from SOHO/MDI magnetograms

	Leader				Follower			
Date	Lat	Long	B_l (G)	δB_l (G)	Lat	Long	B_l (G)	δB_l (G)
11.01.2000	-11.40	243.72	211.29	16.74	-11.57	241.78	171.43	11.99
11.01.2000	-11.10	243.04	218.60	14.44	-11.27	241.26	229.22	4.44
18.01.2000	-8.5	147.72	273.22	17.89	-8.51	146.26	277.33	17.64
19.01.2000	-8.1	159.10	240.49	18.21	-8.12	156.94	278.87	15.21
20.01.2000	11.80	97.4	347.12	7.84	11.87	96.5	222.58	12.11
21.01.2000	11.10	97.08	248.19	2.20	11.19	96.72	302.82	5.36
23.01.2000	10.18	48.18	509.35	22.76	10.72	46.48	538.34	16.77
24.01.2000	10.16	48.38	395.10	21.27	11.70	46.78	384.91	18.29
25.01.2000	6.40	70.14	437.63	133.91	6.80	68.78	243.69	110.70
25.01.2000	6.33	70.30	243.69	100.21	6.79	68.74	198.02	92.12
19.01.2000	10.00	90.50	829.63	19.52	10.04	91.90	110.70	9.56
19.01.2000	9.90	92.14	282.39	10.04	9.94	90.14	117.75	10.11
05.02.2000	6.97	266.74	702.16	2.20	7.12	263.38	288.30	6.49
05.02.2000	6.94	265.68	865.97	12.02	7.09	264.22	247.67	11.29
09.02.2000	-14.60	168.84	702.16	2.20	-14.80	167.2	288.30	6.49
09.02.2000	-14.58	167.44	865.97	8.76	-14.71	165.14	247.67	10.09
23.02.2000	-15.20	351.28	306.88	8.68	-15.80	348.38	728.99	10.54
23.02.2000	-14.55	351.68	272.19	8.68	-15.56	349.04	202.19	10.53
24.02.2000	-10.40	322.66	601.61	18.05	-11.40	320.78	538.34	30.93
24.02.2000	-10.35	322.54	111.11	21.26	-10.66	320.44	236.59	19.87
03.03.2000	-15.60	223.52	393.55	8.07	-17.60	219.5	467.91	7.42
04.03.2000	-15.42	222.44	286.36	9.10	-16.99	226.32	272.28	10.11
06.03.2000	-12.12	194.60	431.63	4.75	-12.33	192.08	297.49	7.79
06.03.2000	-12.02	221.38	415.33	9.67	-12.24	218.46	453.65	10.14
13.03.2000	10.32	154.92	248.59	22.94	10.96	153.56	113.15	15.21
14.03.2000	10.29	155.04	222.17	19.78	10.85	154.4	199.14	16.89
23.03.2000	-10.82	143.66	357.46	11.42	-11.06	142.44	239.80	36.80
23.03.2000	-10.73	144.06	280.57	14.68	-11.01	142.74	201.94	19.89
28.03.2000	-7.74	247.06	529.85	12.43	-7.98	244.98	304.08	17.13
29.03.2000	-7.67	245.66	463.92	13.33	-7.85	245.24	382.77	11.28
19.04.2000	-12.75	334.94	374.20	12.25	-12.77	333.68	241.29	10.77
19.04.2000	-12.66	328.86	196.18	14.61	-12.69	326.28	186.64	15.11
28.04.2000	-11.44	242.02	292.35	6.71	-12.94	239.2	320.99	11.18
28.04.2000	-11.43	233.66	309.35	10.21	-12.89	232.88	371.56	12.36
05.05.2000	13.10	103.3	831.13	31.70	13.38	112.8	872.52	48.46
06.05.2000	13.03	101.24	337.86	23.61	13.29	110.92	377.21	17.14

Continued on next page...

Table 6.1 – continued from previous page

	Leader				Follower			
Date	Lat	Long	B_l (G)	δB_l (G)	Lat	Long	B_l (G)	δB_l (G)
06.05.2000	-12.53	114.08	537.52	29.12	-12.54	113.88	270.40	18.23
06.05.2000	-12.49	112.70	275.12	18.22	-12.52	109.48	225.09	17.54
10.05.2000	10.92	81.74	792.11	14.09	10.93	79.30	283.00	14.85
10.05.2000	10.79	73.74	338.43	18.65	10.88	79.52	167.34	15.88
13.05.2000	5.26	25.46	430.49	39.84	7.82	25.26	411.20	41.44
14.05.2000	5.20	27.1	373.84	25.66	7.77	26.24	443.68	21.26
01.06.2000	7.76	123.72	228.00	10.47	8.20	121.66	311.06	13.55
02.06.2000	7.63	123.92	197.15	11.16	7.99	122.16	198.87	14.12
17.07.2000	-10.10	253.72	483.35	37.84	-10.24	252.56	458.43	43.72
18.07.2000	-9.93	253.86	487.70	36.24	-10.19	252.22	646.96	39.12
29.07.2000	-7.90	66.4	418.24	9.04	-8.00	63.8	472.11	25.15
30.07.2000	-7.86	66.76	250.93	10.58	-7.92	64.44	415.59	21.87
04.08.2000	-10.32	4.64	1128.32	12.51	-10.96	3.38	361.60	6.35
04.08.2000	-10.19	7.72	356.83	18.99	-10.83	6.98	264.52	11.76
04.08.2000	-12.30	16.54	248.91	2.51	-12.96	15.14	241.29	6.35
05.08.2000	-12.19	19.38	356.83	10.45	-12.72	18.54	293.03	16.49
10.08.2000	6.74	329.96	429.37	19.55	6.75	328.64	462.68	9.98
10.08.2000	6.72	330.16	450.92	16.72	6.74	329.18	408.49	11.89
12.08.2000	-11.74	263.22	320.99	7.72	-12.00	260.84	292.35	7.18
13.08.2000	-10.93	284.42	342.04	11.23	-10.94	283.36	397.68	12.36
14.08.2000	-16.21	218.06	311.06	10.53	-16.22	216.70	228.00	8.67
15.08.2000	-15.31	219.76	289.22	11.12	-15.59	218.42	410.57	14.42
03.09.2000	14.78	321.28	443.97	9.77	12.58	317.82	469.76	33.06
04.09.2000	14.75	317.48	315.86	16.52	12.42	315.78	380.66	17.81
04.10.2000	14.56	342.32	288.61	6.82	15.88	339.94	247.26	6.57
04.10.2000	14.44	343.12	286.35	11.47	15.72	340.22	277.65	10.87
09.10.2000	14.06	195.04	328.78	6.59	14.20	198.92	332.71	6.73
09.10.2000	14.04	195.18	464.14	16.72	14.15	193.96	863.98	18.19
12.10.2000	8.88	214.6	749.27	22.98	8.97	205.60	613.61	27.34
12.10.2000	8.83	213.72	512.26	20.64	8.96	205.48	617.15	18.34
18.11.2000	12.98	84.74	388.78	22.35	15.26	84.44	309.70	18.84
19.11.2000	11.99	84.76	359.45	19.18	15.24	84.56	172.03	16.71
30.11.2000	03.80	336.82	435.89	6.82	04.00	323.70	380.56	6.57
30.11.2000	03.74	322.42	335.77	11.23	03.97	321.22	316.57	12.79
07.12.2000	-10.74	283.28	413.85	36.23	-11.90	282.02	397.04	30.85
07.12.2000	-10.68	282.90	200.53	17.29	-11.73	282.22	192.73	12.98
11.12.2000	8.24	84.74	584.22	14.41	8.32	83.38	413.13	17.63
11.12.2000	8.20	84.74	562.04	12.98	8.28	83.42	386.15	14.89
14.12.2000	11.65	72.52	411.72	12.68	11.69	70.06	335.16	16.36

Continued on next page...

Table 6.1 – continued from previous page

	Leader				Follower			
Date	Lat	Long	B_l (G)	δB_l (G)	Lat	Long	B_l (G)	δB_l (G)
14.12.2000	11.49	67.42	254.63	11.66	11.62	64.48	315.42	21.22
28.12.2000	-12.90	245.16	462.94	6.45	-13.78	241.78	265.44	5.43
29.12.2000	-12.85	245.0	647.31	12.91	-13.69	243.4	246.39	14.57
01.01.2000	-13.46	165.68	275.35	12.83	-13.50	164.18	271.22	11.41
01.01.2000	-13.43	165.74	492.06	11.96	-13.45	163.88	375.57	14.72
01.01.2001	-11.59	210.84	572.60	16.51	-11.61	208.88	558.28	15.02
01.01.2001	-11.52	211.10	350.90	12.45	-11.55	208.04	348.52	14.12
18.01.2001	-6.53	310.12	325.63	11.43	-6.55	306.98	477.01	3.51
18.01.2001	-6.42	310.56	371.92	14.11	-6.43	307.14	379.95	11.14
24.01.2001	11.92	233.92	561.24	22.15	12.22	231.86	673.63	7.48
24.01.2001	11.81	233.08	582.56	16.72	11.92	231.76	562.32	18.29
30.01.2001	7.24	159.94	412.77	11.52	6.76	157.70	455.26	18.84
31.01.2001	7.12	159.92	300.20	10.96	6.64	157.98	157.82	15.65
03.02.2001	-7.58	132.30	290.05	14.36	-8.82	130.46	213.15	13.84
03.02.2001	-7.48	131.52	213.64	6.34	-8.74	129.48	214.15	9.21
03.02.2001	-12.83	110.34	275.57	21.61	-12.87	108.48	243.71	13.58
04.02.2001	-12.75	113.98	232.39	6.34	-12.81	113.42	249.26	12.99
06.02.2001	-12.98	69.84	232.39	6.34	-13.50	69.16	249.26	12.99
07.02.2001	-12.96	69.62	171.61	12.49	-12.97	69.28	353.01	11.56
17.02.2001	15.51	255.42	753.17	13.77	15.53	253.60	351.11	5.01
17.02.2001	15.48	256.40	692.32	16.72	15.50	253.88	498.95	20.62
28.02.2001	-12.50	122.44	374.99	13.77	-13.58	120.74	540.12	5.01
28.02.2001	-12.44	122.06	260.44	10.22	-13.49	120.78	153.71	12.24
28.02.2001	-9.87	187.52	361.59	6.34	-9.95	185.46	224.05	5.93
28.02.2001	-9.84	171.84	171.58	8.63	-9.91	170.78	186.81	7.99
07.04.2001	13.60	64.66	463.91	22.24	14.84	64.06	351.11	25.40
07.04.2001	13.57	64.36	294.26	19.82	14.73	64.02	170.26	17.42
07.06.2001	4.66	260.78	379.59	6.44	5.10	258.02	514.45	5.48
08.06.2001	4.34	274.44	336.66	9.98	5.03	271.06	160.29	7.55
09.06.2001	-8.64	232.46	379.59	11.76	-9.24	231.26	264.52	10.58
10.06.2001	-7.91	232.40	503.91	14.58	-8.95	230.58	536.53	15.64
20.06.2001	-7.97	156.46	561.24	12.67	-7.99	155.06	380.56	16.80
20.06.2001	-7.88	156.42	303.11	12.44	-7.89	154.60	373.15	12.60
19.06.2001	-11.46	140.30	295.13	14.11	-12.92	138.50	663.71	5.60
19.06.2001	-11.41	140.28	310.55	16.24	-12.85	138.72	307.56	18.34
23.06.2001	-7.58	62.82	449.89	11.67	-9.40	57.88	360.16	8.86
23.06.2001	-6.89	63.04	326.37	3.08	-9.31	58.04	228.93	3.23
09.07.2001	6.88	285.68	461.34	0.84	7.68	282.64	266.71	0.66
09.07.2001	6.68	264.80	573.29	13.96	6.88	260.18	406.15	4.14

Continued on next page...

Table 6.1 – continued from previous page

	Leader				Follower			
Date	Lat	Long	B_l (G)	δB_l (G)	Lat	Long	B_l (G)	δB_l (G)
09.07.2001	-7.60	189.36	3.32	8.48	-8.04	186.94	0.84	6.16
09.07.2001	-7.53	176.40	236.44	36.95	-7.98	172.34	1.64	14.15
11.07.2001	-5.00	171.80	311.87	15.55	-5.44	167.78	435.97	9.81
11.07.2001	-4.90	170.80	295.55	14.24	-5.31	167.00	233.99	12.65
23.07.2001	14.00	18.38	391.94	7.95	14.16	16.36	333.31	3.98
23.07.2001	13.97	13.98	336.66	9.29	14.08	12.90	581.97	10.12
30.07.2001	-14.81	262.58	336.66	10.11	-14.87	262.33	581.97	19.00
30.07.2001	-14.78	263.82	313.59	9.87	-14.84	261.54	243.71	12.64
01.08.2001	-13.47	326.48	313.59	10.62	-13.82	323.96	243.71	9.78
01.08.2001	-13.27	263.82	300.63	12.14	-13.56	261.54	422.72	14.24
01.08.2001	-9.50	326.48	388.39	10.11	-10.84	323.96	374.23	19.01
02.08.2001	-8.83	326.60	368.13	12.55	-10.74	324.14	231.03	14.64
06.09.2001	-9.18	222.14	567.29	7.97	-11.32	220.62	555.29	12.67
07.09.2001	-8.85	222.62	460.95	10.32	-10.82	214.00	181.41	12.88
20.09.2001	9.18	361.20	593.01	13.80	11.32	358.08	335.77	7.85
20.09.2001	8.67	361.78	269.16	15.69	11.29	358.86	402.41	15.04
30.09.2001	12.68	162.04	358.46	8.28	14.08	157.90	367.03	12.63
01.10.2001	12.54	165.68	329.41	5.53	13.85	162.44	418.72	6.78
05.10.2001	-12.40	147.98	329.41	5.53	-13.38	146.66	418.72	6.78
05.10.2001	-12.29	147.10	402.84	5.16	-13.18	145.56	311.50	4.07
10.10.2001	4.78	65.20	402.84	5.16	5.10	63.18	311.50	4.07
10.10.2001	4.72	65.48	213.46	8.30	5.01	63.72	131.54	8.24
10.10.2001	13.45	65.62	349.62	9.58	14.13	62.80	411.72	12.85
10.10.2001	13.25	65.60	313.58	10.98	14.11	63.72	387.77	4.08
11.10.2001	10.23	33.86	418.52	10.04	10.29	29.88	558.25	7.81
11.10.2001	10.21	32.60	878.53	9.43	10.27	29.76	358.01	9.28
16.10.2001	15.56	317.72	501.36	9.83	16.94	315.62	518.36	14.32
16.10.2001	15.47	317.26	615.28	8.66	16.90	316.02	395.19	8.16
19.10.2001	-12.36	288.38	177.20	8.42	-12.49	285.20	287.89	4.37
19.10.2001	-12.34	288.36	164.79	4.58	-12.47	286.38	269.57	4.39
07.11.2001	06.49	79.36	365.63	11.88	06.88	70.24	213.46	11.86
08.11.2001	06.41	78.92	334.94	14.98	06.79	71.98	332.85	16.59
07.11.2001	13.82	68.00	365.63	14.52	14.08	69.32	360.47	4.22
08.11.2001	13.73	72.92	294.89	11.73	13.88	72.36	268.60	14.45
18.11.2001	-9.87	240.56	555.29	12.86	-9.91	237.56	376.51	14.55
18.11.2001	-9.83	241.88	228.10	17.62	-9.86	239.68	589.28	14.86
22.11.2001	-5.60	201.62	584.33	14.51	-13.54	198.86	234.36	5.87
22.11.2001	-4.95	194.34	571.11	15.19	-13.27	194.04	574.13	12.07
01.12.2001	-15.08	128.90	392.38	32.93	-15.42	128.10	355.97	18.57

Continued on next page...

Table 6.1 – continued from previous page

	Leader				Follower			
Date	Lat	Long	B_l (G)	δB_l (G)	Lat	Long	B_l (G)	δB_l (G)
01.12.2001	-14.83	129.76	263.30	11.80	-14.90	128.92	149.96	17.59
03.12.2001	-11.15	146.56	705.62	10.21	-11.21	145.30	275.57	13.70
03.12.2001	-11.09	142.92	221.96	12.65	-11.18	140.90	223.78	19.90
16.12.2001	-6.14	252.34	551.49	9.12	-6.64	248.58	448.84	26.77
17.12.2001	-5.91	252.84	350.14	19.80	-6.42	251.18	150.13	19.90
19.12.2001	-9.16	226.82	243.45	7.22	-15.64	218.90	217.80	22.98
19.12.2001	-9.00	227.78	243.45	14.20	-15.56	222.70	217.80	13.70
20.12.2001	-12.64	192.16	400.07	15.15	-13.56	189.70	261.76	12.38
21.12.2001	-12.31	192.18	325.01	17.81	-13.35	189.62	227.44	19.12
26.12.2001	5.68	114.0	714.33	31.02	6.80	110.92	468.05	21.55
26.12.2001	5.63	113.40	288.10	26.32	6.79	111.60	250.13	22.34
27.12.2001	14.26	106.32	416.61	12.92	14.68	103.90	382.70	4.15
27.12.2001	14.19	113.74	410.94	14.53	14.64	111.60	160.36	16.44
30.12.2001	-7.00	128.90	518.36	6.45	-8.58	128.10	501.36	7.32
30.12.2001	-6.83	129.76	464.71	9.10	-8.10	128.92	227.44	15.26
09.01.2002	-10.12	70.64	312.27	29.21	-10.32	70.60	288.82	27.09
09.01.2002	-10.08	101.24	325.74	11.25	-10.25	101.30	283.70	7.81
21.03.2002	-13.44	159.06	294.79	16.72	-15.86	157.98	215.37	10.90
22.03.2002	-13.27	141.72	294.79	19.87	-15.76	140.86	215.37	2.85
20.03.2002	-14.24	152.00	288.82	27.09	-14.70	149.12	312.27	24.20
21.03.2002	-14.15	149.24	283.70	393.61	-14.34	148.20	372.96	11.20
22.03.2002	-5.44	111.26	273.67	3.59	-6.78	111.16	253.00	10.41
22.03.2002	-5.37	101.30	221.29	7.12	-6.64	100.44	215.68	7.85
06.04.2002	-8.60	258.96	388.63	6.01	-9.11	261.10	444.55	6.93
07.04.2002	-8.59	258.38	323.71	6.75	-9.03	257.72	324.51	3.55
13.06.2002	-4.32	128.24	259.38	10.52	-5.46	124.28	406.38	27.94
14.06.2002	-4.18	127.48	235.84	3.63	-5.11	124.18	356.54	12.00
06.06.2002	-14.43	138.98	251.36	13.38	-14.55	132.76	259.34	15.28
07.06.2002	-14.39	152.42	217.18	13.38	-14.47	146.04	218.57	115.28
18.06.2002	-5.24	35.30	468.05	10.11	-5.40	34.18	385.07	21.55
19.06.2002	-5.04	21.84	286.71	11.91	-5.29	20.48	264.81	10.03
24.07.2002	-6.44	245.72	546.99	11.03	-7.20	244.72	609.74	15.83
25.07.2002	-6.29	239.28	363.60	16.06	-7.15	236.72	321.81	9.15
23.07.2002	-10.16	217.20	607.84	17.02	-12.32	215.40	281.82	10.89
24.07.2002	-10.11	214.06	545.75	1.93	-12.15	212.46	577.07	25.27
24.07.2002	-11.48	241.06	369.82	2.18	-11.49	239.96	361.39	2.04
25.07.2002	-11.44	240.52	609.74	14.95	-11.47	237.62	546.99	5.76
26.07.2002	-7.78	192.92	363.60	9.70	-7.94	191.98	0.70	8.84
27.07.2002	-7.59	193.58	222.81	10.45	-7.65	191.80	201.40	22.63

Continued on next page...

Table 6.1 – continued from previous page

	Leader				Follower			
Date	Lat	Long	B_l (G)	δB_l (G)	Lat	Long	B_l (G)	δB_l (G)
27.07.2002	-10.78	176.58	219.67	10.45	-11.42	173.92	423.11	21.13
28.07.2002	-10.34	176.36	329.80	14.11	-11.39	173.90	263.44	16.27
18.09.2002	6.40	275.98	535.53	39.27	7.76	277.04	511.93	34.95
18.09.2002	6.33	276.90	323.66	9.41	7.61	276.26	217.30	10.76
15.09.2002	-14.43	234.52	335.52	4.75	-14.57	231.02	435.41	9.13
15.09.2002	-14.39	229.78	717.19	14.61	-14.44	226.00	465.58	8.39
17.09.2002	-14.68	218.18	152.98	10.79	-15.08	214.60	143.85	9.10
18.09.2002	-14.53	208.18	130.98	11.44	-14.97	207.52	130.296	11.47
21.09.2002	-6.84	147.38	426.54	8.27	-6.90	145.76	490.62	13.26
21.09.2002	-6.82	145.69	145.64	8.28	-6.86	143.26	203.36	6.71
06.10.2002	5.30	348.90	349.61	6.56	5.46	347.84	501.74	2.44
06.10.2002	5.19	349.00	175.06	3.07	5.23	347.74	338.58	2.36
11.10.2002	-10.84	342.76	405.52	51.26	-11.10	340.56	402.83	41.46
11.10.2002	-10.20	343.48	422.50	16.72	-10.99	340.64	364.59	15.86
18.10.2002	-4.69	242.38	312.48	6.64	-4.77	240.20	247.49	15.45
18.10.2002	-4.63	242.42	435.45	14.25	-4.74	240.20	257.69	11.10
02.11.2002	-6.01	320.36	238.13	22.39	-6.09	319.02	632.24	13.77
02.11.2002	-5.98	321.82	656.54	19.23	-6.01	324.26	425.40	15.26
06.11.2002	5.18	295.72	436.07	25.00	6.60	291.94	246.52	18.14
06.11.2002	5.12	304.74	275.98	14.65	6.54	303.22	226.59	12.49
10.11.2002	14.21	223.10	155.12	12.42	14.26	219.96	174.89	6.30
11.11.2002	14.18	224.74	108.01	14.62	14.22	223.22	110.63	12.38
18.11.2002	-12.48	121.78	379.24	15.05	-12.84	126.68	340.33	11.09
18.11.2002	-12.32	128.54	387.77	12.98	-12.67	127.36	313.58	17.22
10.12.2002	-6.74	208.64	572.06	10.42	-11.90	201.32	386.17	10.84
10.12.2002	-6.54	209.48	391.65	19.32	-11.88	204.80	256.05	15.26
13.12.2002	-11.78	145.66	396.38	12.53	-11.83	144.38	315.46	4.39
13.12.2002	-11.73	145.00	572.40	7.82	-11.79	143.22	384.99	15.30
20.12.2002	12.56	84.44	329.02	39.48	12.59	83.22	281.93	30.78
20.12.2002	12.53	84.58	291.26	12.50	12.55	83.08	238.38	17.52
22.12.2002	10.72	22.38	307.06	15.20	12.60	19.00	273.72	27.96
22.12.2002	10.51	20.32	345.16	12.45	12.56	18.86	216.36	17.28
30.12.2002	-6.86	283.40	303.51	8.53	-8.06	281.66	294.18	0.69
31.12.2002	-6.55	284.50	142.32	13.82	-7.73	282.58	271.85	12.14
03.01.2003	-8.25	219.54	813.62	11.31	-8.30	217.06	724.29	15.52
03.01.2003	-8.21	219.44	469.61	41.37	-8.27	217.56	174.47	14.62
06.01.2003	8.32	212.62	429.31	36.42	8.82	211.34	417.81	32.49
06.01.2003	8.12	212.16	398.76	18.35	8.45	210.72	436.21	12.32
10.01.2003	11.22	207.30	309.88	4.71	11.34	205.72	368.16	15.02

Continued on next page...

Table 6.1 – continued from previous page

	Leader				Follower			
Date	Lat	Long	B_l (G)	δB_l (G)	Lat	Long	B_l (G)	δB_l (G)
10.01.2003	11.17	207.62	313.32	12.88	11.23	206.14	229.47	18.67
04.01.2003	8.06	193.82	1590.09	22.53	11.07	190.06	641.45	25.12
04.01.2003	7.96	193.00	1358.85	26.69	10.99	191.12	1156.81	14.62
19.01.2003	-3.33	95.82	299.93	13.33	-4.25	94.88	294.81	4.74
19.01.2003	-2.93	97.32	240.85	1.95	-4.16	94.88	319.22	17.41
21.01.2003	9.08	2.1	284.41	8.35	9.34	2.26	271.16	9.44
22.01.2003	8.59	2.22	443.35	2.32	9.25	1.68	186.61	3.46
26.01.2003	-3.62	356.36	397.72	20.80	-3.84	354.52	273.72	21.61
27.01.2003	-3.57	356.86	323.16	27.86	-3.75	355.78	369.26	19.88
04.02.2003	-9.42	189.76	427.77	7.06	-10.26	188.44	380.19	3.84
05.02.2003	-10.16	187.98	233.25	42.71	-10.57	184.76	269.78	16.76
24.02.2003	-11.34	301.70	379.24	12.03	-11.88	300.64	340.33	11.19
25.02.2003	-11.25	301.78	355.26	15.76	-11.67	300.88	272.76	17.66
26.02.2003	-8.72	232.64	698.93	18.76	-10.92	234.18	417.25	7.44
27.02.2003	-8.79	231.90	282.69	1.81	-10.85	232.90	375.46	6.70
03.03.2003	-9.33	192.04	331.92	21.70	-10.25	190.28	299.93	10.58
04.03.2003	-9.25	192.34	317.27	19.20	-10.13	190.54	243.39	14.78
09.03.2003	-15.29	78.90	777.34	15.92	-15.32	75.18	385.84	23.68
09.03.2003	-15.26	82.64	733.43	26.92	-15.29	78.62	477.48	13.17
20.03.2003	11.96	337.84	843.76	18.33	13.92	330.96	309.36	12.04
20.03.2003	11.82	336.82	250.52	15.51	13.86	334.62	195.85	19.58
24.03.2003	3.86	279.60	340.57	11.54	4.40	277.84	174.99	6.17
24.03.2003	3.82	283.96	153.96	16.88	4.62	283.42	150.24	15.35
23.03.2003	12.76	246.22	854.01	6.83	12.79	245.32	756.28	9.13
23.03.2003	12.73	246.72	684.08	11.23	12.75	244.40	690.44	11.23
25.03.2003	-10.82	222.42	895.68	14.84	-11.24	219.48	1287.09	16.72
26.03.2003	-10.77	222.02	826.82	11.05	-10.94	220.16	653.61	26.20
31.03.2003	-9.14	209.02	340.85	7.56	-9.28	206.66	219.67	0.63
01.04.2003	-9.06	209.40	297.64	6.64	-9.15	206.84	215.25	4.46
02.04.2003	2.14	140.18	271.04	5.21	2.28	137.68	287.39	9.26
03.04.2003	1.97	137.24	245.04	5.32	2.15	135.38	213.92	2.99
05.04.2003	-7.84	178.44	236.73	8.27	-9.38	176.58	324.73	12.79
05.04.2003	-7.69	141.58	255.56	8.27	-9.14	139.98	192.94	12.79
23.05.2003	9.20	211.88	458.31	47.44	10.40	205.58	429.49	48.09
23.05.2003	9.18	211.86	422.50	19.29	10.29	206.98	364.59	13.79
02.06.2003	-12.38	75.50	389.11	6.72	-12.85	73.88	333.45	12.99
02.06.2003	-12.21	75.64	267.85	29.40	-12.42	73.14	266.71	37.16
18.06.2003	-5.06	223.30	329.07	6.67	-6.86	221.32	245.44	6.44
18.06.2003	-4.75	223.50	289.41	11.83	-6.67	221.50	342.57	5.85

Continued on next page...

Table 6.1 – continued from previous page

	Leader				Follower			
Date	Lat	Long	B_l (G)	δB_l (G)	Lat	Long	B_l (G)	δB_l (G)
19.06.2003	-11.78	203.36	435.05	2.81	-11.82	200.46	241.50	12.60
19.06.2003	-11.36	201.20	258.85	7.40	-11.45	200.62	225.83	18.11
18.07.2003	11.87	157.94	362.99	15.46	11.91	154.66	217.18	29.21
18.07.2003	11.81	155.94	284.26	10.98	11.86	152.86	410.44	30.14
02.08.2003	5.58	185.40	244.62	15.59	8.94	183.75	218.43	15.48
03.08.2003	4.98	183.78	319.07	11.28	8.10	183.58	369.76	18.16
04.08.2003	15.50	344.50	463.96	17.74	15.60	342.36	470.94	16.95
05.08.2003	15.21	342.68	299.81	18.35	15.30	341.28	278.44	22.12
02.08.2003	-11.32	336.82	244.62	6.64	-11.39	323.70	218.43	7.13
03.08.2003	-11.29	322.42	401.98	6.09	-11.33	471.48	411.11	20.79
21.08.2003	8.06	135.62	210.34	27.37	8.72	133.33	171.60	17.74
22.08.2003	7.96	134.64	160.48	258.85	8.19	132.34	148.37	2.67
23.08.2003	8.84	66.14	672.45	10.56	8.92	63.64	801.14	14.07
23.08.2003	8.81	59.22	666.87	18.76	8.85	52.44	775.75	17.52
25.10.2003	-15.56	300.21	488.37	12.96	-16.94	300.63	355.14	9.02
26.10.2003	-15.42	300.39	407.43	7.47	-16.46	300.67	312.62	5.80
24.11.2003	6.12	251.90	511.60	19.33	6.42	250.78	478.69	12.30
25.11.2003	6.06	250.66	163.79	18.26	6.13	246.72	376.95	6.95
12.12.2003	-13.34	93.56	490.38	4.99	-14.98	92.06	459.02	13.53
12.12.2003	-13.18	93.88	359.03	11.14	-14.55	91.82	296.80	19.82
16.12.2003	13.06	44.98	400.79	35.58	13.40	44.20	388.85	48.47
17.12.2003	13.07	45.50	267.58	4.79	13.29	43.98	422.54	3.09
24.12.2003	-10.36	241.02	366.17	4.46	-11.18	239.54	351.33	2.04
24.12.2003	-10.19	241.18	432.11	2.152	-11.11	239.80	248.84	9.72
13.02.2004	7.26	334.28	540.32	21.35	7.28	336.04	491.51	14.24
14.02.2004	7.22	335.20	130.93	21.35	7.25	332.08	374.63	13.52
04.03.2004	-13.48	12.12	543.25	15.40	-14.04	13.18	268.74	8.90
05.03.2004	-13.22	17.58	398.85	12.68	-13.95	16.12	305.24	9.51
12.04.2004	13.40	241.02	414.18	15.52	14.12	239.54	580.05	12.36
13.04.2004	13.23	241.18	401.98	12.97	14.08	239.80	471.48	23.24
20.04.2004	-4.28	199.18	403.75	39.84	-5.30	197.44	427.46	28.24
21.04.2004	-4.27	203.92	266.15	29.52	-5.11	202.58	212.34	35.11
29.04.2004	9.76	66.22	292.90	13.44	9.92	55.74	528.42	5.98
30.04.2004	9.32	49.66	213.02	19.28	9.79	50.44	209.87	18.79
12.05.2004	-1.02	197.00	495.91	7.56	-5.06	194.54	357.90	6.72
12.05.2004	-0.92	198.72	371.04	12.67	-4.95	195.46	362.64	17.56
17.05.2004	-12.68	139.80	191.87	8.47	-13.38	137.32	268.74	1.15
17.05.2004	-12.39	139.70	339.27	2.28	-13.13	136.46	233.37	1.47
01.06.2004	8.70	329.70	521.84	47.77	9.86	323.78	412.97	48.23

Continued on next page...

Table 6.1 – continued from previous page

	Leader				Follower			
Date	Lat	Long	B_l (G)	δB_l (G)	Lat	Long	B_l (G)	δB_l (G)
01.06.2004	8.35	328.86	500.84	18.54	9.38	327.50	567.99	17.52
04.06.2004	4.60	257.60	543.25	12.34	5.70	256.78	435.32	7.92
05.06.2004	4.29	258.38	118.74	17.41	5.68	257.22	333.57	17.86
07.06.2004	-12.32	217.60	343.29	28.85	-13.32	215.14	368.79	27.43
07.06.2004	-12.29	218.44	468.76	7.58	-13.24	232.70	216.36	22.99
07.06.2004	-4.60	202.66	380.19	25.71	-5.40	203.62	343.29	15.48
07.06.2004	-4.12	207.04	406.11	7.57	-5.13	205.24	239.01	13.23
18.08.2004	11.58	328.22	275.25	15.40	11.96	323.18	232.32	7.99
18.08.2004	11.54	326.64	442.62	6.27	11.89	322.50	495.36	6.27
24.10.2004	-12.98	172.58	434.28	10.02	-13.50	174.56	232.32	12.90
25.10.2004	-12.78	157.08	536.19	2.09	-13.11	155.62	224.05	7.06
19.10.2004	-7.24	293.04	403.51	2.30	-8.64	291.46	389.89	11.77
20.10.2004	-7.71	292.48	217.93	4.33	-7.93	290.08	431.78	8.75
17.10.2004	-10.84	242.38	377.12	6.64	-11.10	240.20	542.93	15.45
18.10.2004	-9.91	242.42	257.69	4.41	-10.96	240.20	435.45	5.90
17.11.2004	11.12	259.56	312.48	0.57	14.56	261.96	247.49	9.99
17.11.2004	10.89	261.78	304.41	2.89	14.44	260.64	145.49	1.56
10.12.2004	12.66	373.88	263.25	5.89	12.74	372.28	316.99	12.68
11.12.2004	12.57	314.46	195.88	14.26	12.53	313.00	208.48	6.07
21.12.2004	-6.42	51.61	398.43	21.35	-7.50	49.62	318.51	12.21
21.12.2004	-5.89	36.06	385.30	15.17	-7.41	30.26	351.28	15.46
31.01.2005	-10.40	29.66	393.98	7.31	-11.18	20.15	318.51	12.22
31.01.2005	-10.18	29.14	231.03	12.31	-10.95	20.58	231.99	11.69
30.10.2005	-7.94	286.78	817.35	4.75	-7.95	286.20	252.27	43.04
31.10.2005	-7.89	288.10	596.98	9.82	-7.90	284.78	636.31	13.39
05.11.2005	-14.98	277.48	232.14	22.53	-14.99	278.34	320.80	21.73
06.11.2005	-14.62	277.06	223.98	3.38	-14.79	276.20	288.41	5.06
19.11.2005	-14.33	105.52	488.20	10.97	-14.54	104.26	499.47	0.96
20.11.2005	-14.16	100.30	357.08	19.47	-14.39	161.95	261.95	8.43
24.11.2005	-5.76	338.14	529.42	19.19	-5.92	336.56	292.90	7.62
26.11.2005	-5.27	338.74	429.33	12.26	-5.37	336.04	160.51	11.34
02.12.2005	10.96	258.04	451.88	18.04	10.99	259.14	411.18	10.20
03.12.2005	10.91	260.50	237.61	14.65	10.95	259.90	179.15	11.26
04.12.2005	-5.84	293.04	179.46	17.84	-6.90	291.46	130.13	16.92
05.12.2005	-5.77	292.48	290.28	7.96	-6.77	290.08	405.80	6.41
09.12.2005	-13.22	232.66	452.29	62.01	-14.24	232.00	445.06	49.92
10.12.2005	-13.16	200.24	423.35	9.52	-14.12	199.38	383.99	7.87

6.3 Results

Irrespective of their sizes, line of sight component of measured field strengths of the whole spots during their initial appearance on the surface are collected in each life span bins (2-3, 3-4 days and so on). For each bin of the life spans, average of magnetic field strengths Bs_1 and Bs_2 with their respective errors $(\sigma/(N)^{1/2}$, where σ is standard deviation and N is number of samples in each life span bins) are computed. The typical number of non-recurrent sunspots in each life span τ bin considered for the present study are illustrated in Fig 6.1(a). Irrespective of their direction from the central meridian (*i.e.,* whether in East or West) and for different life spans, in Fig 6.1(b), distribution of sunspots is presented. In Fig 6.2(a), irrespective of their sizes, average strength of line of sight component *Bs1* of the magnetic field structure for each life span bin is presented. Irrespective of their sizes, strength of the measured line of sight component of magnetic field structure of the whole spot on the surface varies from $\sim$ 450 G for the life span of two days to $\sim$ 300 G for the life span of twelve days.

The observed SOHO/MDI magnetograms yield only the line of sight component of the magnetic field structure. However, bipolar sunspots are part of toroidal magnetic field structure that emerge from the interior. In principle, the toroidal component of the field structure can be separated from the observed line of sight component. Following the pioneering studies (Duvall et al. 1979; Shrauner & Scherrer 1994; Rust 1999; Ulrich et al. 2002; Ulrich & Boyden 2005), we decompose the line of sight component B_l of sunspot magnetic field structure into *toroidal* B_φ and *poloidal* B_θ components as

$$B_l = B_\varphi sin\vartheta + B_\theta cos\vartheta\,, \tag{6.2}$$

where ϑ is the sunspots' longitudinal distance from the central meridian. It is to be noted that present study uses the magnetogram data of bipolar spots during their initial appearance on the surface, whereas aforementioned pioneering studies use the magnetogram data irrespective of their time of appearance and lifespan.

In each life span bins, with measured strength of average B_l values from the ini-

tial observations, and by applying a linear least-square fit, B_φ and B_θ are separated. These separated components of the field structures are presented in Fig 6.2(b). From Fig 6.2(b), one can notice that contribution of strength of average toroidal component of magnetic field structure of the sunspots when they have initial appearances on the surface varies from $\sim$ 10 G for the life span of 2 days to $\sim$ 700 G for the life span of 12 days bipolar spots. Another important result is that, for each life span bin, strengths of the separated toroidal and poloidal field structures are inversely proportional to each other. Using this observed property, in the following, strength of toroidal field structure at different anchoring depths in the convective envelope will be inferred.

In order to compute toroidal field structure at different anchoring depths of the bipolar spots, one should need observations of the well developed sunspots with their initial appearance on the surface, a sunspot (flux tube) model and, a life-span anchoring depth information in the solar convective envelope. In this study Parker's (1955b) flux tube model derived in spherical coordinates (see in Appendix A) and Hiremath's (2002) life-span anchoring depth information in the solar convective envelope is used.

The salient features of the Parker's flux tube model are : (i) the tube is considered to be slender, (ii) vertical to the surface, (iii) a homogeneous magnetic flux along the cross section of the tube and, (iv) the tube is in thermal equilibrium with the surroundings. The solution of this flux tube model yields the exponential decrease of magnetic flux towards the surface such that $B\,\alpha\,(P_e)^{1/2}$,where B is strength of the magnetic field and P_e is external ambient pressure. With simple algebra, one can obtain the relation $B_a = (P_{ea}/P_{es})^{1/2} B_s$ that yields the strength of magnetic field B_a at different anchoring depths in the convection zone with the ambient plasma pressure P_a (where as B_s is the strength of the flux tube and P_s is the ambient plasma pressure at the surface). This simple concept is used in the previous chapter for inference of longitudinal component of the magnetic field structure in the convective envelope (Hiremath & Lovely 2007). However, in this chapter as toroidal and poloidal components are separated, one can not use the same concept to infer the toroidal component of the magnetic field structure. Hence, as in Appendix A,

Parker's (1955b) equations in spherical coordinates are redrived and similar relationship (equation 6.12) is obtained such that $(B_r^2 + B_\varphi^2 + B_\theta^2) = Cr^2(P_e)^{1/2}$, where B_r is the radial component, B_φ and B_θ are the components of the toroidal and poloidal magnetic field structures respectively and, C is integrational constant. Integrational constant C can be eliminated by taking the ratio at different anchoring depths 'a' and at the surface 's'. Hence, the same relationship can be transformed into $(B_r^2 + B_\varphi^2 + B_\theta^2)_a = (B_r^2 + B_\varphi^2 + B_\theta^2)_s x^2(P_{ea}/P_{es})$, where $x = r/R_\odot$ and $R_\odot$ is radius of the sun.

From the results presented in Fig 6.2b, it is clearly evident that strengths of toroidal and polidal components on the surface are inversely proportional to each other (*i.e.,* $B_\theta = \frac{K}{B_\varphi}$, K is constant of inverse relationship and is found to be equal to -1 from the correlative analysis). With the assumption that constant $K = -1$ is almost same through out the convective envelope, solution of such a quadratic equation yields the relation $B_{\varphi a} \sim [(B_r^2 + B_\varphi^2 + B_\theta^2)_s\, x^2(P_{ea}/P_{es}) - B_r^2]^{1/2}$, where subscripts s and a represent surface and different anchoring depths respectively. Hence by knowing strengths of line of sight (from which radial field follows from the relation $B_r = B_l sec\theta$, where B_l is observed line of sight component and θ is heliographic latitude) and toroidal field component structures with the ambient pressure values on the surface and at different anchoring depths in the convective envelope, one can compute strength of toroidal field structure at different depths where sunspots are anchored. As for the ambient pressure in the convective envelope, the helioseismic inferred results are considered (Shibahashi et al. 1998, 1999).

In the recent study (Hiremath 2002), using 103 years of non-recurrent sunspot group data, it is shown that variation of rotation rates of the spot groups that have initial appearances on the surface for different life spans is almost similar to the radial variation of internal rotation rate inferred from the helioseismology. This result is not surprising as the solar plasma in the convective envelope has infinite conductivity, the flux tubes isorotate with the solar plasma and due to buoyancy rise towards the surface along the isorotation contours. Hence the flux tube that initially appears on the surface must have similar rotation rate at it's anchoring depth. With physical significance, this strong life span-anchoring depth relationship

in the same study is further justified from the observed variation of initial rate of change of rotation rates and life-span of the sunspot groups and the radial variation of rotational gradient as inferred from the helioseismology (for further details see Fig 5(b) and discussion part in the section 4 of Hiremath (2002)). For each life span of the sunspots, this study has given us sunspots' anchoring depth information uniquely in the convective envelope. That is sunspots that have 2-3 days life spans are anchored close to the surface and the sunspots that have 11-12 days life spans are anchored near base of the convection zone.

Hence, using these two basic physical concepts, *viz.*, Parker's modified flux tube model in spherical coordinates and Hiremath's (2002) life-span anchoring depth information, strength of line of sight and the toroidal components of magnetic field structure of the bipolar spots are inferred in the convective envelope from the measured longitudinal and estimated toroidal components on the surface. For different life spans of the bipolar spots with their initial appearances on the surface, radial variation of the inferred line of sight and the toroidal components of the sunspot magnetic field structure of the bipolar spots in the convective envelope are presented in Fig 6.3(a) and 6.3(b) respectively. For the life spans less than 8 days it appears from Fig 6.3 that strengths of inferred radial variation of line of sight and toroidal field structures are almost zero. That is not right and in order to avoid this ambiguity, separately in Table 6.2, the inferred results are presented. In Table 6.2, first to sixth columns represent the life span, anchoring depth (normalized with the solar radius), strength of inferred longitudinal and toroidal components of magnetic field structures, strength of theoretically computed toroidal field structure (Hiremath (2001), equation (21)) and rate of emergence ($\frac{dB_\varphi}{dt}$) of toroidal magnetic activity respectively.

It is interesting to compare inferred toroidal component of magnetic field structure with the theoretical toroidal field structure in the convective envelope. As the observed data set is considered from the equator to 15° latitude zones, for both the hemispheres combined together, for the intervals of two degrees in this latitude zone, theoretical toroidal field structure (Hiremath (2001), equation (21)) is computed and average curve is over plotted as a red dashed line in Fig 6.3(b). It is to be noted

that, except near base of convection zone, both the strength and the inferred radial variation of theoretical and inferred toroidal magnetic field structures are almost similar.

It is not clear whether such a inferred toroidal field structure in the convective envelope results from the perturbation of toroidal field structure of fossil origin or from the traditional dynamo mechanism. In case the inferred toroidal field structure is of fossil origin, except near base of the convection zone, radial variation is almost similar to strength and radial variation of theoretical toroidal field structure (Hiremath 2001) that is consistent with the internal isorotation contours as inferred from the helioseismology. Moreover, inferred strength of the toroidal magnetic field structure is also strikingly consistent with the inferred strength of the toroidal magnetic field structure from the helioseismic studies (Basu 1997; Antia et al. 2000; Antia 2002; Baldner et al. 2009) and from the MHD computations (Choudhuri & Gilman 1987; D'Silva & Howard 1994).

With the first two consecutive initial appearances of the bipolar spots on the surface and for different life spans, strengths of line of sight components B_{l1} and B_{l2} of the bipolar spots are measured and toroidal components $B_{\varphi 1}$ and $B_{\varphi 2}$ are separated by the least square fit. Strengths of line of sight and toroidal components at different anchoring depths in the convective envelope are inferred. Irrespective of their sizes and for different life spans, rate of change $((B_{\varphi 2} - B_{\varphi 1})/(t_2 - t_1)$, where t_1 and t_2 are consecutive observed times) of toroidal magnetic field structure $(\frac{dB_\varphi}{dt})$ of the bipolar spots that represents the emergence of toroidal magnetic flux is computed at different anchoring depths in the solar convective envelope and is illustrated in Fig 6.4. One can notice that emerging toroidal component of magnetic flux near base of the convective envelope is found to be $\sim 10^3$ times the emerging toroidal component of the magnetic flux near the surface.

In the previous chapter and in the published (Hiremath & Lovely 2007) study, strength of inferred line of sight component of the magnetic field structure is found to be too high when we compare with the equipartition field strength at different anchoring depths. However, present study yields the correct strength of inferred ($\sim 10^4$ G) line of sight component of the sunspots' magnetic field structure at different

anchoring depths near base of the convective envelope.

6.4 Discussion and conclusions

The origin and formation of the sunspots are not yet understood completely. The unknown dynamo mechanism that sustains the solar magnetic cycle and activity phenomena may be responsible for origin and formation of the flux tubes. Moreover, it is also not clear and debatable whether toroidal field structures are formed by the turbulent dynamo mechanism (Hiremath & Lovely 2007) or perturbation of the underlying steady toroidal field structure in the convective envelope (Hughes 1992; Hiremath 2001). For example, if one accepts the existence of such a steady part of toroidal magnetic field structure with the strength B_φ at different depths, then perturbations result in creation of MHD waves whose amplitudes are $\sim \delta B_\varphi$. Superposition of amplitudes of such MHD waves in turn leads to constructive interference and form the sunspots. When the magnetic field structure of resulting sunspots attains a critical strength, due to buoyancy, sunspots erupt towards the surface along the isorotational contours. Hence, it is not surprising that the red dashed line (over plotted in Fig 6.3(b)) that represents radial variation of steady part of toroidal magnetic field structure in the convective envelope (Equation 21 of Hiremath (2001)) nearly matches with the radial variation of toroidal magnetic field structure inferred from the observations. There are also many alternative ideas (Schüssler & Rempel 2005) for the formation and emergence of the sunspots towards the surface.

Important conclusions of the present study are : (i) when the bipolar spots emerge initially on the surface, irrespective of their sizes, measured average strength of line of sight component for the whole spot varies from $\sim$ 450 G for two days life span to $\sim$ 300 G for the twelve days life span, (ii) strength of toroidal component of magnetic field structure separated by a least square fit from the line of sight component on the surface is estimated to be $\sim$ 10 G for the 2-3 days life span to $\sim$ 700 G for the 11-12 days life span, (iii) inference by using modified Parker's (1955b) flux tube model in spherical coordinates and Hiremath's (2002) life span

anchoring depth information yields both the strength of line of sight and toroidal field components at different anchoring depths with similar strength and radial variation in the convection zone and, (iv) rate of emergence of toroidal component of the magnetic field structure near base of the convective envelope is found to be $\sim 10^3$ times the rate of emergence of toroidal component of the magnetic field structure near the surface.

6.5 Appendix

As the flux tube is embedded in the sun, the vector magnetic field **B** is expanded in the following form

$$\mathbf{B} = B_r\hat{\mathrm{I}}_r + B_\theta\hat{\mathrm{I}}_\vartheta + B_\varphi\hat{\mathrm{I}}_\varphi \ , \tag{6.3}$$

where B_r, B_θ and B_φ are radial, latitudinal and azimuthal components parallel to the sun's radial, latitudinal and the azimuthal directions. Correspondingly $\hat{\mathrm{I}}_r$, $\hat{\mathrm{I}}_\vartheta$ and $\hat{\mathrm{I}}_\varphi$ are the unit vectors in the same directions.

The current **j** can be expressed as

$$\mathbf{j} = \frac{1}{r^2 sin\theta}[\frac{\partial}{\partial\theta}(rsin\theta B_\varphi) - \frac{\partial}{\partial\varphi}(rB_\theta)]\hat{\mathrm{I}}_r - \frac{1}{rsin\theta}[\frac{\partial}{\partial r}(rsin\theta B_\varphi) - \frac{\partial}{\partial\varphi}(B_r)]\hat{\mathrm{I}}_\theta + \frac{1}{r}[\frac{\partial}{\partial r}(rB_\theta) - \frac{\partial}{\partial\theta}(B_r)]\hat{\mathrm{I}}_\varphi. \tag{6.4}$$

Following (Parker 1955b), assume that **B** is homogeneous across the tube. This condition implies that $\frac{\partial}{\partial\theta}(B_r) = \frac{\partial}{\partial\varphi}(B_r) = 0$.

Therefore radial component of the Lorentz force is

$$[\mathbf{j} \times \mathbf{B}]_r = -\frac{1}{r}(B_r^2 + B_\varphi^2 + B_\theta^2) - \frac{1}{2}\frac{d}{dr}(B_r^2 + B_\varphi^2 + B_\theta^2) + \frac{1}{2r^2}\frac{d}{dr}(r^2 B_r^2). \tag{6.5}$$

Hence, radial component of the momentum equation for static equilibrium inside sunspot is

$$\frac{dP_i}{dr} = -g\rho_i - \frac{1}{r}(B_r^2 + B_\varphi^2 + B_\theta^2) - \frac{1}{2}\frac{d}{dr}(B_r^2 + B_\varphi^2 + B_\theta^2) + \frac{1}{2r^2}\frac{d}{dr}(r^2 B_r^2) \ , \tag{6.6}$$

where P_i and ρ_i are the internal pressure and density structures of the tube and g is acceleration due to gravity. Where as radial component of the momentum equation

for the static equilibrium outside the tube is

$$\frac{dP_e}{dr} = -g\rho_e \ , \tag{6.7}$$

where P_e and ρ_e are pressure and density structures of the ambient medium. Following Parker (1955b), hydrostatic equilibrium requires that the magnetic pressure P_m be balanced by the external gas pressure P_e outside the tube. Then we have

$$P_e = P_i + P_m \ , \tag{6.8}$$

where $P_m = B_r^2 + B_\varphi^2 + B_\theta^2$

Differentiating equation (6.8) and by using equations (6.6) and (6.7) , we get

$$\frac{dP_m}{dr} = \frac{d}{dr}(B_r^2 + B_\varphi^2 + B_\theta^2) = g(\rho_i - \rho_e) + \frac{1}{r}(B_r^2 + B_\varphi^2 + B_\theta^2) + \frac{1}{2}\frac{d}{dr}(B_r^2 + B_\varphi^2 + B_\theta^2) - \frac{1}{2r^2}\frac{d}{dr}(r^2 B_r^2). \tag{6.9}$$

Following Parker (1955b), it is is assumed that tube is in thermal equilibrium with it's surroundings such that temperature T_i inside the flux tube must be same as that of ambient temperature T_e. This condition implies that

$$\rho_i - \rho_e = -\frac{m}{2kT_e}(B_r^2 + B_\varphi^2 + B_\theta^2). \tag{6.10}$$

Integrating equation (6.9) on both sides, we get

$$B_r^2 + B_\varphi^2 + B_\theta^2 = [Cr^2]\exp[-\int \frac{mg}{kT_e}dr - \int \frac{1}{2[(B_r^2 + B_\varphi^2 + B_\theta^2)r^2]}\frac{d}{dr}(r^2 B_r^2)dr] \ , \tag{6.11}$$

where C is a integrational constant and T_e is temperature of the ambient medium. This equation is similar to Parker's (1955b) equation (16), except that LHS is a summation of square of strength of all the three components of magnetic field structure of the sunspot with also an additional integral term in the exponential of RHS. As the ambient pressure P_e is decreasing from the deep interior to surface, flux tube must expand from the interior to the surface. Although general solution of equation (6.11) is necessary, in this study, we make a reasonable assumption that radial

component of the magnetic field structure B_r varies as $1/r$. In this case the second integral term in exponential of equation (6.11) vanishes leading to a solution similar to Parker's solution (equation 16) such that

$$(B_r^2 + B_\varphi^2 + B_\theta^2) = Cr^2(P_e)^{1/2}. \tag{6.12}$$

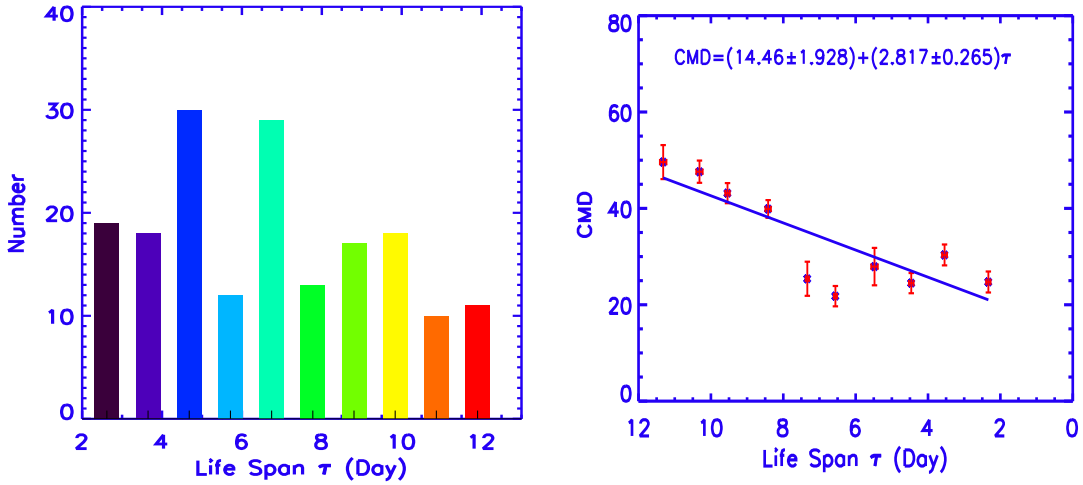

Figure 6.1: Irrespective of their sizes and for different life spans of the bipolar spots with their initial appearance on the surface, figure on the left side (Fig 6.1(a)) represents variation of number of spots and figure on the right side (Fig 6.1(b)) represents central meridian distances (in degrees) of the bipolar spots considered for the analysis. In the right figure, blue continuous line represents a linear least-square fit with a law $CMD = C_1 + C_2\tau$ (where CMD is central meridian distance, τ is life span in days and, C_1 and C_2 are the coefficients determined from the least-square fit).

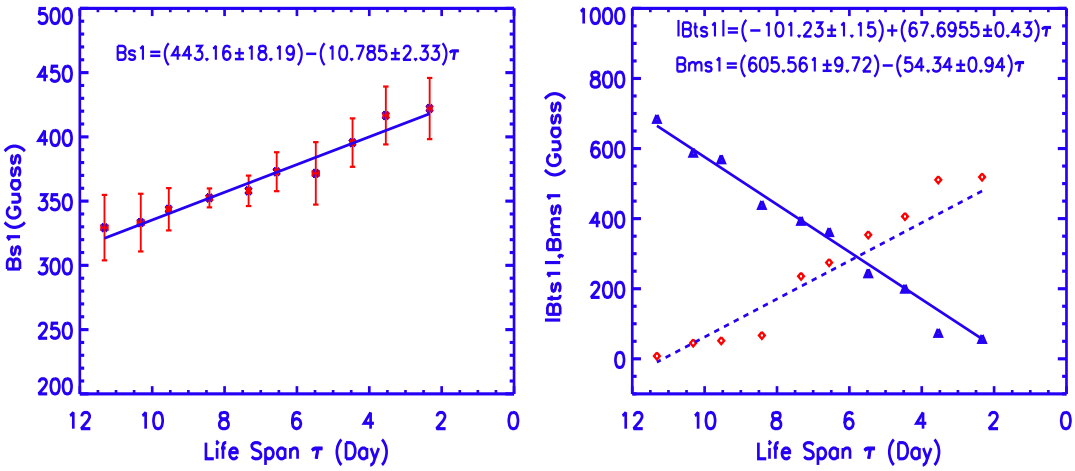

Figure 6.2: Irrespective of their sizes and for different life spans of the bipolar spots with their initial appearance on the surface, figure on the left side (Fig 6.2(a)) represents variation of measured average strength of line of sight component *Bs1* of the magnetic field structure and figure on the right side (Fig 6.2(b)) illustrates the estimated toroidal *Bts1* (blue triangles with blue continuous line) and poloidal *Bms1* (red diamonds with blue dashed line) components of the magnetic field structure. In both the figures, the blue continuous and dashed line represent the linear least-square fit with a law $B = C_1 + C_2\tau$ (where B is longitudinal or toroidal or poloidal field structures, τ is life span in days and, C_1 and C_2 are the coefficients determined from the least-square fit).

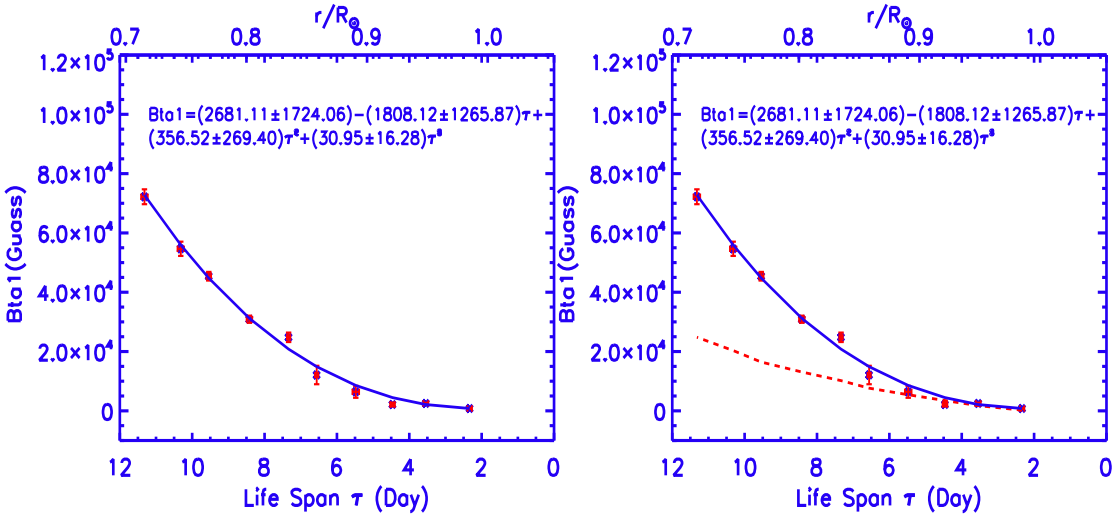

Figure 6.3: Irrespective of their sizes and for different life spans, inferred strengths of line of sight (*Ba*1, left figure -Fig 6.3(a)) and toroidal (*Bta*1, right figure - Fig 6.3(b)) components of magnetic field structure at different anchoring depths in the convective envelope. The blue continuous line in both the figures represents the polynomial fit with the laws indicated on the figures. The dashed red line over plotted on the Fig 6.3(b) is the radial variation of steady part of toroidal component of the magnetic field structure computed from the equation (21) of Hiremath (2001).

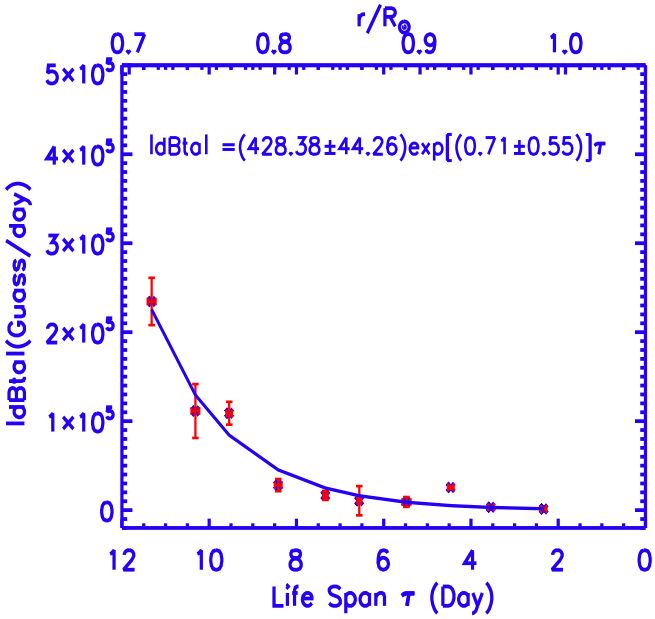

Figure 6.4: Irrespective of their sizes and for different life spans, rate of emergence of toroidal magnetic field structure $\frac{dB_\phi}{dt}$ at different anchoring depths in the convective envelope. Blue continuous line represents the exponential fit with a law indicated on the figure.

Table 6.2: Strength of inferred magnetic field at different anchoring depths in the convective envelope

$LifeSpan$ τ $Days$	$r/R_\odot$ $(Anc$ $dep)$	$Inferred$ B_l (G)	$Inferred$ B_φ (G)	$Theory$ B_φ (G)	$Emergof$ $Tor.Field$ (G/day)
$2-3$	0.995	464.4	787.41	236.2	1305.81
$3-4$	0.965	1182.4	2500.00	1757.9	3251.62
$4-5$	0.935	3501.7	2140.00	3479.2	25477.10
$5-6$	0.905	6164.6	6420.00	5432.1	9190.36
$6-7$	0.875	9493.3	12090.00	7654.9	10582.30
$7-8$	0.845	12795.4	24800.00	10193.8	16505.40
$8-9$	0.815	16684.5	30900.00	13104.4	28112.10
$9-10$	0.785	20995.8	45400.00	16454.5	108919.00
$10-11$	0.755	25155.6	54650.00	20326.8	111419.00
$11-12$	0.725	38568.5	72200.00	24823.1	234519.00

Chapter 4

Rotation rates of the sunspots during their initial appearance

4.1 Introduction

Sun rotates differentially and it's equator rotate faster than the poles. On average sun rotates on it's equator of ~ 2 km/sec. During its early phase of the evolutionary history, sun was rotating faster than the present phase. The question remains still open as to how the sun has lost it's high angular momentum from its initial phase. One possibility is that, as planetary system has high angular momentum, sun might have transferred it's high angular momentum to the solar system. Although how sun has transferred it's angular momentum to the solar system is debatable, it is interesting to know whether sun has very high angular momentum and hence might be rotating faster in the solar interior. Knowing of internal rotation of the sun is very crucial for understanding not only dynamical and thermal evolutionary history of the sun, but also the sun's internal rotation, especially near the core, is important either to confirm or disprove Einstein's general theory of relativity.

Before the advent of helioseismology, solar oblateness measurements (Dicke 1970) implied that the solar core may be rotating ~ 10 times faster than the surface. However, such a rapidly rotating core is ruled out by the helioseismic inferences and by the following studies. In the recent decade, helioseismology-a tool to probe the solar internal structure and interior dynamics-has changed our conventional perception of the large-scale internal dynamics. Observations from the ground based (GONG, BISON, IRIS, *etc.,*) and from the space (like SOHO) provided frequency

data of very high precision that are measured from the surface oscillations.

Though understanding of internal structure obtained from the solar evolutionary models is almost compatible with the solar seismic structure (Antia 1995; Takata & Shibahashi 1998; Shibahashi et al. 1998), internal dynamics, especially, internal rotation inferred from the helioseismology is not compatible with the rotation expected from earlier theoretical works. Most of the theories based on hydrodynamical works were developed before the advent of helioseismology and their main aim was to explain surface differential rotation. In the axisymmetric models, anisotropic *Reynolds stresses* and the resulting meridional circulations are supposed to play a dominant role in maintaining the differential rotation (Hiremath & Gokhale 1995; Hiremath & Gokhale 1996). Except some of (Kueker et al. 1993; Elliott et al. 1998) hydrodynamical works which simulate internal rotational isocontours approximately similar to rotational isocontours inferred from the helioseismology. From all these simulations it indicates that *Reynolds stresses alone cannot be responsible for the maintenance of differential rotation.* In addition to Reynolds stresses in the momentum equation, Maxwell stresses due to ubiquitous large-scale toroidal magnetic field of primordial origin in the solar interior may be necessary (Hiremath 2001) in order to reproduce proper rotational isocontours.

A typical inferred isorotational profile (Antia et al. 1998) from the GONG helioseismic splittings data is presented in the left figure of Fig 4.1(a). In Fig 4.1(b), isorotational profile obtained from the solution of MHD equations (Hiremath 2001) is presented. Right from the surface, *differential rotation* persists throughout the convective envelope and core is rotating quasi-rigidly. There appears to be a sharp transition near base of the convective envelope from differential rotation to quasi-rigid body rotation called *tachocline*. In the most reliable part of the inferred rotation, there is a decrease of angular velocity towards the center.

Sun's internal rotation, especially in the convective envelope, can also be inferred from movements or longitudinal displacements of positions of the sunspots, over the surface of the sun. Very first hint that sun's internal rotational profile does not increases from surface to the interior, as expected by the solar turbulent dynamo mechanisms for correct simulation of the solar butterfly diagrams, was suggested

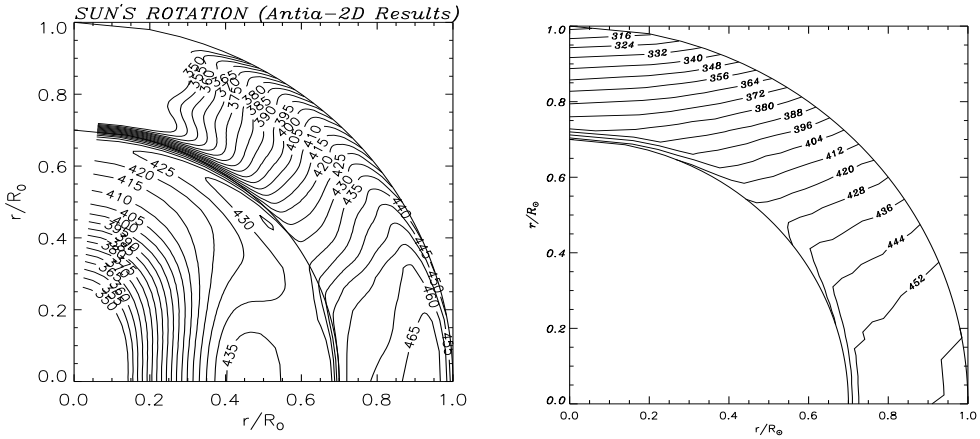

Figure 4.1: Left figure represents rotational isocontours inferred from the helioseismology (Antia & Chitre 1997) and right figure represents rotational isocontours obtained by the solution of MHD equations (Hiremath & Gokhale 1996). Isocontours of both the figures are in nHz.

from the study of changes in the sunspots' rotation rates (Gokhale & Hiremath 1984) during their life span. In fact, stunningly, this result was latter confirmed from the helioseismic studies of internal rotational profile in the convective envelope inferred from the observed helioseismic rotational splittings.

The sunspots are supposed to be tracers of internal dynamics and magnetic field structure of solar convective envelope. For example, morphological and dynamical properties of sunspots for first appearance on the surface for different life spans represent the different anchoring depths of the flux tubes. Due to the very high conductivity of the solar plasma, sunspots isorotate with the internal plasma, and due to buoyancy rise toward the surface along the path of rotational isocontours. Hence, if the sunspots with different life spans that originate at different depths have first and second observations on the surface, and if one computes their initial rotation rates, then one can infer the rotation rate of the internal solar plasma where sunspots' footprints are anchored. By matching the profile of variation of initial rotation rates of the sunspot groups for different life spans and the radial variation of the internal rotation of the solar plasma as inferred from Helioseismology (Anita et al.1997), it is possible to estimate different anchoring depths of the flux tubes in the convective envelope.

Using non-recurrent rotation rates of the sunspot groups during their initial appearances on the surface, in the recent study many authors (Javaraiah & Gokhale 1997; Javaraiah 2001; Sivaraman et al. 2003; Hiremath 2002) found that, for different life spans, variation of profile of observed initial rotation rates is almost similar to the radial variation of rotation profile in the convective envelope as inferred from the helioseismology. Inference of gist of these studies is that non-recurrent spots that have larger life spans (say 10-12 days) might be originated and anchored near base of the convection zone, where as the spots that have smaller life spans (2-3 days) might be originated and anchored near the surface.

Irrespective of their polarity, aforementioned studies compute rotation rates of the sunspots during their initial appearance on the surface. By knowing individual initial rotation rates and latitudinal separation of the leader and follower bipolar spots, one can get an idea of their separation at different anchoring depths in the convective envelope.

Irrespective of their life spans, from the Mount Wilson white light pictures and for the years 1917-1983, Gilman & Howard (1985) (here onwards referred as GH85) computed rotation rates of the leader and the follower bipolar spots and found that at all latitudes, leader spots rotate faster than follower spots by $\sim 0.1^0$ per day. For different phases of the solar cycle, these authors also found that leaders and followers show the same variation of rotation rates with respect to phase of the solar cycle.

However, as shown in the previous study (Hiremath 2002) that sunspots' rotation rates during their initial appearance is different for different life spans, yielding clues to internal rotation profile and anchoring depths of different flux tubes in the convective envelope. However, for different life spans, it would be interesting to know the rotation rates of the leader and follower respectively.

Keeping these ideas in mind, in the present study, for different life spans, rotation rates of the leader and the follower during their initial appearance on the surface are computed. Although present study is similar to GH85, following are the main differences: (i) data of bipolar spots of the SOHO/MDI magnetograms are considered, (ii) rotation rates are computed for the leader and the follower during their initial appearance on the surface and, (ii) initial rotation rates of the leader

and follower are classified according to different life spans.

4.2 Data and analysis

For a period of six years (2000-2005), bipolar spots from SOHO/MDI primary (at 1.8 level) magnetograms data is considered for estimating the initial rotation rates of the leader and follower. For the same period 2000-2005, times of observation (the first, second, and last observations during the lifetime of a spot on the same part of the solar disk) are noted. The SOHO/MDI magnetograms are observed in the Ni I 6768 A^0 line (Scherrer et al. 1995). Non recurrent sunspots that are born and vanish on same part of visible disk are considered. The combined data set for both the solar hemispheres and in the latitude range 0-15 degree is considered. The reason for combining the data set in this latitude range is that the information of anchoring depth (Hiremath 2002) of sunspots is available. Details of data selection and the analysis can be found from the previous published study (Hiremath & Lovely 2007).

Peter Meadows Helioviewer software is used for measuring heliographic latitudes and longitudes of the leader and the follower of the bipolar spots. Helioviewer is a software for the location of position of sunspots and estimation of their area. Peter Meadows Helioviewer software works in Windows operating system and accepts only the bitmap formated images. Hence, full disk SOHO/MDI solar magnetogram fits images are converted into bitmap images and by using Peter Meadows Helioviewer software, heliographic coordinates of the leader and the follower are computed. In order to determine rotation rate of the sunspots, consecutive two observations of the well developed bipolar spots that appear first on the solar surface are needed. For a given date and time of a well developed bipolar spot and by using Peter Meadows Helioviewer software, heliographic latitude and longitude for five different positions of the leader for the very first appearance are considered. Similar readings are also considered for the follower. Then average of five readings for each of the leader and follower is separately determined. Similar method is adopted for measurement of the heliographic coordinates for the consecutive second observation. For the

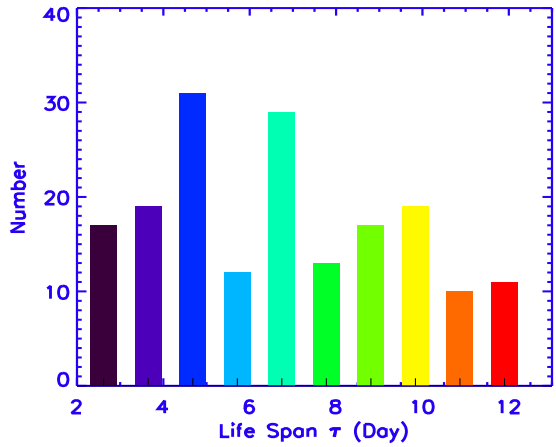

Figure 4.2: The selected number N of sunspots for different life spans are considered for the analysis.

two consecutive observations, as sun rotates on it's axis, there are displacements of positions of the leader and follower in the longitudinal direction. Hence, rotation rates of the leader and follower during their initial appearance on the surface can be computed as follows

$$\Omega_i = \frac{\phi_2 - \phi_1}{t_2 - t_1} \ , \tag{4.1}$$

where $i = l, f$ (symbols l and f are for the leader and the follower), ϕ_i $(i = 1, 2)$ are consecutive longitudinal displacements and t_i $(i = 1, 2)$ are consecutive time of observations.

As rotation rates computed from the observations are in the units of degree/day, these results are converted into the units of nHz for the sake of comparison with radial variation of solar internal rotational profile as inferred from helioseismology (Antia et al. 1998).

4.3 Results and conclusion

For different life span bins of 2-3, 3-4, etc., rotations rates are collected and average rotation rates are determined separately for the leader and the follower of bipolar spots. Uncertainty in the rotation rates of the leader and the follower are computed from the relation $\sigma/N^{1/2}$ (where σ is the standard deviation in the rotation rates and N is the number of samples used in each life span bin).

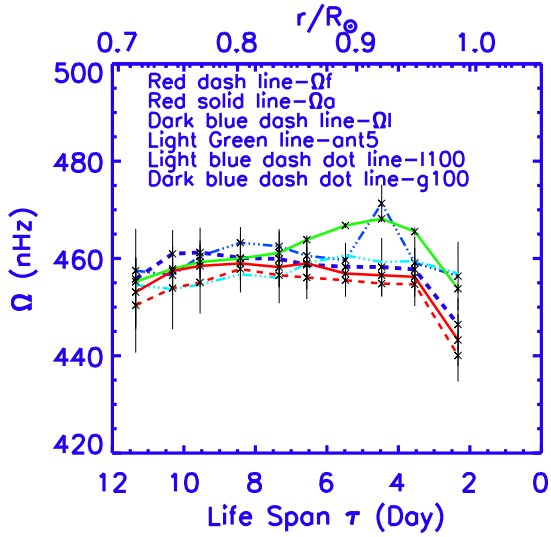

Figure 4.3: Irrespective of their sizes and for different life spans, variation of rotation rates of bipolar spots during their initial appearance on the surface are compared with radial variation of rotation profile, at heliographic latitude of 5 degree, inferred from the helioseismology (continuous light green curve) from (Antia & Chitre 1997).

For different life span bins, number of bipolar sunspots considered for the analysis is illustrated in Fig 4.2. In all the three figures (4.3-4.5) , for different life spans τ, variation of rotation rates Ω of the leader (dark blue dashed line), the follower (red dashed line) and average rotation rate (red solid line)of leader and follower are presented. In the same figures, initial rotation rates of the sunspot groups (Hiremath 2002) without polarity, for the areas less than 100 mh (dark blue dashed with three dotted line), the areas greater than 100 mh (light blue dashed dotted line) and radial variation of rotation rate (Green solid line) inferred by helioseismology (Antia et al. 1998) are presented. For the sake of comparison, radial $\frac{r}{R_\odot}$ coordinate is presented on the top of each plots.

One can notice, especially for the average radial variation of rotation profile taken for three heliographic latitude zones (5, 10 and 15 degrees) that are inferred from the helioseismology (Antia et al. 1998), that all the four profiles of initial rotation rates that are computed from the leader and follower of bipolar spots and from sunspot groups (with area < 100 mh and > 100 mh) are almost similar to radial variation of the rotation profile inferred from the helioseismology suggesting that rotation rates of the sunspots during their initial appearance on the surface give the clue to radial variation of internal rotation of the solar plasma. In order to further strengthen this

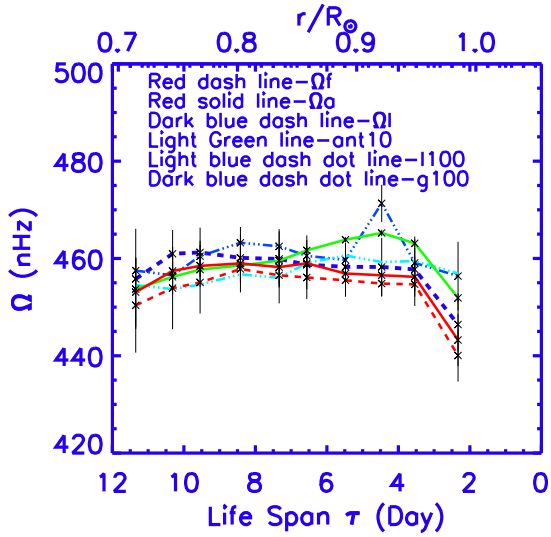

Figure 4.4: Irrespective of their sizes and for different life spans, variation of rotation rates of bipolar spots during their initial appearance on the surface are compared with radial variation of rotation profile,at heliographic latitude of 10 degree, inferred from the helioseismology (continuous light green curve) from (Antia & Chitre 1997).

view, for different life spans, difference in angular velocity $d\Omega$ between 5 degree and 15 degree latitudes of radial variation of solar plasma inferred by helioseismology and difference in rotation rates ($d\Omega = \Omega_l - \Omega_f$) between the leader and the follower are computed and are presented in Fig 4.6 (left figure). Further, for different life spans, rates of latitudinal rotational rates gradient ($\frac{\Omega_l - \Omega_f}{d\theta}$) (blue continuous curve) between the leader and follower spots are computed and is presented in the same figure (right illustration) . For comparison, radial variation of angular velocity gradient ($\frac{d\Omega}{d\theta}$) (between the latitudes 5 and 15 degrees) is computed and overplotted (Fig 4.6, right illustration red crossed curve). Again by strengthening the view (that rotation rates of the sunspots that have initial appearance on the surface can be used for inferring the radial variation of the internal rotational profile), both the profiles of $d\Omega$ and $\frac{d\Omega}{d\theta}$ that are computed from the rotation rates of the sunspots are almost similar to the radial variations of $d\Omega$ and $\frac{d\Omega}{d\theta}$ profiles inferred from the helioseismology. Correlation coefficient between these two profiles is found to be $\sim$ 90%.

Thus these results strongly suggest that, for different life spans of the sunspots, rotation rates of the sunspots during their initial appearance on the surface represent the rotation rate of the sunspots at different anchoring depths of the convective

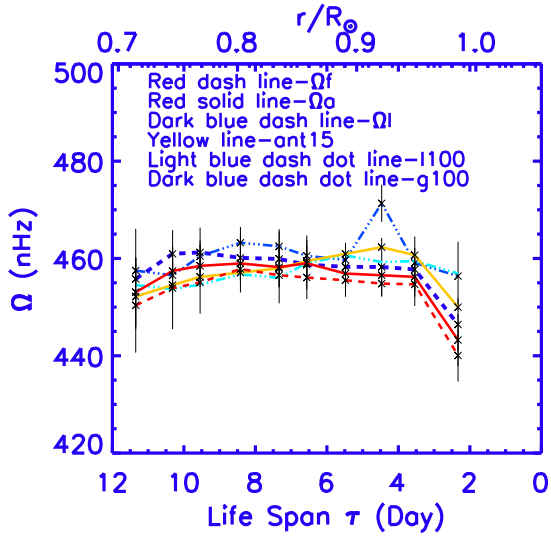

Figure 4.5: Irrespective of their sizes and for different life spans, variation of rotation rates of bipolar spots during their initial appearance on the surface are compared with radial variation of average rotation profile (for the heliographic latitudes of 5, 10 and 15 degrees) inferred from the helioseismology (continuous light yellow curve) from (Antia & Chitre 1997).

envelope yielding radial variation of the rotation profile in the convective envelope. These results obtained by bipolar spots confirm the previous results (Gokhale & Hiremath 1984; Javaraiah & Gokhale 1997; Hiremath 2002; Sivaraman et al. 2003; Zuccarello & Zappalá 2003).

This result is not surprising, in the convective envelope, owing to very high conductivity sunspots isorotate with the solar internal plasma rotation and travel along the isorotational contours while raising towards the surface. Hence, during their initial appearance on the surface, rotation rates of the sunspots on surface and rotation of the solar plasma where sunspot's foot point is anchored must be same. These inferences have far reaching implications. For example, one hidden assumption in the inference of solar internal rotation profile inverted from the rotational splittings is that sun is rotating slowly. This condition is true for the sun and the stars that rotate slowly. However, if the stars are fast rotators, similar method that is used in helioseismology can not be used for inference of internal rotation of the star from the stars' rotational splittings determined from the asteroseismology. In that case and in future, for fast rotating stars and for different life spans, if one measures rotation rates of the star-spots during their initial appearance on the surface, one can infer

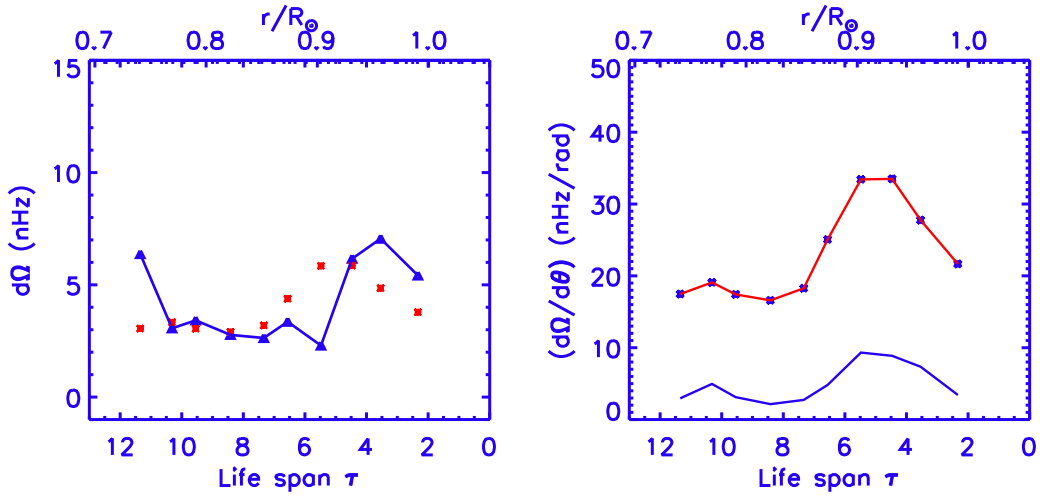

Figure 4.6: For different life spans, in the left illustration blue continuous line represents difference in rotation rates of leader and the follower of the bipolar spots and a over plotted red crossed curve represents radial variation of difference of the angular velocity between two latitudes 5 and 15 deg inferred from the helioseismology. Where as right figure illustrates the variation of latitudinal rotational rates gradient for different life spans from the sunspots (blue continuous curve) and radial variation of latitudinal angular velocity gradient $\frac{d\Omega}{d\theta}$ inferred from helioseismology (red continuous curve).

(without any knowledge of internal structure such as pressure, density, etc., that are needed for the kernels which are necessary for the inversion in case of rotation profile as inferred from the asteroseismology) the internal rotational profile. Off course this method of inference of internal rotational profile from the sunspots (during their initial appearance) presented in this study cam also be used for the sun like slow rotating stars and will give complementary results with the results inferred from the star's rotational splittings.

Another interesting result (see the left illustration of Fig 4.6) from this study is that, similar to results ofGH85 results, irrespective of area and their life spans, leader of the bipolar spots have faster rotation rates by ~ 5 nHz compared to rotation rates of the follower. This difference in rotation rates of the leader and the follower is due to difference in their heliographic latitudes. As the leaders in both the hemisphere are closer to the equator that rotate faster compared with the followers which are situated slightly at the higher latitudes that rotate slower, hence the leader of the bipolar spots rotate faster than the follower.

Finally it is interesting to know the heliographic latitudinal difference of positions

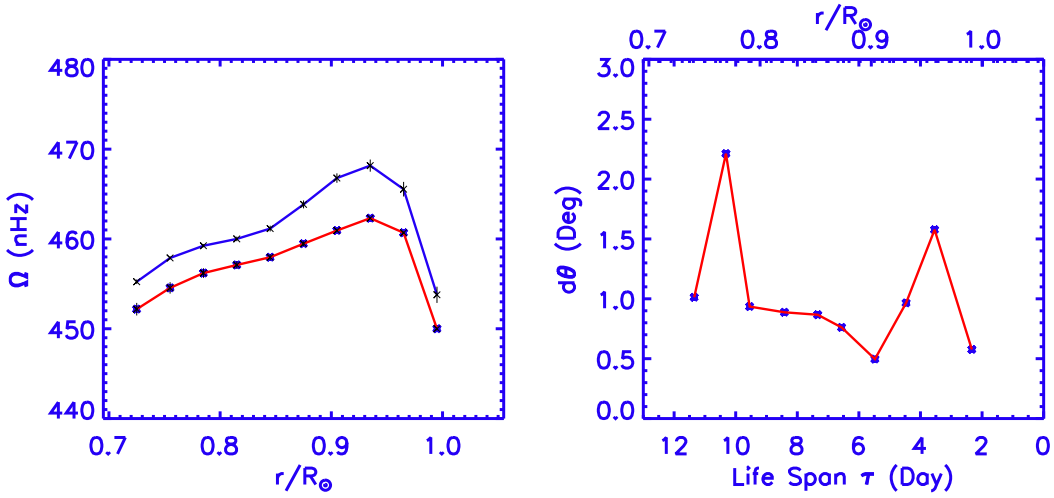

Figure 4.7: In the left figure red crossed curve represents angular velocity for latitude 15 deg over plotted blue curve represents the angular velocity for latitudes 5 deg inferred from the helioseismology. Where as right figure illustrates the difference in latitude between leader and follower (red crossed curve).

between the leader and the follower during their initial appearance on the surface. These results are presented in Fig 4.7 (right illustration). Except for the life spans of 11 and 3 days, for all life spans, on an average leader and follower of the bipolar spots have latitudinal difference of 1°. As the spots with 11 and 3 days have anchoring depths near base and near $0.935R_{\odot}$ where rotational shear and gradients exist, it is expected that difference $d\theta$ between leader and follower has a high gradient. In fact according to expectations, latitudinal difference of positions of the leader and follower spots shows such high gradients (in Fig 4.7, right illustration) in $d\theta$ at 11 and 2 day lifespans whose anchoring depths must be in the regions of two rotational shears, via., near base and near surface.

Overall conclusions from this study are : (i) irrespective of their sizes and for different life spans, leaders of the bipolar spots during their initial appearance on the surface rotate faster by $\sim 5\ nHz$ than the followers, (ii) irrespective of their sizes, variation of rotation rates of the leader and follower of bipolar spots with respect to their different life spans have almost similar radial variation of the rotation profile in the convective envelope inferred from the helioseismology and, (iii) this study suggests an independent method for inference of internal rotational profile of the sun and the stars without any information regarding internal structure that is needed in case of either helioseismic or asteroseismic inversion methods and, except for the

life span of 11 and 3 days, during their initial appearance on the surface, leader and follower of the bipolar spots have a latitudinal positional difference of $\sim 1^{\circ}$.

Chapter 5

Inference of longitudinal magnetic flux in the convective envelope

5.1 Introduction

The sunspots have been observed since the invention of telescope. Understanding of their evolution and their origin ultimately may give clue to the sun's internal dynamo mechanism that is supposed to be sustaining the solar cycle and the activity phenomena. On the surface though sunspots' dynamical and morphological properties are well understood, recently only Helioseismic investigations (Kosovichev 2004; Gizon & Birch 2005) reveal the jelly fish like structure below the surface consistent with Parker's (1979) idea, though stability of such a structure can not be guaranteed (Lites 1992; Chitre 1992; J. H. Thomas & N. O. Weiss 1992).

On the surface, sunspots erupt and are oriented in the east-west direction nearly parallel to the equator suggesting that they are supposed to be formed by the perturbation of the underlying diffused toroidal magnetic field structure. In the convective envelope, such a toroidal field structure may be prone to dynamical instabilities due to buoyancy (Parker 1979; Hughes & Proctor 1988; Hughes 1991). Toroidal field structure is also unstable if it varies continuously in the solar convective envelope (Gilman 1970), although simulations of the compressible numerical convection alleviate the problem of flux storage (Nordlund et al. 2000; Dorch & Nordlund 2001; Tobias et al. 2001). Yet it is not clear whether instability of the underlying toroidal field structure that represents the dynamo activity occurs near base or occurs everywhere in the convective envelope as recently proposed by Brandenburg (2005). Moreover

it is a unsettled problem whether sunspots are formed due to conventional turbulent dynamo mechanism or formed due to the perturbation of a diffused toroidal field structure in the convective envelope (Hughes 1992). If somehow sunspots are formed below the surface, still a crucial question is what is the magnitude of the magnetic field or magnetic flux at the sites of sunspots' anchoring depths.

Present consensus is that the sunspots originate below the solar surface. In the convective envelope, owing to differential rotation and cyclonic turbulence, the *dynamo mechanism* is supposed to wind the poloidal magnetic field structure into a toroidal magnetic field structure leading to formation of the sunspot structures. It is believed that the solar cycle and the activity phenomena are produced and maintained by such a dynamo mechanism (Parker 1955a; Babcock 1961; Steenbeck et al. 1966; Leighton 1969; Wang et al. 1991; Fan et al. 1993; Caligari et al. 1995; Durney 1997; Choudhuri 1999; Stix 2002; Ossendrijver 2003; Dikpati 2005; Charbonneau 2005; Gilman 2005; Browning et al. 2006; Solanki et al. 2006). Due to very high conductivity of the solar plasma (and assuming that rising flux tube does not acquire extra flux from the ambient medium), sunspots isorotate with the internal plasma and due to buoyancy raise towards the surface along the path of rotational isocontours. This implies that sunspots are very good tracers of the internal dynamics and magnetic field structure of the solar convective envelope. Hence if the sunspots with different life spans that originate at different depths have first and second observations on the surface and if one computes their initial rotation rates, then one can infer rotation rate of the internal solar plasma where the sunspots' foot points are anchored. In fact recent studies (Gokhale & Hiremath 1984; Javaraiah & Gokhale 1997; Javaraiah 2001; Hiremath 2002; Sivaraman et al. 2003; Zuccarello & Zappalá 2003; Meunier 2005) and from the results presented in the previous chapter substantiate this fact and show that the variation of initial rotation rates of the sunspot groups with different life spans is almost similar to the radial variation of internal rotation as inferred from the helioseismology. By matching the profile of variation of initial rotation rates of the sunspot groups for different life spans and the radial variation of the internal rotation of the solar plasma as inferred from the helioseismology (Antia et al. 1998), it is possible to estimate different anchoring

depths of the flux tubes in the convective envelope. Based on the analysis of rate of change of initial rotation rates of the sunspot groups and the radial gradient of rotation inferred from the helioseismology, Hiremath (2002, see the sections 3.3 and 4) further concludes that the spot groups that have life spans of $\geq$ 12 days may originate near base of the convective envelope and spot groups that have life spans $\leq$ 3 days may originate near the surface. However, the spot groups that have life spans 4-11 days may originate at different depths in the convective envelope.

Aims of the present study are two fold : (i) after measuring strength of magnetic flux of the sunspots that have their first and second observations on the solar disk, estimate the strength of magnetic field and the rate of emergence of the magnetic flux at different anchoring depths of the flux tubes in the solar convective envelope by using *anchoring depth-life span* information from the Hiremath's (2002) analysis and, (ii) to confirm whether the dynamo activity is distributed in the entire convection zone or confined to near region of base of the convective envelope. In section 5.2, the data used and the method of analysis are presented. The results are presented in section 5.3 and discussion with overall conclusions that emerge from this study are presented in section 5.4.

5.2 Data and analysis

For the period of seven years (1999-2005), full disk SOHO/MDI primary (at 1.8 level) calibrated 1 minute magnetogram data are used for estimating the magnetic flux of the individual spots. The SOHO/MDI magnetograms are observed in Ni I 6768 $\AA$ line (Scherrer et al. 1995). A typical magnetogram taken by SOHO/MDI is shown in Fig 5.2. A typical bipolar spot taken from SOHO/MDI observations is shown in Fig 5.1. Non-recurrent sunspots that are born and vanish on the visible part of the solar disk are considered. The combined data set for both the solar hemispheres and in the range of 0-15 degree latitude range is considered. The reason for combining the data set in this latitude range is that the information of anchoring-depth (Hiremath 2002) of the sunspots is available. Following criteria (Balthasar et al. 1986; Hiremath 2002) in selecting the spot groups are adopted. On the visible solar disk : (i)

the spot groups that occur in the latitude belt $\leq \pm 15$ degrees, (ii) in order to avoid the projectional effects (especially for the life spans of 10-12 days as they emerge near the limb), the spot groups that emerge within 65 degree longitudinal distance from the central meridian are considered and, (iii) the initial rotation rates of the spot groups (computed from the first and the second observations) should lie between 11-16 degree/day in order to safeguard from the effects due to either torsional oscillations (Howard & Labonte 1980) or due to abnormal rotation rates (Hiremath & Suryanarayana 2003) that are associated with the development of the abnormal magnetic flux and the flares. *Life span* τ of a spot group is defined to be total number of days between the first and the last observation on the same part of the solar disk satisfying the aforementioned criteria. Life span data are binned in the range of 2-3 days, 3-4 days, *etc.* Further number of sunspots and their life spans are collected in each bin and average life span is computed. In Fig 5.3(a), number of selected spots versus different averaged life spans are illustrated. For the same period 1999-2005, Positional measurements (such as latitude and longitude from the central meridian) and time of observations (the first, the second and the last observations during life time of a spot on the same part of the solar disk) from the Solar Geophysical data (USA) are used.

The magnetograms of the first and second observations are used for measurement of initial fluxes and rate of emergence of the magnetic flux. The times of observations of the first and last observations from the Solar Geophysical data are used for estimation of different life spans of the spot groups. With the positional measurements alone, ambiguity arises especially if the two spot groups are too close. Thus it is very difficult to match the positions of the sunspots on the magnetograms. Hence in order to locate the sunspots' positions on the magnetograms, sunspots' positions on the active region maps from the Mees Solar Observatory (http://www.solar.ifa.hawaii.edu/ARMaps/Archive/) are manually matched. Once position of a sunspot group on a magnetogram is located and keeping in mind the noise level in the MDI magnetograms is of $\sim$ 20 G (Scherrer et al. 1995), from the threshold of 20 isogauss contours, boundary of a sunspot group is determined. The MDI magnetograms provide the line-of-sight component of magnetic field in

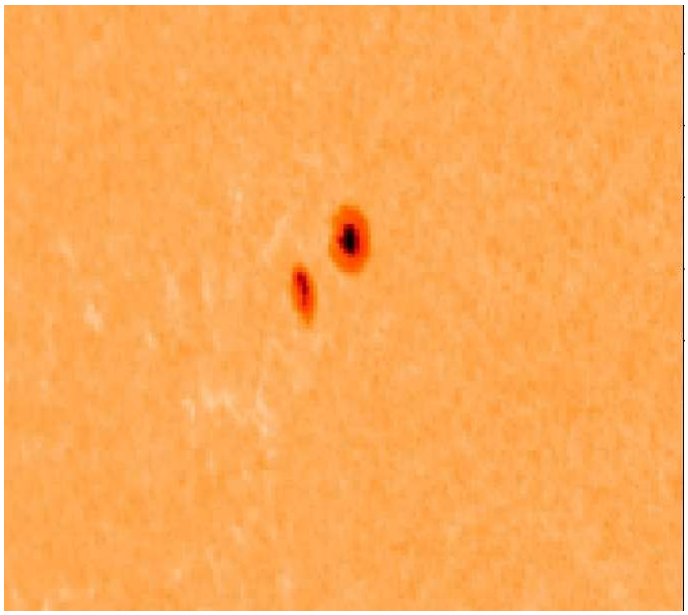

Figure 5.1: A typical bipolar spot taken from SOHO/MDI observations.

Gauss. Using *FV* interactive FITS file editor[1], strength of *average magnetic field* (with errors) that is averaged over total number of pixels considered in the detected boundary of a sunspot is estimated. Correspondingly, area of a sunspot group within a region of 20 isogauss contour is determined. The *average magnetic flux* of a spot group is determined by multiplying the average magnetic field and the area.

Irrespective of their life spans, Harvey (1993) mainly concentrated on measuring the magnetic flux of the active regions during their maximum developmental stage. Meunier (2003) computed flux-area relationship for the regions at any time during their lifetime. However present study is different in the following two crucial aspects. For different life spans : (i) determination of strength of the *initial* average magnetic field/flux of the bipolar regions and (ii) rate of emergence of the flux at the initial stage of development.

Since the line formation of the observed magnetograms occurs at 200 kms above the photosphere (Jones 1989; Meunier 1999), there is every possibility that the measured sunspot flux partly contains the plage flux also. Assuming that Parker's

[1] (http://heasarc.gsfc.nasa.gov/docs/software/ftools/fv/)

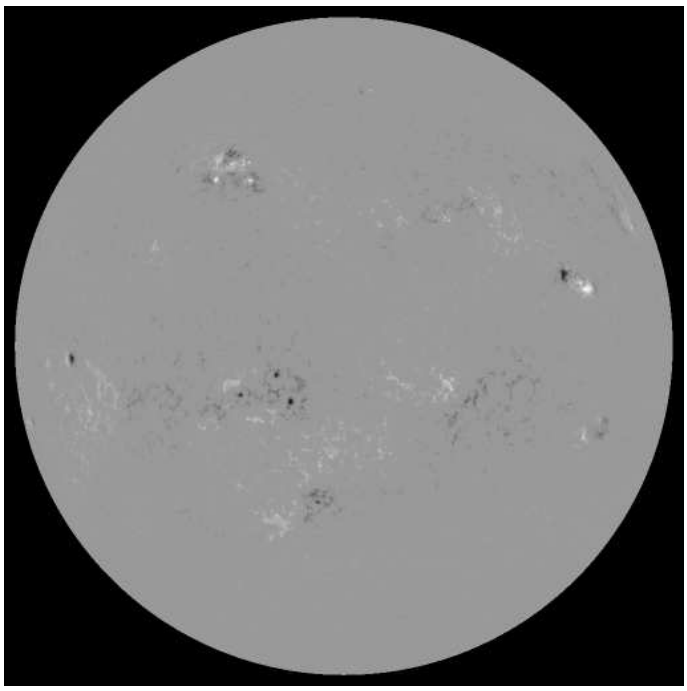

Figure 5.2: A typical magnetogram taken by SOHO/MDI on Feb 9^{th}, 2000.

(1955b) flux tube model is valid (i.e, strength of the flux tube is directly proportional to square root of the ambient plasma pressure; as this idea is used in the following discussion) and by knowing the observed average magnetic field and the pressure (Vernazza et al. 1981) at the height of the line formation ($\sim$ 200 kms above the photosphere), strength of average magnetic field and the flux at the photosphere are computed. Such a measured and corrected data set from the SOHO/MDI magnetograms is presented in Table 5.1. In Table 5.1, first column represents date of observation, second to fifth columns represent measured parameters for the leader and columns sixth to ninth represent measured parameters for the follower spots. As for the measured and corrected parameters, B_l and δB_l represent strength of line of sight of component and its measured uncertainty respectively; Area and MF are the measured area and magnetic flux of the bipolar spots.

Here onwards, computed average magnetic field/flux measured from the first two observations on the surface is called as *initial* magnetic field B_i $(i = 1, 2)$ and *initial* magnetic flux F_i $(i = 1, 2)$ of the spots. It is to be noted that time interval

between the two *initial* observations are considered from the observations compiled from the Solar Geophysical Data and it is not 96 min time interval as considered in the MDI magnetograms. However, the magnetogram data is considered when the time of observations from the Solar Geophysical Data are very close to the time of observations of the magnetograms.

Table 5.1: Measurements of line of sight component of magnetic field of the bipolar spots from SOHO/MDI magnetograms.

	Leader				Follower			
Date	B_l (G)	δB_l (G)	Area $\times 10^{17}$ (cm^2)	MF $\times 10^{19}$ (Max)	B_l (G)	δB_l (G)	Area $\times 10^{17}$ (cm^2)	MF $\times 10^{19}$ (Max)
11.01.2000	805.07	26.74	1.12	9.02	501.79	21.28	1.07	5.36
11.01.2000	674.70	51.96	0.75	5.06	528.48	53.84	0.84	4.44
15.01.2000	490.19	60.21	1.03	5.05	339.63	34.53	0.94	3.19
16.01.2000	349.57	20.27	1.12	3.92	435.06	52.21	1.03	4.48
18.01.2000	638.02	99.67	0.61	3.89	754.13	107.20	1.73	13.05
19.01.2000	518.39	35.27	1.72	8.92	547.09	49.86	1.12	6.13
20.01.2000	530.30	48.64	0.89	4.72	667.47	63.76	0.42	2.80
21.01.2000	523.23	81.94	0.42	2.20	547.09	49.86	0.98	5.36
23.01.2000	834.27	95.36	0.65	5.42	667.47	95.41	0.65	4.34
24.01.2000	772.12	92.41	0.89	6.87	586.82	66.11	1.59	9.33
25.01.2000	523.45	39.29	0.98	5.13	750.46	93.78	0.56	4.20
25.01.2000	964.59	93.37	0.89	8.59	952.56	89.27	0.87	8.29
19.01.2000	758.85	63.90	2.48	18.82	567.99	50.27	3.08	17.49
19.01.2000	731.97	55.42	3.69	27.01	731.97	55.40	3.69	27.01
09.02.2000	254.04	66.61	0.51	1.30	768.65	20.41	1.92	14.76
09.02.2000	773.42	124.61	0.70	5.41	741.00	59.44	0.16	1.19
22.02.2000	704.96	44.08	1.87	13.18	666.16	42.65	1.08	7.20
23.02.2000	413.12	39.82	0.79	3.26	640.81	38.14	1.12	7.18
23.02.2000	600.87	51.78	2.10	12.62	711.65	69.41	2.66	18.93
23.02.2000	539.10	67.01	2.94	15.85	663.35	59.44	0.93	6.17
24.02.2000	241.94	44.57	0.47	1.14	324.80	28.49	0.94	3.05
24.02.2000	317.20	21.18	0,19	0.60	339.68	30.02	0.89	3.02
03.03.2000	475.12	103.99	0.33	1.57	472.99	64.96	0.56	2.65
04.03.2000	553.25	50.72	0.75	4.15	497.16	97.44	0.74	3.68
07.03.2000	811.42	129.48	0.47	3.81	704.63	66.22	0.42	2.96
07.03.2000	791.75	143.18	0.65	5.15	874.00	53.81	1.40	12.24
13.03.2000	773.20	73.05	1.17	9.05	773.20	73.05	1.17	9.05
14.03.2000	1012.49	106.53	1.12	11.34	896.98	94.33	0.98	8.79
23.03.2000	782.23	78.16	1.12	8.76	679.74	62.46	1.22	8.29

Continued on next page...

Table 5.1 – continued from previous page

	Leader				Follower			
Date	B_l (G)	δB_l (G)	Area $\times 10^{17}$ (cm^2)	MF $\times 10^{19}$ (Max)	B_l (G)	δB_l (G)	Area $\times 10^{17}$ (cm^2)	MF $\times 10^{19}$ (Max)
23.03.2000	426.60	40.37	0.70	2.99	750.87	55.30	0.93	6.98
28.03.2000	588.04	37.33	1.73	10.17	586.92	35.94	1.87	10.98
29.03.2000	764.67	35.08	1.64	12.54	368.98	43.68	1.12	4.13
31.03.2000	355.80	89.66	2.34	8.33	377.99	24.06	1.22	4.61
31.03.2000	463.04	21.64	1.96	9.08	356.45	22.38	1.40	4.99
10.04.2000	253.61	24.20	0.94	2.38	252.74	52.06	0.19	0.48
10.04.2000	392.60	158.99	0.19	0.75	392.60	158.99	0.19	0.75
19.04.2000	543.55	63.01	0.75	4.08	873.76	119.18	0.79	6.90
19.04.2000	282.17	42.15	0.61	1.72	436.28	27.17	0.94	4.10
28.04.2000	618.02	57.50	1.17	7.23	480.58	118.00	1.40	6.73
28.04.2000	530.49	40.97	1.12	5.94	1120.71	119.20	0.61	6.84
28.04.2000	830.47	119.32	0.79	6.56	459.21	85.97	0.19	0.87
28.04.2000	719.92	72.19	0.18	1.30	638.31	117.52	0.28	1.79
28.04.2000	784.53	82.71	0.89	6.98	550.93	66.73	1.49	8.21
28.04.2000	690.54	98.67	2.10	14.50	526.15	44.25	5.66	29.78
29.04.2000	244.44	50.08	0.14	0.34	248.10	67.71	0.33	0.82
29.04.2000	239.93	50.70	0.33	0.79	239.93	50.70	0.28	0.67
05.05.2000	277.86	30.79	1.82	5.06	376.09	51.27	1.31	4.93
06.05.2000	254.12	24.06	0.31	0.79	336.13	34.26	2.19	7.36
10.05.2000	833.01	85.61	2.15	17.91	642.38	48.04	4.53	29.10
10.05.2000	620.00	77.25	2.06	12.77	329.42	28.80	1.08	3.56
13.05.2000	620.39	30.91	1.73	10.73	451.57	52.88	2.29	10.34
14.05.2000	376.05	34.38	6.45	24.26	364.04	28.34	3.08	11.21
15.05.2000	450.78	45.33	0.75	3.38	457.10	58.82	0.75	3.43
15.05.2000	373.98	40.61	4.02	15.03	290.51	14.86	0.98	2.85
01.06.2000	587.16	83.48	1.40	8.22	860.85	94.64	1.36	11.71
02.06.2000	569.28	40.47	4.53	25.78	623.50	80.58	1.54	9.60
03.06.2000	467.14	67.30	0.47	2.20	799.94	51.27	0.47	3.76
03.06.2000	302.08	49.17	0.98	2.96	666.29	58.92	0.98	6.53
11.06.2000	991.64	88.56	5.00	49.58	880.71	96.32	4.95	43.60
11.06.2000	876.97	55.11	1.28	11.22	726.91	100.34	5.84	42.45
11.06.2000	282.94	101.92	0.28	0.79	689.65	100.75	1.08	7.45
11.06.2000	600.07	10.11	0.09	0.54	660.26	63.71	4.72	31.16
16.06.2000	991.64	88.65	5.00	49.58	552.73	29.30	4.95	27.36
17.06.2000	357.43	16.68	12.80	45.75	726.67	100.32	5.84	42.44
17.06.2000	527.47	33.2	0.61	3.22	343.37	59.44	0.51	1.75
17.06.2000	426.75	79.55	0.56	2.39	613.27	70.99	0.75	4.60
23.06.2000	997.06	42.60	0.65	6.48	863.39	86.30	0.89	7.68

Continued on next page...

Table 5.1 – continued from previous page

	Leader				Follower			
Date	B_l (G)	δB_l (G)	Area $\times 10^{17}$ (cm^2)	MF $\times 10^{19}$ (Max)	B_l (G)	δB_l (G)	Area $\times 10^{17}$ (cm^2)	MF $\times 10^{19}$ (Max)
23.06.2000	873.23	115.73	2.01	17.55	777.27	99.46	2.38	18.50
17.07.2000	671.76	87.69	1.03	6.92	488.73	61.82	1.12	5.47
18.07.2000	406.04	76.67	2.06	8.37	370.61	58.92	1.36	5.04
29.07.2000	672.72	29.26	0.65	4.37	756.50	61.29	0.89	6.73
30.07.2000	681.03	103.27	1.12	7.63	487.58	49.55	1.68	8.19
04.08.2000	563.79	49.55	0.23	1.30	380.79	24.01	0.19	0.72
05.08.2000	915.81	51.42	1.64	15.02	707.72	70.42	2.06	14.58
10.08.2000	527.30	96.22	1.31	6.91	554.76	67.93	0.65	3.61
10.08.2000	810.53	63.25	1.36	11.02	544.46	86.52	0.94	5.12
12.08.2000	796.08	98.21	0.33	2.63	675.40	91.70	0.28	1.89
13.08.2000	379.34	79.09	1.12	4.25	179.43	11.93	1.17	2.10
14.08.2000	246.69	43.51	0.37	0.91	443.88	91.70	0.18	0.80
15.08.2000	379.38	35.46	0.37	1.40	179.43	11.93	1.17	2.10
30.08.2000	704.99	43.51	0.65	4.58	453.10	23.41	1.73	7.84
31.08.2000	568.01	44.09	0.33	1.87	623.14	81.34	0.33	2.06
03.09.2000	837.79	86.95	1.11	9.30	363.08	26.91	1.11	4.03
04.09.2000	536.67	47.44	4.52	24.26	430.65	59.59	1.92	8.27
13.09.2000	331.55	42.43	1.73	5.73	630.76	38.70	3.83	24.16
14.09.2000	321.63	47.44	3.83	12.32	349.19	26.07	4.35	15.19
21.09.2000	660.74	33.21	1.4	9.25	879.58	77.75	1.31	11.52
21.09.2000	925.13	90.64	2.10	19.42	1226.21	55.06	3.08	37.77
04.10.2000	532.09	69.05	0.65	3.46	668.86	63.25	1.31	8.76
04.10.2000	464.94	77.15	7.62	35.43	621.11	53.93	4.16	25.84
04.10.2000	278.27	50.84	1.03	2.86	400.13	21.18	2.19	8.76
04.10.2000	758.95	50.32	2.19	16.62	383.40	19.36	1.54	5.90
09.10.2000	672.45	109.11	1.03	6.92	642.38	48.04	1.45	9.32
09.10.2000	618.16	68.17	1.03	6.37	645.64	45.86	1.08	6.97
12.10.2000	894.01	70.15	1.5	13.41	1032.71	56.83	0.75	7.75
12.10.2000	783.36	72.19	0.98	7.67	278.27	50.24	1.03	2.87
18.11.2000	556.20	126.96	0.56	3.12	574.77	50.53	0.61	3.51
19.11.2000	725.91	43.85	0.61	4.43	491.08	35.87	1.92	9.43
27.11.2000	485.52	62.58	0.98	4.76	783.38	115.49	1.22	9.56
27.11.2000	658.77	43.37	1.03	6.79	826.94	120.16	1.26	10.42
28.12.2000	560.37	84.43	2.29	12.83	705.32	80.75	0.94	6.63
29.12.2000	573.19	37.14	0.37	2.12	573.19	73.70	3.6	20.64
01.01.2001	285.53	73.70	1.08	3.08	581.02	43.75	0.98	5.69
01.01.2001	512.45	44.33	0.84	4.31	841.08	68.48	0.42	3.53
06.01.2001	991.19	38.55	0.84	8.33	990.73	84.63	0.79	7.83

Continued on next page...

Table 5.1 – continued from previous page

	Leader				Follower			
Date	B_l (G)	δB_l (G)	Area $\times 10^{17}$ (cm^2)	MF $\times 10^{19}$ (Max)	B_l (G)	δB_l (G)	Area $\times 10^{17}$ (cm^2)	MF $\times 10^{19}$ (Max)
06.01.2001	872.73	84.63	1.96	17.10	870.73	71.86	1.73	15.10
16.01.2001	476.65	71.83	1.68	8.01	481.80	29.97	1.73	8.34
17.01.2001	372.41	26.84	1.78	6.63	311.98	29.23	1.87	5.83
24.01.2001	535.98	33.14	1.03	5.52	368.88	35.87	0.42	1.55
24.01.2001	883.92	54.15	0.65	5.75	648.80	40.99	0.23	1.49
27.01.2001	370.66	72.69	0.28	1.04	630.14	90.04	0.56	3.53
27.01.2001	565.06	58.94	0.75	4.24	362.03	24.39	2.94	10.64
30.01.2001	327.22	49.33	0.51	1.67	628.25	50.99	1.36	8.54
30.01.2001	328.63	36.90	3.31	10.88	652.97	32.66	2.15	14.04
30.01.2001	878.12	25.33	1.78	15.63	667.11	74.71	2.10	14.01
31.01.2001	822.73	71.40	1.40	11.52	562.40	59.83	1.36	7.65
06.02.2001	688.89	76.91	1.73	11.92	932.61	47.51	3.08	28.72
07.02.2001	546.78	54.63	4.95	27.07	1158.14	55.30	1.59	18.41
10.02.2001	419.70	36.71	0.61	2.56	308.55	37.26	2.80	8.64
10.02.2001	581.26	54.15	0.33	1.92	654.89	39.17	0.19	1.24
28.02.2001	644.01	77.13	0.42	2.71	675.59	45.43	0.61	4.12
28.02.2001	724.54	65.17	0.79	5.72	631.70	48.90	0.75	4.74
28.02.2001	606.95	37.04	2.43	14.75	624.53	162.83	0.14	0.87
28.02.2001	857.42	88.20	2.71	23.23	635.29	48.90	2.85	18.11
03.03.2001	377.89	65.12	0.65	2.46	298.73	42.39	0.98	2.93
03.03.2001	388.29	20.87	3.93	15.26	388.29	20.87	3.92	15.22
14.03.2001	541.70	56.57	9.35	50.65	741.74	61.77	1.5	11.13
15.03.2001	1059.47	68.24	2.01	21.29	824.85	76.65	3.55	29.28
24.03.2001	745.29	124.35	0.47	3.50	443.23	47.70	1.45	6.43
25.03.2001	318.09	58.13	0.56	1.78	485.73	92.80	0.42	2.04
24.03.2001	430.46	64.62	1.03	4.43	608.38	50.24	1.31	7.97
24.03.2001	395.96	51.44	1.26	4.99	502.60	46.10	2.01	10.10
26.03.2001	469.25	55.85	0.42	1.97	331.70	44.92	0.7	2.32
27.03.2001	444.04	90.62	0.19	0.84	502.60	46.07	2.01	10.10
01.04.2001	347.34	61.91	0.56	1.95	316.70	39.70	0.61	1.93
01.04.2001	316.70	39.73	0.65	2.06	295.14	59.20	0.51	1.51
07.04.2001	527.81	94.88	0.56	2.96	686.42	70.49	1.73	11.88
07.04.2001	260.85	28.63	0.33	0.86	281.60	46.87	0.28	0.79
03.04.2001	406.50	69.03	0.89	3.62	252.58	17.56	0.89	2.25
03.04.2001	331.75	56.38	1.78	5.91	265.04	20.68	1.49	3.95
11.04.2001	854.95	74.92	1.50	12.82	813.86	62.03	1.31	10.66
11.04.2001	564.23	70.66	1.73	9.76	903.37	73.46	1.68	15.18
11.04.2001	860.25	73.46	0.84	7.23	677.75	100.27	1.03	6.98

Continued on next page...

Table 5.1 – continued from previous page

	Leader				Follower			
Date	B_l (G)	δB_l (G)	Area $\times 10^{17}$ (cm^2)	MF $\times 10^{19}$ (Max)	B_l (G)	δB_l (G)	Area $\times 10^{17}$ (cm^2)	MF $\times 10^{19}$ (Max)
11.04.2001	1028.80	71.47	1.03	10.60	474.28	75.52	0.70	3.32
17.04.2001	703.10	110.17	0.61	4.29	578.05	47.61	0.84	4.86
18.04.2001	736.57	61.91	0.37	2.73	1028.80	71.47	1.78	18.31
29.04.2001	961.12	39.73	0.42	4.04	746.82	86.40	0.56	4.18
29.04.2001	746.82	94.88	0.37	2.76	799.39	120.57	0.56	4.48
29.04.2001	613.44	28.63	2.62	16.071	511.18	73.10	0.95	4.86
29.04.2001	943.32	70.97	1.31	12.35	658.67	26.24	2.99	19.69
02.05.2001	798.84	30.96	2.80	22.37	657.40	40.47	0.75	4.93
02.05.2001	784.34	29.78	3.13	24.55	583.54	29.52	0.94	5.48
09.05.2001	737.48	87.14	1.45	10.69	562.02	90.14	1.36	7.64
09.05.2001	1051.95	116.49	1.96	20.62	902.97	67.90	1.92	17.34
14.05.2001	844.98	116.25	0.47	3.97	679.23	89.61	0.42	2.85
14.05.2001	889.12	65.27	1.73	15.38	553.25	47.46	2.24	12.39
11.05.2001	959.44	90.33	0.79	7.58	365.89	48.04	0.28	1.03
12.05.2001	523.23	55.73	0.42	2.20	426.34	48.83	0.37	1.58
26.05.2001	878.98	101.35	0.98	8.61	737.67	99.48	0.89	6.57
27.05.2001	869.83	53.45	1.31	11.40	406.48	56.31	1.22	4.96
07.06.2001	715.60	42.3	1.12	8.02	417.90	53.45	0.37	1.56
08.06.2001	417.90	48.02	1.22	5.10	464.15	40.73	0.61	2.83
09.06.2001	704.82	55.42	0.94	6.63	672.09	60.91	0.28	1.88
10.06.2001	479.19	84.82	2.43	11.64	416.78	35.60	0.84	3.50
18.06.2001	559.80	87.12	0.42	2.35	456.73	62.99	0.42	1.92
18.06.2001	611.67	14.71	0.84	2.35	459.20	36.13	0.47	2.16
20.06.2001	736.52	74.95	0.23	1.69	736.52	55.40	0.23	1.69
20.06.2001	870.79	21.76	0.42	3.65	692.65	100.13	0.47	3.26
19.06.2001	693.68	179.70	0.37	2.57	666.87	62.34	0.94	6.27
19.06.2001	359.66	113.07	0.14	0.50	355.15	36.30	0.14	0.50
23.06.2001	541.03	33.66	0.14	0.76	562.21	46.55	0.42	2.36
23.06.2001	410.64	26.43	0.75	3.08	701.59	54.05	0.46	3.23
06.07.2001	842.04	37.86	0.51	4.29	696.89	42.55	0.51	3.55
07.07.2001	439.54	97.13	0.17	0.74	573.35	66.97	1.12	6.42
09.07.2001	443.09	35.46	0.19	0.84	287.18	84.17	0.23	0.66
09.07.2001	981.53	46.58	0.42	4.12	353.79	24.61	0.37	1.31
09.07.2001	472.96	41.55	3.32	15.70	802.58	123.68	0.84	6.74
09.07.2001	731.63	48.16	5.05	36.95	862.79	93.40	1.64	14.15
11.07.2001	541.03	87.12	0.94	5.09	667.25	69.34	0.42	2.80
11.07.2001	725.26	84.46	1.68	12.18	1022.36	120.18	0.75	7.67
18.07.2001	559.82	71.09	0.42	2.35	456.74	62.99	0.79	3.61

Continued on next page...

Table 5.1 – continued from previous page

	Leader				Follower			
Date	B_l (G)	δB_l (G)	Area $\times 10^{17}$ (cm^2)	MF $\times 10^{19}$ (Max)	B_l (G)	δB_l (G)	Area $\times 10^{17}$ (cm^2)	MF $\times 10^{19}$ (Max)
18.07.2001	611.67	31.24	0.84	5.14	459.21	36.13	0.47	2.16
23.07.2001	600.55	47.82	0.65	3.90	439.44	36.63	0.61	2.68
23.07.2001	429.48	57.60	1.08	4.64	245.01	15.14	2.43	5.95
01.08.2001	836.91	51.95	0.14	1.17	623.31	60.98	2.43	15.15
01.08.2001	918.76	42.43	2.71	24.89	827.81	33.78	2.85	23.59
01.08.2001	371.78	49.81	0.42	1.56	526.89	78.08	0.94	4.95
02.08.2001	776.82	61.82	4.07	31.62	762.32	93.16	1.50	11.43
11.08.2001	395.93	52.71	1.17	4.63	881.24	34.43	1.07	9.43
12.08.2001	444.76	104.08	0.65	2.89	401.20	56.57	0.98	3.93
22.08.2001	379.38	80.74	0.28	1.06	1011.58	71.64	0.65	6.58
23.08.2001	988.86	47.56	0.65	6.43	708.87	72.50	1.12	7.94
06.09.2001	335.60	22.62	0.47	1.58	392.05	39.34	0.42	1.65
07.09.2001	817.89	41.21	1.92	15.70	568.01	39.32	0.75	4.26
20.09.2001	514.61	39.56	1.92	9.88	447.45	25.64	1.92	8.59
20.09.2001	684.93	42.03	2.29	15.69	656.71	24.22	2.29	15.04
30.09.2001	283.13	73.03	0.89	2.52	158.97	16.01	0.89	1.42
01.10.2001	651.06	22.62	2.10	13.67	580.25	48.18	1.5	8.70
10.10.2001	548.63	41.21	0.94	5.16	456.79	66.22	0.89	4.07
10.10.2001	846.66	39.56	0.98	8.30	840.43	58.65	0.98	8.24
10.10.2001	527.81	42.03	0.56	2.96	295.54	28.32	1.17	3.46
10.10.2001	634.62	73.03	1.73	10.98	299.98	19.60	1.36	4.08
11.10.2001	501.21	85.18	0.37	1.86	257.93	29.23	0.56	1.44
11.10.2001	628.94	94.88	1.50	9.43	492.71	75.59	0.61	3.01
16.10.2001	560.18	57.12	1.17	6.55	632.53	35.29	1.08	6.83
16.10.2001	920.96	54.05	0.94	8.66	792.03	45.74	1.03	8.16
19.10.2001	986.85	33.50	0.19	1.88	621.44	62.32	0.98	6.09
19.10.2001	704.05	30.43	0.65	4.58	556.20	47.82	0.79	4.39
24.10.2001	284.90	72.29	1.73	4.93	581.26	38.89	1.82	10.58
24.10.2001	1040.97	43.87	2.52	26.23	354.79	38.14	1.92	6.81
07.11.2001	524.19	103.51	0.84	4.40	682.13	34.67	0.89	6.07
08.11.2001	619.67	109.06	1.68	10.41	868.49	82.97	0.89	7.73
07.11.2001	968.11	41.21	1.50	14.52	691.48	97.20	0.61	4.22
08.11.2001	266.10	62.63	0.65	1.73	593.74	66.11	0.75	4.45
19.11.2001	722.77	106.38	1.31	9.47	552.25	38.43	1.03	5.69
19.11.2001	313.85	39.68	0.56	1.76	383.59	31.36	1.17	4.49
22.11.2001	294.30	92.84	1.12	3.30	414.53	30.30	0.84	3.48
22.11.2001	834.54	65.19	1.82	15.19	491.75	65.77	0.42	2.07
22.11.2001	717.57	25.64	1.12	8.04	918.68	37.47	0.47	4.32

Continued on next page...

Table 5.1 – continued from previous page

	Leader				Follower			
Date	B_l (G)	δB_l (G)	Area $\times 10^{17}$ (cm^2)	MF $\times 10^{19}$ (Max)	B_l (G)	δB_l (G)	Area $\times 10^{17}$ (cm^2)	MF $\times 10^{19}$ (Max)
22.11.2001	651.94	82.97	1.73	11.28	821.46	44.40	0.75	6.16
01.12.2001	1022.17	87.41	1.5	15.33	662.32	44.28	1.03	6.82
01.12.2001	967.16	72.81	1.17	11.32	967.16	65.19	1.73	16.73
01.12.2001	612.48	40.01	1.96	12.01	575.99	21.83	2.01	11.58
02.12.2001	784.77	76.65	0.37	2.90	714.76	43.85	0.09	0.64
02.12.2001	950.48	100.25	0.75	7.13	809.64	84.02	0.75	6.07
02.12.2001	792.35	72.93	1.12	8.87	713.33	66.32	0.98	6.99
16.12.2001	451.35	74.99	1.4	6.32	516.79	31.60	1.49	7.70
17.12.2001	1087.98	112.75	1.82	19.80	640.90	49.86	0.95	6.09
19.12.2001	796.56	75.71	0.84	6.69	556.97	30.98	0.84	4.68
19.12.2001	749.82	83.69	0.56	4.20	440.02	68.55	0.84	3.70
20.12.2001	787.41	80.27	0.33	2.60	669.22	78.99	0.19	1.27
21.12.2001	780.56	23.36	0.94	7.33	787.63	82.52	0.75	5.91
26.12.2001	692.70	43.61	1.82	12.61	473.20	41.74	0.65	3.08
26.12.2001	954.50	50.56	1.45	13.84	777.83	112.68	0.84	6.53
27.12.2001	691.14	54.80	1.87	12.92	578.43	80.55	0.89	5.15
27.12.2001	348.52	73.41	2.06	7.18	348.52	23.36	9.75	33.98
01.01.2002	657.02	56.81	0.51	3.35	568.35	46.77	0.47	2.67
01.01.2002	561.88	87.02	2.1	11.80	561.88	50.56	3.13	17.59
09.01.2002	716.20	20.58	0.98	7.02	561.28	52.74	1.12	6.29
09.01.2002	893.17	27.58	1.26	11.25	722.84	70.15	1.08	7.81
20.01.2002	753.00	28.42	2.06	15.51	609.94	87.24	1.12	6.83
20.01.2002	869.62	77.85	2.8	24.35	463.81	57.31	1.08	5.01
15.01.2002	552.85	100.39	1.96	10.84	375.18	21.06	2.06	7.73
16.01.2002	624.46	50.60	2.01	12.55	521.36	25.64	2.10	10.95
20.01.2002	770.14	16.48	2.34	18.02	473.59	61.58	0.94	4.45
20.01.2002	840.29	19.10	1.36	11.43	754.13	34.21	2.66	20.06
23.01.2002	1140.0	50.65	0.79	9.01	191.44	45.02	0.75	1.44
23.01.2002	801.33	64.26	1.59	12.74	172.68	28.06	1.5	2.59
22.01.2002	475.96	117.76	1.17	5.57	255.79	10.85	1.21	3.10
22.01.2002	486.14	73.34	6.08	29.56	291.25	11.62	8.27	24.09
31.01.2002	657.84	96.19	1.50	9.87	247.29	14.83	1.59	3.93
31.01.2002	754.32	98.45	1.68	12.67	197.02	12.24	2.71	5.34
16.02.2002	705.59	37.38	0.33	2.33	455.19	47.01	1.45	6.60
16.02.2002	532.07	34.50	2.06	10.96	340.37	51.47	1.22	4.15
21.02.2002	800.71	34.67	1.26	10.09	722.00	31.99	76.65	9.46
21.02.2002	793.76	71.59	1.64	13.02	800.71	96.17	1.26	10.09
3.02.2002	335.60	74.61	0.98	3.29	388.48	14.09	0.94	3.65

Continued on next page...

Table 5.1 – continued from previous page

	Leader				Follower			
Date	B_l (G)	δB_l (G)	Area $\times 10^{17}$ (cm^2)	MF $\times 10^{19}$ (Max)	B_l (G)	δB_l (G)	Area $\times 10^{17}$ (cm^2)	MF $\times 10^{19}$ (Max)
24.02.2002	356.38	72.79	1.4	4.99	340.97	30.86	1.4	4.77
03.03.2002	318.64	95.36	3.18	10.13	451.86	50.51	1.03	4.65
03.03.2002	510.68	96.03	0.89	4.54	491.36	47.03	0.89	4.37
04.03.2002	834.23	81.51	2.80	23.36	429.29	14.43	34.57	6.43
04.03.2002	949.50	31.79	3.22	30.57	1012.34	96.03	2.80	28.35
03.03.2002	961.09	64.45	1.03	9.90	833.63	92.58	1.22	10.17
03.03.2002	989.17	140.38	1.08	10.68	1020.82	80.41	1.36	13.88
05.03.2002	1012.34	78.59	0.75	7.59	741.48	152.96	0.28	2.08
06.03.2002	822.30	108.94	3.88	31.91	721.23	56.55	0.84	6.06
21.03.2002	669.70	124.85	0.61	4.09	386.49	48.04	0.19	0.73
22.03.2002	559.84	57.19	3.55	19.87	291.04	25.92	0.98	2.85
20.03.2002	695.36	31.89	1.96	13.62	1109.28	130.25	0.61	6.77
21.03.2002	660.64	80.17	0.89	5.88	572.66	43.77	0.75	4.29
22.03.2002	403.50	71.59	0.89	3.59	743.73	99.10	1.4	10.41
22.03.2002	588.43	99.50	1.21	7.12	365.19	39.39	2.15	7.85
06.04.2002	554.64	112.75	3.22	17.86	577.79	56.11	0.7	4.05
07.04.2002	803.65	41.35	0.84	6.75	422.03	67.49	0.84	3.55
18.04.2002	443.85	39.03	0.51	2.26	468.51	43.66	0.56	2.62
18.04.2002	1053.89	75.04	0.84	8.85	646.17	95.17	0.84	5.43
18.04.2002	559.67	75.62	0.94	5.26	868.82	48.66	1.36	11.82
18.04.2002	960.69	105.83	0.84	8.07	1521.87	76.12	0.84	12.78
19.04.2002	1460.84	66.76	1.54	22.50	523.09	44.66	1.54	8.06
20.04.2002	936.94	47.20	2.43	22.77	518.34	40.59	1.68	8.71
24.04.2002	741.81	56.57	2.20	16.32	736.81	96.94	0.65	4.79
24.04.2002	776.12	79.52	2.52	19.59	1053.86	65.12	1.73	18.23
15.05.2002	834.23	126.12	0.98	8.18	973.12	99.50	0.98	9.54
16.05.2002	973.12	30.17	1.12	10.89	757.22	112.75	1.12	8.48
11.05.2002	757.22	43.63	1.26	9.54	417.04	31.99	0.56	2.34
11.05.2002	571.46	113.09	1.31	7.49	925.90	109.45	1.4	12.96
21.05.2002	707.77	76.82	1.03	7.29	725.38	77.61	0.65	4.72
22.05.2002	1103.87	75.04	1.50	16.56	690.25	58.17	0.7	4.83
30.05.2002	972.83	40.28	0.89	8.66	881.45	114.82	1.12	9.87
31.05.2002	609.82	83.62	1.49	9.09	785.61	75.45	1.50	11.78
13.06.2002	785.40	92.70	0.56	4.40	723.53	72.31	0.56	4.05
14.06.2002	648.42	44.81	0.56	3.63	587.71	107.32	0.42	2.47
06.06.2002	367.01	67.21	0.42	1.54	975.37	123.32	0.42	4.10
07.06.2002	948.30	40.01	0.65	6.16	831.16	37.09	0.19	1.58
09.06.2002	514.15	70.68	0.65	3.34	401.54	38.07	0.61	2.45

Continued on next page...

Table 5.1 – continued from previous page

	Leader				Follower			
Date	B_l (G)	δB_l (G)	Area $\times 10^{17}$ (cm^2)	MF $\times 10^{19}$ (Max)	B_l (G)	δB_l (G)	Area $\times 10^{17}$ (cm^2)	MF $\times 10^{19}$ (Max)
10.06.2002	274.53	66.61	0.37	1.02	416.78	52.28	0.42	1.75
18.06.2002	695.36	71.09	1.86	12.93	818.01	157.37	0.23	1.88
19.06.2002	578.27	80.34	0.33	1.91	367.30	62.08	0.28	1.03
08.07.2002	483.58	43.66	0.42	2.03	318.23	26.33	0.51	1.62
09.07.2002	438.49	78.59	0.93	4.08	255.12	46.63	0.37	0.94
24.07.2002	554.52	90.54	0.37	2.05	617.78	77.39	0.61	3.77
25.07.2002	675.02	32.90	2.38	16.06	425.93	51.80	2.15	9.15
23.07.2002	508.23	23.36	0.42	2.13	773.63	64.55	0.94	7.27
24.07.2002	379.07	58.56	0.51	1.93	580.93	45.26	4.35	25.27
24.07.2002	389.22	79.50	0.56	2.18	485.83	78.71	0.42	2.04
25.07.2002	615.24	44.99	2.43	14.95	323.38	49.19	1.78	5.76
26.07.2002	379.95	68.96	0.56	2.13	410.02	37.16	0.70	2.87
27.07.2002	1051.71	71.16	1.64	17.24	606.18	74.47	1.26	7.64
27.07.2002	816.81	55.83	1.12	9.15	552.845	39.56	1.96	10.84
28.07.2002	505.81	21.20	2.29	11.58	558.45	55.85	2.24	12.51
18.09.2002	813.02	46.00	0.75	6.10	632.37	70.39	0.98	6.20
18.09.2002	840.43	55.56	1.12	9.41	717.09	76.59	1.50	10.76
15.09.2002	494.86	101.59	2.15	10.64	360.14	25.181	2.29	8.25
15.09.2002	396.05	56.14	3.69	14.61	320.14	24.18	2.62	8.39
17.09.2002	367.28	23.24	1.17	4.30	260.18	82.66	1.12	2.91
18.09.2002	661.23	26.81	1.73	11.44	613.37	48.97	1.87	11.47
21.09.2002	383.88	65.55	0.98	3.76	241.01	23.91	0.98	2.36
21.09.2002	804.30	51.03	1.03	8.28	651.82	64.40	1.03	6.71
06.10.2002	764.17	155.28	0.37	2.83	404.86	46.82	0.33	1.37
06.10.2002	313.32	95.12	0.98	3.07	241.01	23.91	0.98	2.36
07.10.2002	390.49	53.31	0.75	2.93	504.76	31.48	0.56	2.83
07.10.2002	288.16	121.28	1.92	5.53	677.56	60.59	2.34	15.86
08.10.2002	277.52	33.16	0.33	0.92	277.76	46.07	0.33	0.91
09.10.2002	437.19	70.44	0.79	3.45	305.61	38.31	0.33	1.01
09.10.2002	613.92	93.18	0.33	2.03	709.83	53.72	0.61	4.33
09.10.2002	621.15	43.58	0.65	4.04	808.90	64.04	1.45	11.73
08.10.2002	159.21	31.94	1.36	2.17	77.86	9.13	7.57	5.90
12.10.2002	437.19	63.06	0.84	4.09	366.30	35.43	1.36	4.98
12.10.2002	613.92	109.02	1.17	5.63	479.96	37.88	1.40	6.72
15.10.2002	621.15	89.18	1.22	10.33	1054.89	130.77	0.65	6.86
15.10.2002	159.21	22.88	0.56	2.91	368.55	33.38	7.62	28.08
31.10.2002	236.60	20.73	0.87	5.38	434.34	41.67	0.75	3.26
31.10.2002	487.34	47.92	0.42	1.23	429.45	57.10	0.65	2.79

Continued on next page...

Table 5.1 – continued from previous page

	Leader				Follower			
Date	B_l (G)	δB_l (G)	Area $\times 10^{17}$ (cm^2)	MF $\times 10^{19}$ (Max)	B_l (G)	δB_l (G)	Area $\times 10^{17}$ (cm^2)	MF $\times 10^{19}$ (Max)
02.11.2002	480.94	98.57	0.79	4.81	493.33	52.66	0.75	3.70
02.11.2002	846.85	135.13	1.22	7.11	495.99	39.85	5.00	24.80
06.11.2002	521.00	107.46	1.12	7.59	520.43	47.85	1.08	5.62
06.11.2002	619.45	27.77	1.82	9.05	480.25	31.39	1.82	8.74
10.11.2002	293.17	34.02	1.17	6.39	506.46	50.39	1.12	5.67
11.11.2002	609.05	48.85	2.38	12.37	519.97	63.09	2.38	12.38
19.11.2002	582.75	29.28	0.94	7.76	275.68	31.77	2.57	7.09
20.11.2002	678.49	90.06	0.47	2.92	905.65	120.16	1.12	10.14
27.11.2002	497.38	44.99	2.90	20.02	451.81	37.74	1.87	8.45
27.11.2002	545.94	47.73	0.51	3.34	439.52	23.05	3.37	14.81
10.12.2002	519.97	72.31	0.42	1.24	317.82	50.84	0.42	1.34
10.12.2002	825.24	51.35	0.65	4.25	795.24	104.58	0.69	5.49
13.12.2002	621.15	51.03	0.51	3.32	543.55	87.88	0.65	3.53
13.12.2002	690.47	54.08	1.12	7.82	698.47	107.46	2.19	15.30
17.12.2002	655.01	64.07	1.12	4.51	543.24	59.76	1.21	6.57
17.12.2002	295.26	77.73	0.61	3.67	959.80	71.18	0.61	5.86
22.12.2002	464.29	107.89	1.12	5.20	212.57	28.82	2.48	5.27
22.12.2002	344.64	44.73	1.31	4.52	85.56	15.48	2.76	2.36
28.12.2002	644.30	39.27	1.78	11.47	978.70	88.94	0.84	8.22
29.12.2002	498.46	89.47	1.08	5.38	644.30	90.06	0.98	6.31
30.12.2002	495.73	125.17	0.51	2.53	546.40	76.17	0.51	2.78
31.12.2002	691.14	44.45	0.56	3.87	521.07	79.57	0.51	2.66
07.01.2003	359.56	58.77	1.31	4.71	366.32	35.44	1.36	4.98
08.01.2003	480.94	39.61	1.22	5.87	251.03	37.88	2.56	6.43
03.01.2003	1016.30	63.78	2.28	23.17	1092.99	98.12	0.65	7.10
03.01.2003	1029.19	81.68	4.02	41.37	974.32	48.69	1.50	14.62
06.01.2003	527.38	67.90	0.51	2.69	506.46	108.97	0.19	0.96
06.01.2003	810.46	66.73	1.03	8.35	552.73	77.25	0.42	2.32
10.01.2003	408.09	42.27	0.94	3.84	491.15	87.17	0.79	3.88
10.01.2003	403.55	94.31	0.47	1.90	572.66	43.77	0.47	2.69
04.01.2003	774.45	126.36	0.42	3.25	465.49	80.36	0.42	1.96
04.01.2003	1588.64	71.62	1.68	26.69	821.43	119.20	1.78	14.62
19.01.2003	272.45	23.15	0.70	1.91	911.16	90.02	1.08	9.84
19.01.2003	278.17	37.57	0.70	1.95	1061.72	102.26	1.64	17.41
21.01.2003	291.73	65.48	0.47	1.37	529.51	61.43	0.56	2.97
22.01.2003	357.17	72.84	0.65	2.32	461.75	30.40	0.75	3.46
26.01.2003	849.92	50.34	1.50	12.74	786.45	96.17	1.50	11.80
27.01.2003	865.16	60.76	3.22	27.86	785.28	66.78	2.01	15.78

Continued on next page...

Table 5.1 – continued from previous page

	Leader				Follower			
Date	B_l (G)	δB_l (G)	Area $\times 10^{17}$ (cm^2)	MF $\times 10^{19}$ (Max)	B_l (G)	δB_l (G)	Area $\times 10^{17}$ (cm^2)	MF $\times 10^{19}$ (Max)
26.01.2003	905.32	82.35	0.61	5.52	714.19	72.48	1.36	9.71
27.01.2003	784.32	50.17	3.69	28.94	865.16	67.90	1.73	14.97
04.02.2003	462.25	47.58	1.26	5.82	787.46	53.84	1.03	8.11
05.02.2003	1576.21	47.08	2.71	42.71	823.21	49.96	2.24	18.44
06.02.2003	1344.68	97.49	1.40	18.83	1147.30	110.67	1.08	12.39
06.02.2003	1062.63	100.56	1.50	15.94	852.99	100.56	1.73	14.76
24.02.2003	1026.12	45.24	12.52	5.52	781.54	122.96	0.47	3.67
25.02.2003	557.04	34.05	0.28	1.56	318.95	40.44	0.56	1.79
26.02.2003	321.56	51.71	2.10	6.75	123.22	36.73	1.31	4.23
27.02.2003	241.20	102.36	0.75	1.81	548.94	45.40	1.22	6.70
03.03.2003	438.46	60.98	0.37	1.62	247.53	29.97	0.37	0.92
04.03.2003	492.95	82.83	0.47	2.32	585.79	88.22	0.61	3.57
09.03.2003	257.16	75.04	0.94	2.42	576.45	61.94	0.89	5.13
09.03.2003	736.18	63.35	0.94	6.92	675.64	56.90	0.47	3.17
20.03.2003	852.22	39.34	0.89	7.59	400.01	73.39	0.84	3.36
20.03.2003	359.51	36.49	0.61	2.19	510.80	71.88	0.33	1.69
24.03.2003	389.66	33.74	0.42	1.64	425.12	71.21	0.42	1.79
24.03.2003	507.63	4.43	0.33	1.68	463.55	47.82	0.33	1.53
23.03.2003	663.74	1.63	1.12	7.44	663.87	45.21	1.12	7.44
23.03.2003	630.74	55.47	1.78	11.23	630.74	45.40	1.78	11.23
25.03.2003	449.58	38.36	1.31	5.89	598.87	54.05	1.31	7.84
26.03.2003	657.50	63.35	1.68	11.05	898.68	66.94	0.69	6.20
31.03.2003	629.76	39.34	0.98	6.17	810.08	77.20	0.69	5.59
01.04.2003	677.22	55.47	0.98	6.64	594.15	49.45	0.75	4.46
02.04.2003	801.04	38.36	0.65	5.21	944.85	102.76	0.98	9.26
03.04.2003	475.24	38.36	1.12	5.32	267.46	60.83	1.12	2.99
05.04.2003	615.60	63.35	1.12	6.90	280.99	26.96	1.12	3.14
05.04.2003	247.79	39.34	0.61	1.51	291.04	25.92	0.19	0.55
23.04.2003	392.82	55.47	1.03	4.04	671.76	49.29	0.75	5.04
23.04.2003	394.09	38.36	1.54	6.07	789.66	57.53	0.98	7.74
30.04.2003	220.31	38.36	3.18	7.01	122.41	1.53	4.11	5.03
01.04.2003	253.40	103.15	1.12	2.84	405.54	5.08	4.39	17.80
23.04.2003	690.88	59.01	1.03	7.12	286.03	35.44	0.75	2.15
23.04.2003	505.17	70.47	1.54	7.78	270.86	26.79	0.98	2.66
04.05.2003	394.09	615.59	0.61	3.76	280.99	26.96	0.19	0.53
05.05.2003	247.79	27.65	3.55	8.80	291.04	25.92	0.98	2.85
23.05.2003	690.83	29.28	0.15	1.04	286.03	35.44	1.26	3.60
23.05.2003	505.17	73.96	0.94	4.75	270.86	26.79	1.40	3.79

Continued on next page...

Table 5.1 – continued from previous page

	Leader				Follower			
Date	B_l (G)	δB_l (G)	Area $\times 10^{17}$ (cm^2)	MF $\times 10^{19}$ (Max)	B_l (G)	δB_l (G)	Area $\times 10^{17}$ (cm^2)	MF $\times 10^{19}$ (Max)
02.06.2003	896.40	104.75	0.75	6.72	1111.03	115.72	1.17	12.99
02.06.2003	1139.37	67.06	2.58	29.40	1327.09	101.80	2.80	37.16
18.06.2003	377.46	38.26	2.94	11.10	321.25	31.56	1.73	5.56
18.06.2003	395.65	54.29	2.99	11.83	338.17	39.03	1.73	5.85
19.06.2003	352.57	25.95	0.61	2.15	361.05	55.04	0.61	2.20
19.06.2003	986.25	35.94	0.75	7.40	1159.19	74.18	0.70	8.11
20.06.2003	249.40	41.88	0.47	1.17	474.55	48.06	0.89	4.22
20.06.2003	501.76	45.28	1.68	8.43	337.04	34.86	1.45	4.89
23.06.2003	986.11	83.26	1.08	10.65	339.63	34.53	3.74	12.70
23.06.2003	508.14	44.83	0.37	1.88	965.89	86.45	1.73	16.71
26.06.2003	651.07	43.89	0.75	4.88	726.15	43.08	0.75	5.45
26.06.2003	567.87	32.80	1.03	5.85	375.90	30.12	0.61	2.29
18.07.2003	869.69	37.04	1.68	14.61	520.34	69.98	2.15	11.19
18.07.2003	681.06	26.31	4.07	27.72	983.37	72.21	4.11	40.42
02.08.2003	292.67	30.64	0.94	2.75	502.17	38.41	1.59	7.99
03.08.2003	752.02	43.92	1.50	11.28	485.78	38.34	1.68	8.16
04.08.2003	689.46	23.74	1.31	9.03	564.99	128.28	1.22	6.89
05.08.2003	637.59	31.84	1.31	8.35	549.56	79.14	4.11	22.59
02.08.2003	608.93	36.11	1.36	8.28	400.49	26.91	1.78	7.13
03.08.2003	303.19	55.63	2.01	6.09	505.76	64.09	4.11	20.79
21.08.2003	503.95	65.58	0.33	1.66	411.14	42.50	0.37	1.52
22.08.2003	384.49	27.86	0.94	3.61	355.48	53.48	0.75	2.67
23.08.2003	275.25	63.16	0.65	1.79	245.78	21.56	1.03	2.53
23.08.2003	313.32	63.78	0.33	1.03	368.14	30.31	0.33	1.22
25.08.2003	533.37	37.62	9.03	9.71	414.05	30.38	1.68	6.96
25.08.2003	376.38	50.24	8.35	4.07	376.36	34.55	1.08	4.07
29.08.2003	844.94	43.92	1.12	9.46	690.90	29.71	1.22	8.43
29.08.2003	636.08	23.74	1.83	11.64	744.76	29.21	0.19	1.42
03.09.2003	326.71	31.84	1.36	4.44	373.82	36.73	1.45	5.42
04.09.2003	573.67	36.11	2.52	14.46	505.76	64.09	0.89	4.50
20.10.2003	443.78	55.63	0.89	3.95	320.20	13.06	2.29	7.33
20.10.2003	718.72	63.16	1.17	8.41	334.17	33.99	3.13	10.46
25.10.2003	632.87	63.78	0.98	6.20	506.63	55.68	0.94	4.76
26.10.2003	533.22	37.62	1.40	7.47	414.53	43.20	1.40	5.80
27.10.2003	328.77	50.24	0.28	0.93	813.55	146.56	0.33	2.69
28.10.2003	759.04	94.62	0.75	5.69	533.51	54.92	0.51	2.72
26.10.2003	531.47	90.33	0.56	2.98	910.97	118.86	0.51	4.65
27.10.2003	543.55	99.94	0.37	2.01	768.75	114.79	0.37	2.84

Continued on next page...

Table 5.1 – continued from previous page

	Leader				Follower			
Date	B_l (G)	δB_l (G)	Area $\times 10^{17}$ (cm^2)	MF $\times 10^{19}$ (Max)	B_l (G)	δB_l (G)	Area $\times 10^{17}$ (cm^2)	MF $\times 10^{19}$ (Max)
14.11.2003	609.25	53.62	1.68	10.23	266.55	22.98	1.64	4.37
14.11.2003	549.83	23.55	2.57	14.13	277.17	32.08	1.68	4.65
24.11.2003	767.95	89.47	0.61	4.69	677.60	86.54	0.70	4.74
25.11.2003	1026.02	84.91	1.78	18.26	880.11	56.95	0.79	6.95
12.12.2003	441.50	104.08	0.91	4.02	442.34	119.58	0.19	0.84
12.12.2003	494.14	117.62	0.23	1.14	293.91	6.73	0.09	0.27
16.12.2003	384.84	17.11	0.89	3.43	245.04	14.16	0.89	2.18
17.12.2003	570.29	46.75	0.84	4.79	347.61	17.95	0.89	3.09
23.12.2003	387.69	29.49	1.82	7.05	485.99	27.34	1.73	8.41
23.12.2003	434.84	21.90	2.52	10.96	391.98	21.01	2.48	9.72
07.01.2004	857.71	83.97	0.75	6.43	366.27	35.44	1.26	4.62
08.01.2004	624.53	82.78	0.94	5.87	479.98	71.38	1.40	6.72
01.01.2004	304.41	58.27	0.79	2.40	494.70	54.08	4.21	20.83
02.01.2004	397.99	53.07	1.50	5.97	406.93	39.29	0.67	2.73
31.12.2003	459.59	62.18	1.03	4.73	576.99	70.47	0.47	2.71
02.01.2004	259.15	27.77	6.78	17.57	1095.46	104.85	1.40	15.34
13.01.2004	750.54	82.37	0.70	5.25	458.54	40.90	0.23	1.06
14.01.2004	420.90	72.29	0.84	3.54	932.05	110.81	1.45	13.52
20.01.2004	60.18	0.34	1.40	0.84	78.06	0.84	2.94	2.30
20.01.2004	65.58	0.43	2.24	1.47	78.13	0.60	2.62	2.05
22.01.2004	412.66	62.94	0.65	2.68	319.09	48.30	0.47	1.50
23.01.2004	747.95	108.99	0.75	5.61	863.19	95.31	0.56	4.83
23.01.2004	747.97	57.24	0.47	3.52	478.79	55.32	0.47	2.25
23.01.2004	743.11	43.22	0.61	4.53	501.52	98.55	0.61	3.06
04.03.2004	611.74	47.49	1.68	10.28	655.92	62.51	1.22	8.00
05.03.2004	630.62	53.05	2.01	12.68	495.51	34.67	1.92	9.51
08.03.2004	465.99	41.40	0.84	3.91	735.75	41.38	0.84	6.18
10.03.2004	558.04	61.29	1.03	5.75	488.20	38.98	2.29	11.18
12.04.2004	250.07	43.51	0.75	1.88	332.70	33.83	0.75	2.50
13.04.2004	396.39	45.33	0.75	2.97	463.09	60.57	0.70	3.24
16.04.2004	352.57	31.75	1.22	4.30	390.49	33.14	1.17	4.57
17.04.2004	357.26	29.97	1.68	6.00	324.20	32.61	2.10	6.81
18.04.2004	515.80	48.69	1.12	5.78	653.19	59.80	1.12	7.32
19.04.2004	494.53	45.81	1.82	9.00	502.55	52.14	1.73	8.69
20.04.2004	967.35	95.45	0.79	7.64	1024.15	67.66	0.79	8.09
21.04.2004	637.67	70.73	1.36	8.67	508.75	84.12	1.36	6.92
29.04.2004	594.75	68.36	1.36	8.09	419.20	19.29	3.18	13.33
30.04.2004	494.53	526.13	1.45	7.63	397.99	53.07	6.68	26.59

Continued on next page...

Table 5.1 – continued from previous page

	Leader				Follower			
Date	B_l (G)	δB_l (G)	Area $\times 10^{17}$ (cm^2)	MF $\times 10^{19}$ (Max)	B_l (G)	δB_l (G)	Area $\times 10^{17}$ (cm^2)	MF $\times 10^{19}$ (Max)
12.05.2004	659.15	80.43	1.50	9.89	558.12	79.12	1.45	8.09
12.05.2004	459.86	36.52	1.82	8.37	543.91	67.42	1.82	9.90
12.05.2004	823.49	75.04	0.28	2.31	678.49	80.74	0.61	4.14
12.05.2004	355.42	89.06	0.75	2.67	674.66	69.77	1.12	7.56
17.05.2004	611.67	77.03	0.98	5.99	573.57	85.68	0.98	5.62
17.05.2004	689.51	80.07	0.33	2.28	523.59	111.72	0.28	1.47
23.05.2004	1081.73	106.07	0.75	8.11	835.78	127.01	0.42	3.51
24.05.2004	609.05	63.11	0.79	4.81	675.57	74.56	2.52	17.02
22.05.2004	212.38	18.02	0.56	1.19	92.92	20.34	0.28	0.26
23.05.2004	177.88	14.64	3.50	6.23	180.29	61.10	0.33	0.60
01.06.2004	479.84	61.07	0.75	3.60	362.65	63.28	0.42	1.52
01.06.2004	637.18	94.93	1.31	8.35	616.46	91.45	1.22	7.52
04.06.2004	638.50	93.29	0.47	3.00	423.25	58.68	0.56	2.37
05.06.2004	508.16	72.09	1.17	5.95	523.95	68.64	1.50	7.86
07.06.2004	711.58	106.24	0.84	5.98	531.71	67.85	0.56	2.98
07.06.2004	601.94	96.20	1.26	7.58	337.09	37.67	0.61	2.06
07.06.2004	837.80	121.81	0.98	8.21	734.44	113.78	0.89	6.54
07.06.2004	700.48	111.13	1.08	7.57	707.24	106.12	1.87	13.23
09.06.2004	837.80	612.38	0.47	2.88	585.60	57.65	1.31	7.67
09.06.2004	279.73	44.97	2.24	6.27	395.14	43.03	2.90	11.46
11.08.2004	317.25	41.50	0.56	1.78	460.15	96.92	0.51	2.35
12.08.2004	392.03	27.48	0.28	1.10	476.08	83.24	0.19	0.91
18.08.2004	358.51	26.88	3.27	11.72	273.36	45.48	1.22	3.35
18.08.2004	197.12	22.07	3.18	6.27	197.14	22.04	3.18	6.27
24.10.2004	684.62	66.32	0.42	2.88	554.71	84.96	0.42	2.33
25.10.2004	278.32	35.89	0.75	2.09	539.09	48.57	1.31	7.06
19.10.2004	1008.84	92.15	1.22	12.31	826.08	135.95	0.42	3.47
20.10.2004	709.11	72.65	0.61	4.33	717.26	75.83	1.22	8.75
16.10.2004	772.12	97.49	2.90	22.39	506.15	24.99	1.54	7.80
17.10.2004	765.01	66.63	2.43	18.59	364.45	25.28	3.83	13.96
17.10.2004	620.67	103.05	0.33	2.05	583.20	27.12	0.19	1.11
18.10.2004	469.35	93.49	0.94	4.41	966.44	95.96	0.61	5.90
17.11.2004	698.74	116.23	0.33	2.31	492.11	91.12	0.19	0.94
17.11.2004	613.73	93.97	0.47	2.89	422.12	41.40	0.37	1.56
23.11.2004	539.69	75.02	0.37	1.99	562.19	46.55	0.42	5.57
24.11.2004	400.17	49.57	0.37	1.48	703.89	95.12	0.42	2.96
10.12.2004	812.69	74.37	0.75	6.10	761.05	83.55	0.65	4.95
11.12.2004	1088.70	92.22	1.31	14.26	808.69	81.49	0.75	6.07

Continued on next page...

Table 5.1 – continued from previous page

	Leader				Follower			
Date	B_l (G)	δB_l (G)	Area $\times 10^{17}$ (cm^2)	MF $\times 10^{19}$ (Max)	B_l (G)	δB_l (G)	Area $\times 10^{17}$ (cm^2)	MF $\times 10^{19}$ (Max)
31.01.2005	186.53	51.61	1.22	2.28	395.07	49.62	0.56	2.21
31.01.2005	380.31	36.06	1.36	5.17	601.60	30.26	2.57	15.46
30.05.2005	226.44	29.66	1.40	3.17	295.71	20.15	0.75	2.22
1.05.2005	211.16	29.14	0.56	1.18	277.52	20.58	0.61	1.69
18.06.2005	281.55	31.58	0.98	2.76	84.75	10.47	0.28	0.24
18.06.2005	245.32	36.23	0.23	0.56	83.91	13.85	0.19	0.16
11.07.2005	1329.38	55.52	1.54	20.47	535.95	57.36	0.23	1.23
11.07.2005	506.507	34.79	2.43	12.31	364.45	25.28	3.83	13.96
23.07.2005	729.52	92.39	0.75	5.47	611.91	74.37	0.70	4.28
23.07.2005	433.21	67.49	1.22	5.29	500.68	69.44	0.79	3.96
29.07.2005	921.99	62.13	0.65	5.99	363.08	77.46	0.37	1.34
29.07.2005	380.53	48.61	1.22	4.64	904.74	65.72	0.56	5.07
10.10.2005	872.95	32.68	3.32	28.98	612.55	36.35	4.39	26.89
11.10.2005	793.16	30.88	5.33	42.28	596.98	25.73	4.30	25.67
30.10.2005	602.99	72.89	0.89	5.37	549.47	50.53	0.98	5.39
31.10.2005	749.34	79.28	1.31	9.82	1022.00	65.99	1.31	13.39
05.11.2005	379.38	52.74	0.89	3.38	699.77	93.56	0.84	5.87
06.11.2005	328.58	60.28	1.03	3.38	490.89	37.16	1.03	5.06
19.11.2005	1064.69	97.01	1.03	10.97	291.95	45.07	0.33	0.96
20.11.2005	1069.94	93.59	1.82	19.47	463.28	56.40	1.82	8.43
24.11.2005	790.43	76.50	1.82	14.39	1040.95	89.92	1.82	18.95
26.11.2005	521.36	80.43	2.24	11.68	569.26	41.81	2.15	12.24
02.12.2005	1136.33	131.18	0.33	3.75	1081.51	149.72	0.33	3.57
03.12.2005	591.23	50.84	1.12	6.62	706.40	93.04	0.94	6.64
28.11.2005	393.15	49.48	0.98	3.85	301.94	52.52	0.51	1.54
29.11.2005	516.57	43.75	0.56	2.89	442.03	41.12	0.61	2.70
4.12.2005	638.02	99.55	0.61	3.89	393.15	49.45	0.37	1.46
05.12.2005	516.57	43.75	1.54	7.96	442.03	41.12	1.45	6.41
30.11.2005	346.43	23.12	2.06	7.14	340.85	21.85	1.03	3.51
01.12.2005	889.12	93.18	1.45	12.89	817.93	47.25	0.70	5.73
01.12.2005	422.12	88.48	0.75	3.17	623.19	57.95	0.65	4.05
01.12.2005	994.73	105.76	1.08	10.74	995.57	67.54	1.03	10.25
09.12.2005	569.93	54.63	2.90	16.53	781.44	68.53	0.98	7.66
10.12.2005	598.54	36.78	1.59	9.52	836.89	61.84	0.94	7.87
17.12.2005	733.14	42.96	2.90	21.26	308.86	36.32	0.47	1.45
17.12.2005	638.12	35.63	2.62	16.72	223.23	54.34	0.19	0.42
21.12.2005	377.08	46.03	0.75	2.83	264.92	28.44	0.65	1.72
22.12.2005	299.99	61.96	0.47	1.41	368.64	40.90	0.47	1.73

Continued on next page...

Table 5.1 – continued from previous page

	Leader				Follower			
Date	B_l (G)	δB_l (G)	Area $\times 10^{17}$ (cm^2)	MF $\times 10^{19}$ (Max)	B_l (G)	δB_l (G)	Area $\times 10^{17}$ (cm^2)	MF $\times 10^{19}$ (Max)
22.12.2005	497.74	9.79	0.14	0.70	627.34	72.14	0.56	3.51
22.12.2005	357.65	54.70	0.33	1.18	556.49	77.80	0.56	3.12
09.11.1999	629.80	102.36	0.51	3.21	810.05	77.22	0.28	2.27
09.11.1999	441.03	49.69	0.65	2.87	594.15	49.45	0.33	1.96
15.11.1999	686.92	84.91	0.33	2.27	248.75	61.36	0.37	0.92
16.11.1999	423.70	44.30	0.79	3.35	422.96	68.31	0.75	3.17
06.12.1999	286.94	28.06	1.03	2.96	760.96	86.26	0.42	3.20
06.12.1999	245.96	20.15	3.04	7.48	406.07	50.17	1.36	5.52

Using *initial* two observations, the *rate of emergence of the magnetic flux* (REF) from the following relation is computed

$$REF = \frac{(F_2 - F_1)}{(t_2 - t_1)}, \tag{5.1}$$

where F_1 and F_2 are measured fluxes, t_1 and t_2 are the time of observations for the first and second *initial* observations respectively. For different life spans, time difference between the second and the first observations are collected and averaged over each life span bin. For different life-spans, the averages of such observed time differences dt with their error bars along both the axes are presented in Fig 5.3(b). The errors are determined using the formula $\sigma/(N)^{1/2}$, where N is the total number of observed events in different life span bins and, σ is the standard deviation. One can notice from Fig 5.3(b) that, for different life spans, on average the time difference between initial two observations are $\sim 12 \pm 2$ hours.

5.3 Results

It is found that majority of the sunspots during their initial observation on the surface are bipolar. Thus strengths of initial magnetic field and magnetic flux for each of the leading and following bipolar spots respectively are computed. Keeping in mind the Hale's law (*i.e* in a particular solar cycle, polarities of the leading

and the following sunspots in both the northern and southern hemispheres are in opposite signs) of magnetic polarity, irrespective of their polarities in the northern and southern hemispheres, strengths of initial magnetic field for the leading and the following spots are separately collected. Similar procedure is adopted and strength of magnetic fluxes for the leading and the following spots in the northern and southern hemispheres respectively are collected. For the sake of statistical significance, both the leading and following spots data set is merged.

For the first and the second observations, after classifying into different life spans, measured strength of average magnetic field and the flux values with their respective average errors are computed. Then a linear least square fit of the form $y = C_1 + C_2\tau$ to both the observed data set is computed, where y is the observed initial magnetic field/flux values, τ is the life span of the spots and, C_1 and C_2 are the unknown coefficients to be determined. For different life spans, in Fig 5.4, variation of strength of the measured *initial* average magnetic field is illustrated and in Fig 5.5., strength of *initial* average magnetic fluxes that are derived from *initial* two observations of the bipolar spots on the surface are illustrated. The corresponding law of fits, the rank correlation coefficients and significance of the rank correlation coefficient are computed from IDL software and are over plotted on each of the figures. According IDL, significance of the rank correlation coefficient is the two-sided significance of its deviation from zero.

One can notice in Fig 5.5 that the bipolar spots with their first and second observations have strong and significant negative correlations between life span and measured *initial* magnetic fluxes that are in the range of $\sim 2X10^{19} - 4X10^{20}$ Mx over the surface and are consistent with the conclusion of the previous study (Harvey 1993).

Similarly, for the bipolar spots that have first and second observations (Fig 5.4), we find strong and significant negative correlations between the life span and measured *initial* average magnetic field strengths that are in the range of $\sim 400 - 600$ G.

For all the life spans combined together, the maximum values of the *initial* magnetic flux and the area are determined. In Fig 5.6., for all the life spans, the normal-

ized (with respect to their maximum values) *initial* areas versus *initial* magnetic flux of the bipolar spots are presented for their first and second observations suggesting a strong linear relationship between these variables. Hence, linear least square fit of the form $F = C_1 + C_2 A$ (where F and A are the normalized flux and area values, C_1 and C_2 are the constants determined from the least square fit) is done. With a very high probability, we find significant correlations between these variables. This area-flux relationship is useful for measuring strength of the initial fluxes for a long stretch of sunspot data set (for example, the Greenwich Photoheliographic results wherein the information of magnetic flux is not available). It is to be noted that, in the previous studies, Harvey (1993) computed the flux-area relationship when the active regions reached their maximum area and Meunier (2003) computed the flux-area relationship for the regions at any time during their life time. However, present study is for the spot groups when they are at the initial stages of the development. Moreover, slope ($log_{10}C_2$ is 2.66 for figure 5.6(a) and is 1.66 for figure 5.6(b)) of the area-flux relationship of the present study is much greater than the slopes of area-flux relationship in the previous studies. This result suggests that most of the magnetic flux contribution within the threshold 20 G contour is from the sunspots only.

The rate of emergence (REF) of magnetic flux versus the life span for both the leading and following spots is presented in Fig 5.7. From the law of least-square fit, the rate of emergence of magnetic flux of the bipolar spots during their *initial* developmental stage is found to be $\sim 6X10^{19}$ Mx/day for the spot groups with 12 days life span (that might originate near base of the convective envelope). However, the spot groups with 2 days life span (that might originate near the surface) emerge with $\sim 4X10^{19}$ Mx/day, nearly 65% of the emergence rate near the base.

All the results related to linear least square fits that are over plotted on different scatter plots ($\tau - B$, $\tau - Flux$, $Area - Flux$ and $\tau - dF$) such as the intercepts, slopes and correlation coefficients with probability of significance of correlation coefficient are summarized in Table 5.2.

5.4 Discussion and conclusions

The sunspot groups have very large concentration of magnetic flux compared to the surrounding medium. Present study shows that majority of the spot groups that have first and second observations are bipolar. This suggests that sunspots that are observed on the surface are parts of emerging Ω-shaped loops from the convective envelope. Previous study (Hiremath 2002) shows that the initial rotation rate of sunspot groups with respect to their life spans is almost similar to the radial variation of internal rotation of the solar plasma (Fig 3a and Fig 5 of (Hiremath 2002)) as inferred from helioseismology (Antia et al. 1998) suggesting that the sunspot groups of different life spans are anchored at different depths in the solar convection zone. That is the sunspot groups with life span of $\sim$ 12 days are anchored near base of the convective envelope and the spot groups of life spans $<$ 2 days are anchored near the surface ($\geq$ $0.96R_{\odot}$). The strength of magnetic field B of the flux tube (at the site of the anchoring depth) is directly proportional to the square root of the ambient plasma pressure (P) (Parker 1955b). To be precise, the relation $B_a = (P_a/P_s)^{1/2}B_s$ yields the strength of magnetic field B_a at different anchoring depths in the convection zone with the ambient plasma pressure P_a (where as B_s is the strength of the flux tube and P_s is the ambient plasma pressure at the surface). From the inferred pressure from helioseismology (Shibahashi et al. 1998, 1999) and the results from Fig 5.4 (average surface field strength B_s of $\sim$ 500 G), we get magnetic field strength of $\sim 10^6$ G near base of the convection zone and $\sim 10^4$ G at $0.96R_{\odot}$. These results are strikingly consistent with the helioseismic inversions (Dziembowski & Goode 1989; Basu 1997; Antia et al. 2000; Antia 2002) and the MHD calculations (Choudhuri & Gilman 1987; D'Silva & Howard 1994; Hiremath 2001)

If the source of formation of the sunspots, *viz.*, the dynamo activity is confined to base of convection zone, one would expect that all the spot groups irrespective of their size and life span should have same strength of magnetic field over the surface. However, both the results of Fig 5.4 that are derived from the *initial* two measurements show a strong negative and significant correlation suggesting that ,

irrespective of their sizes on the surface, the spot groups that have longer life spans have small magnetic field strength compared to the spot groups that have shorter life spans. This is possible only when the dynamo activity is distributed everywhere in the convective envelope. This result is also consistent with the recent argument for the case of a distributed dynamo (Brandenburg 2005) in the whole region of convective envelope.

If we accept this fact that the source of dynamo activity is distributed everywhere in the convective envelope, the results presented in Fig 5.7 show that the rate of flux emergence from the dynamo activity varies at different depths. For example, the spot groups that have longer life spans with their foot points anchored near base of the convection zone emerge with more flux compared with the spot groups that have shorter life spans and whose foot points are anchored close to the surface. This implies that dynamo activity produces more flux near base of the convection zone compared to the dynamo activity near the surface. It would be interesting to know whether models based on the turbulent dynamo and full MHD simulations reproduce these inferred results.

It is not surprising that the sun has such a source of distributed dynamo activity in the convective envelope. The recent analysis (Donati et al. 2003) of brightness and magnetic surface images of the young K0 dwarfs AB Doradus and LQ Hydrae, and of the K1 subgiant of the RS CVn system HR 1099, reconstructed from Zeeman-Doppler imaging spectropolarimetric observations shows that the dynamo activity is distributed throughout the entire convection zone.

In the present study, initial magnetic flux of the sunspots from their first observation on the surface is measured. However, the line of sight component of the magnetic field structure is a combination of poloidal and toroidal parts of the magnetic field structure that are computed in the previous studies (Shrauner & Scherrer 1994; Ulrich & Boyden 2005). Using Mount Wilson line of sight magnetic data averaged over each Carrington rotation, Ulrich and Boyden (2005) computed both the poloidal and toroidal parts of the global magnetic field structure. It would be interesting to know both of these magnetic field components from the initial magnetic field measurements for the localized field structure such as sunspots used in

this study.

In the next chapter, from the observed line of sight component of magnetic field structure, poloidal and toroidal components of magnetic field structure of sunspot are separated and, after rederiving Parker's (1955b) flux tube model in spherical coordinates, poloidal and toroidal components of the sunspots at different anchoring depths in the convective envelope are inferred.

To conclude, analysis of the initial magnetic field/flux of the sunspot groups derived from the SOHO/MDI magnetograms yields the following results : (i) majority of the sunspots that are observed initially on the surface are bipolar, (ii) irrespective of their sizes, bipolar spots have average initial magnetic field strength of $\sim$ 500 G for different life spans, (iii) the field strength at the sites of the anchoring depths is estimated to be $\sim 10^6$ G near base of the convective envelope and $\sim 10^4$ G near the surface ($\geq 0.96 R_\odot$) and, (iv) the dynamo-a source of sunspot activity-is distributed everywhere in the convective envelope and, (v) the rate of emergence and hence the dynamo activity is strong near base of the convective envelope compared to near the surface.

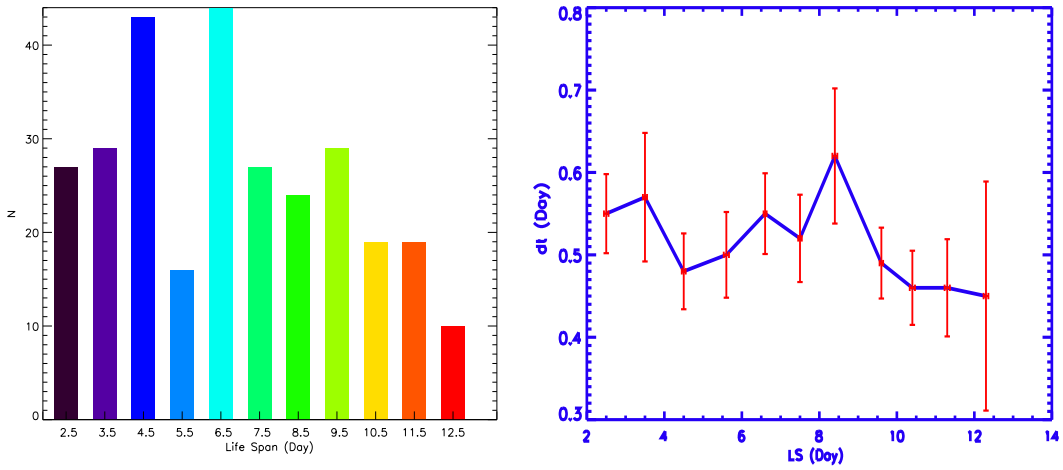

Figure 5.3: The selected number N of sunspots for different life spans are considered for the analysis i.e., represented on the left side figure(Fig 5.3(a)) and right side figure (Fig 5.3(b)) represents the average time difference dt between the initial two observations, for different life spans.

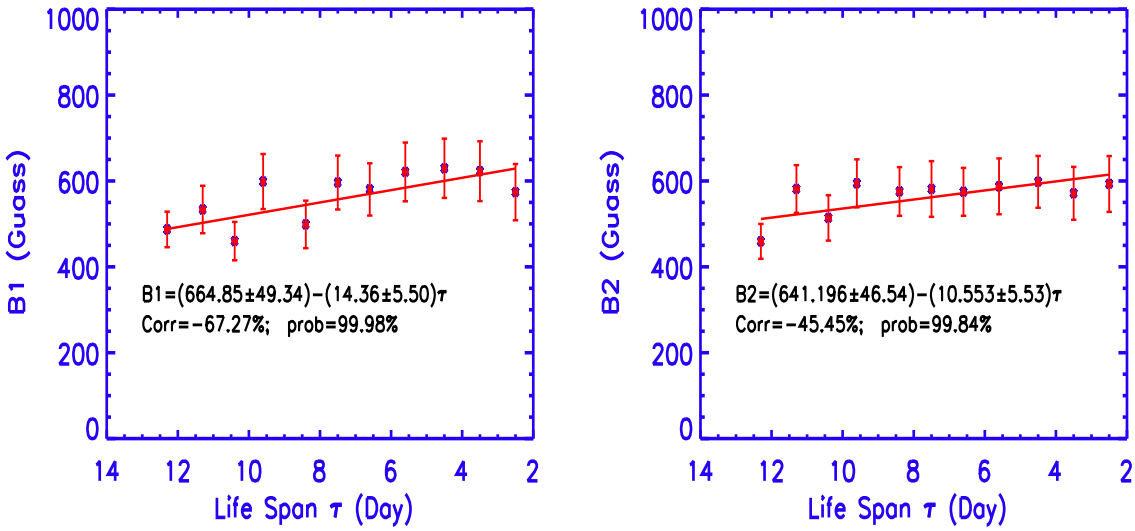

Figure 5.4: For different life spans, measured initial magnetic field strength of the bipolar spots. **(a)** The left figure represents variation of the magnetic field strength of the bipolar spots during their first observation on the solar disk. **(b)** The right figure represents variation of the magnetic field strength of the bipolar spots during their second observation on the solar disk. In both the illustrations, the red continuous line represents the linear least-square fit with a law $B_i = C_1 + C_2\tau$ (where $B_i, i = 1, 2$, are the measured initial magnetic field strengths,τ is life span in days and, C_1 and C_2 are the coefficients determined from the fit) is fitted to both the data set.

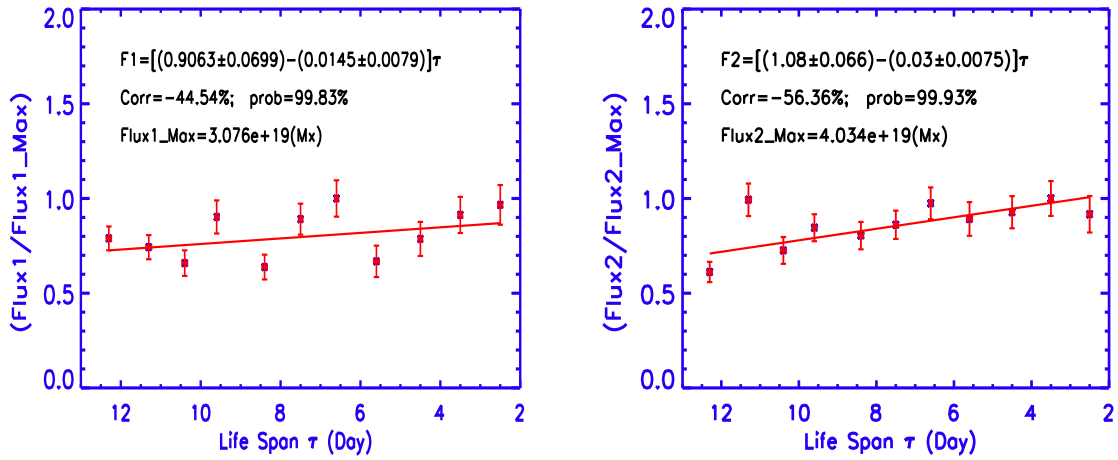

Figure 5.5: For different life spans, measured initial magnetic flux of the bipolar spots. **(a)**The left figure represents variation of the magnetic flux of the bipolar spots during their first observation on the solar disk. **(b)** The right figure represents variation of the magnetic flux of the bipolar spots during their second observation on the solar disk. In both the left and right illustrations, the normalized (with their maximum values Flux1_Max and Flux2_Max) flux values during their first and second observations respectively are presented. The red continuous line represents the linear least-square fit to the normalized flux values with a law $F_i = C_1 + C_2\tau$ (where $F_i, i = 1, 2$, are the measured initial magnetic fluxes, τ is life span in days and, C_1 and C_2 are the coefficients determined from the fit) is fitted to both the data set.

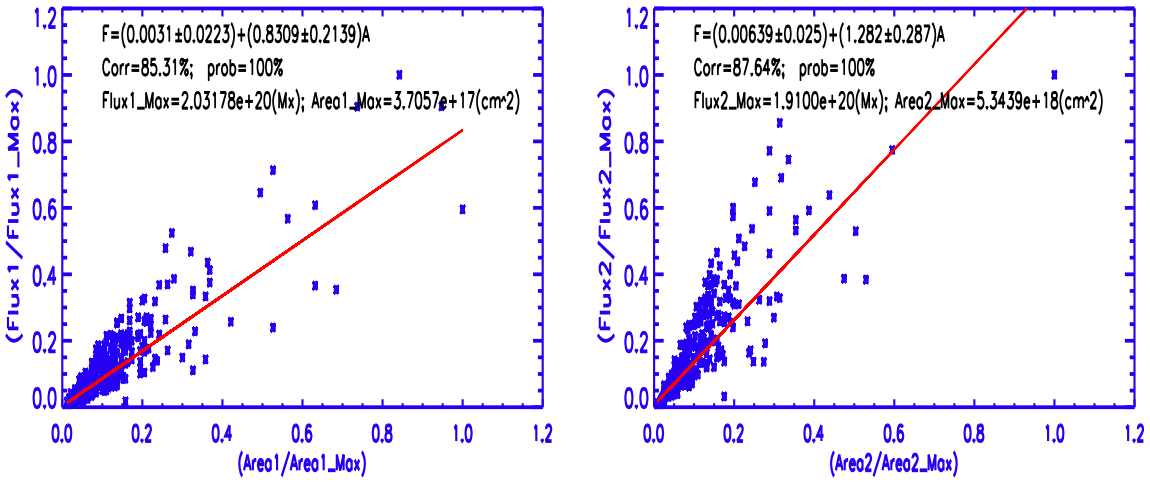

Figure 5.6: Irrespective of their life spans, measured initial area versus initial magnetic flux of the bipolar spots. Both the left **(a)** and right **(b)** illustrations represent the normalized (with their maximum area values Area1_Max and Area2_Max and, the flux values Flux1_Max and Flux2_Max) area and flux values during their first and second observations respectively. The red continuous line represents the linear least-square fit with a law $F_i = C_1 + C_2 A$ (where $F_i, i = 1, 2$, and A are the normalized flux and area and, C_1 and C_2 are the coefficients determined from the fit).

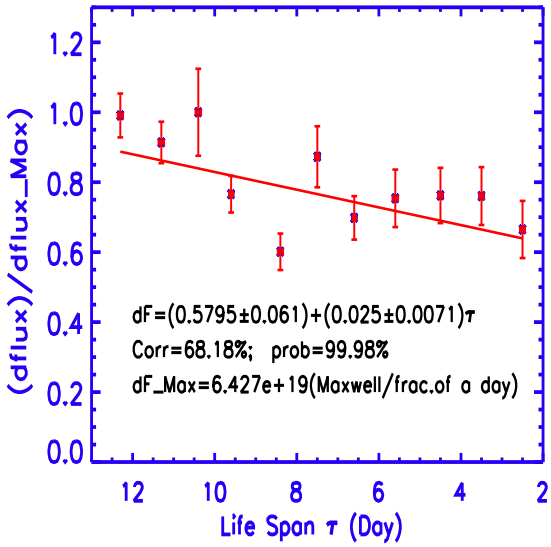

Figure 5.7: For different life spans, the normalized (with the maximum value of dF_Max) rate of emergence of magnetic flux of the bipolar spots respectively. The red continuous line represents the linear least-square fit with a law $dF = C_1 + C_2\tau$ (where dF (in the units of Mx/day) is the rate of emergence of initial flux, τ (in days) is the life span and, C_1 and C_2 are the coefficients determined from the fit) is fitted to both the data set.

Table 5.2: Parameters of the linear least square fit

Observations	Intercept	Slope	Corr	Prob
$(\tau - B)$ First	654.85±49.34	14.31±5.50	-67.27	99.98
$(\tau - B)$ Second	641.20±46.54	10.55±5.53	-45.54	99.83
$(\tau - Flux)$ First	(2.79±0.22)x10^{19}	(0.04±0.02)x10^{19}	-44.54	99.83
$(\tau - Flux)$ Second	(4.36±0.27)x10^{19}	(0.12±0.03)x10^{19}	-56.36	99.93
$(Area - Flux)$ First	(0.06±0.45)x10^{19}	(455.58±115.43)	85.3	99.99
$(Area - Flux)$ Second	(0.01±0.05)x10^{20}	(45.85±10.27)	87.6	99.99
$(\tau - dF)$	(3.72±0.39)x10^{19}	(0.16±0.05)x10^{19}	68.2	99.98

(a) For the first and second observations of $(\tau - B)$ relationship, the intercepts and the slopes are in the units of Guass.
(b) For the first and second observations of $(Area - Flux)$ relationship, the intercepts are in units of Maxwell and the slopes are in the units of Guass.
(c) For $(\tau - dF)$ and the first and second observations of $(\tau - Flux)$ relationships, the intercepts and the slopes are in the units of Maxwell.